

Dissertation  
submitted to the  
Combined Faculties for the Natural Sciences and for Mathematics  
of the Ruperto-Carola University of Heidelberg, Germany  
for the degree of  
Doctor of Natural Sciences

presented by

Dipl. Biomathematikerin Anna Schulze

born in Lehre Kr Helmstedt

Oral-examination: .....



# Data – driven modeling of T cell activation

Referees: Prof. Dr. Thomas Höfer  
Prof. Dr. Ursula Klingmüller



# Contents

<b>Summary</b>	<b>i</b>
<b>Zusammenfassung</b>	<b>iii</b>
<b>1. Introduction</b>	<b>1</b>
1.1. T cell receptor triggering . . . . .	1
1.1.1. Early signaling events . . . . .	2
1.1.2. ZAP70 is an essential molecule in TCR triggering . . . . .	3
1.1.3. Signal propagation . . . . .	4
1.1.4. The high discriminative power of the TCR is explained by different mechanisms . . . . .	5
1.2. Src-family kinase regulation . . . . .	9
1.2.1. CD45 is an important regulator of Lck activity . . . . .	11
1.3. Structure of this work . . . . .	12
<b>2. Mathematical Methods</b>	<b>13</b>
2.1. Modeling . . . . .	13
2.2. Parameter estimation and identifiability . . . . .	14
2.2.1. The profile likelihood approach . . . . .	15
2.2.2. Prediction confidence intervals can be estimated by using the profile likelihood method . . . . .	16
<b>3. A mechanistic model of early T cell receptor signaling</b>	<b>19</b>
3.1. Modeling basal activation of the T cell receptor . . . . .	19
3.1.1. Basal TCR activation is measured by stimulating T cells with the phosphatase inhibitor pervanadate . . . . .	20
3.1.2. A model of early events in TCR signaling . . . . .	22
3.1.3. Estimation of the basal rates from kinetic measurements . . .	25
3.2. Ligand binding can induce kinetic proofreading . . . . .	32
3.2.1. Adding ligand binding to the basal model . . . . .	32
3.2.2. Regulated kinase access or phosphatase exclusion can trigger TCR signaling . . . . .	35
3.2.3. Kinetic proofreading requires a synergistic effect of enhanced phosphorylation and reduced dephosphorylation . . . . .	38

<b>4. Modeling the dynamics of Lck regulation</b>	<b>43</b>
4.1. Modeling Lck regulation: two different approaches . . . . .	43
4.1.1. Bistability in the model with enzymatic kinetics . . . . .	43
4.1.2. A mass-action kinetics model without bistability . . . . .	45
4.1.3. Flow cytometry data does not show bistability . . . . .	48
4.2. A more detailed view on the mass action kinetics model . . . . .	50
4.2.1. Phosphorylation of Lck was measured for different Lck chimeras	50
4.2.2. Parameters can be estimated from dose-response data . . . . .	53
4.3. Model simulations show the regulation of Lck activity . . . . .	58
4.3.1. Autoactivation of Lck occurs in trans . . . . .	58
4.3.2. Csk phosphorylates the primed and the single active Lck differently . . . . .	60
4.3.3. CD45 has an inhibitory effect on Lck activity . . . . .	62
<b>5. Discussion</b>	<b>65</b>
<b>References</b>	<b>74</b>
<b>A. Appendix</b>	<b>83</b>
A.1. Additional material for the T cell signaling model . . . . .	83
A.1.1. ODE-System for the basal model . . . . .	83
A.1.2. ODE-System of the model with ligand binding . . . . .	84
A.1.3. Prediction profile likelihoods . . . . .	87
A.2. Additional material for the Lck regulation model . . . . .	88
A.2.1. Flow cytometry data of pY505 . . . . .	88
A.2.2. Steady state solution of the Lck model . . . . .	88
A.2.3. Csk kinase activity with two different rates . . . . .	89
<b>Abbreviations</b>	<b>90</b>
<b>Acknowledgments</b>	<b>93</b>

## Summary

T cells accurately discriminate between antigens that have only moderately different affinities. The decision of whether the cell is activated or not is made during the initial stages of membrane-proximal signaling triggered by the T cell receptor (TCR). Several mechanistic models have been proposed to explain the highly specific and sensitive recognition of peptide-MHC ligands. Prominent among them is the kinetic proofreading model that accounts for the high specificity of the ligand discrimination by the TCR based on ligand dwell time. Open questions of central importance are (1) whether kinetic proofreading is indeed realized in TCR signal transduction and (2) how information about ligand binding to the TCR is transduced to the cell interior. In this work, we addressed these questions quantitatively by means of two data-based models. Our models describe the dynamics of two core modules of TCR activation: the TCR signaling module and the Src-family kinase regulation module.

The model of TCR signaling accounts for the reversible phosphorylation of immunoreceptor tyrosine-based activation motifs (ITAMs) in the TCR complex by the kinase Lck and the phosphatase CD45, and the subsequent recruitment and phosphorylation of the pivotal kinase ZAP70. We parameterize the model using kinetic measurements of phosphorylation status and protein-protein interactions. The model constrained by these data allows for kinetic proofreading of ligand dwell time; however, this capacity depends on the mechanism of signal initiation. Neither an enhancement of phosphorylation nor a reduction of phosphatase activity alone allow the TCR to discriminate ligand dwell times, whereas a combination of both effects yields kinetic proofreading behavior.

TCR signaling is driven by the Src-family kinase Lck: thus we investigated the dynamic regulation of Lck activity in the second model. The parameterization of this model is based on dose-response data of wild type Lck and Lck chimeras with altered membrane targeting. These data allow us to determine the model parameters within narrow confidence bounds enabling us to make quantitative predictions with the model. We find that Lck activity is regulated jointly by its subcellular localization, trans-autophosphorylation of the activating tyrosine residue and the activity of the phosphatase CD45 in the proximity of Lck. Mechanistically, CD45 mediates both activating and inhibitory dephosphorylations of Lck. Physiologically, we find that CD45 has a solely inhibitory effect on Lck activity. Interestingly, this inhibitory action could synergize with the mechanisms modeled in the TCR signaling model to support kinetic proofreading.

In summary, our results show how data-driven mathematical modeling, can be used to dissect the complexity of TCR activation on a quantitative basis.



## Zusammenfassung

T-Zellen sind in der Lage exakt zwischen Antigenen mit moderaten Affinitätsunterschieden zu differenzieren. Ob die Zelle aktiviert wird, entscheidet sich während des Beginns der vom T-Zell-Rezeptor (TCR) initiierten Signaltransduktion an der Zellmembran. Die hohe Spezifität und Sensitivität in der Erkennung von Liganden kann durch verschiedene mechanistische Modelle erklärt werden. Ein wichtiger Vertreter ist das sogenannte *kinetic proofreading*-Modell (im folgenden kinetische Fehlerkorrektur genannt), welches die spezifische Diskriminierung von Liganden anhand ihrer Verweildauer am TCR erklärt. Offene Fragen von zentraler Bedeutung sind (1) ob eine kinetische Fehlerkorrektur durch die Signaltransduktion des TCR realisiert werden kann und (2) wie die Information, dass ein Ligand an den TCR bindet, ins Innere der Zelle übermittelt wird. In dieser Arbeit adressieren wir diese Fragen auf quantitativer Weise mit Hilfe von zwei, auf Messdaten basierenden, Modellen. Diese Modelle beschreiben das dynamische Verhalten von zwei Hauptmodulen der TCR- Aktivierung: Das TCR Signaltransduktions Modul und das Modul welches die Regulation der zur Src-Familie gehörenden Kinasen zusammenfasst.

Das TCR-Signaltransduktionsmodell berücksichtigt sowohl die reversible Phosphorylierung der ITAMs (immunoreceptor tyrosine-based activation motifs) des TCR-Komplexes durch die Kinase Lck und Phosphatase CD45 als auch die anschließende Rekrutierung und Phosphorylierung der zentralen Kinase ZAP70. Wir parametrisieren das Modell mit zeitaufgelösten Messungen des Phosphorylierungsstatus und von Protein-Protein Interaktionen. Das so durch die Daten beschränkte Modell hat die Fähigkeit, Liganden anhand ihrer Verweildauer am TCR zu unterscheiden, allerdings hängt das Verhalten dieser kinetischen Fehlerkorrektur von dem Mechanismus der Signalinitiierung ab. Weder eine verstärkte Phosphorylierung noch die Reduzierung der Phosphataseaktivität alleine ist ausreichend für den TCR um Liganden anhand ihrer Verweildauer zu unterscheiden. Erst eine Kombination beider Effekte resultiert in der Möglichkeit zur kinetischen Fehlerkorrektur.

Regulierung der Aktivität von Lck untersuchen. In diesem Modell basiert die Parametrisierung auf Dosis-Wirkungs-Messungen des Wildtyps und verschiedener Chimaeren von Lck, die sich durch unterschiedliches Assoziierungsverhalten mit der Membran unterscheiden. Die Parameter des Modells können durch diese Daten vollständig innerhalb kleiner Konfidenzintervalle identifiziert werden, was quantitative Modellvorhersagen erlaubt. Wir können beobachten, dass die Aktivierung von Lck gleichzeitig durch die zelluläre Lokalisierung von Lck, die Trans-Autophosphorylierung des aktivierenden Tyrosinrests und die Aktivität der Phosphatase CD45 reguliert wird. Mechanistisch gesehen kann CD45 sowohl die Aktivierung als auch die Inhibierung von Lck vermitteln. Physiologisch können wir einen ausschließlich inhibierenden Effekt von CD45 auf Lck feststellen. Interessanterweise könnte dieser inhibitorische Mechanismus den für die kinetische Fehlerkorrektur des TCR-Signaltransduktionsmodells wichtigen synergistischen Effekt auslösen.

Zusammenfassend zeigen unsere Resultate, dass die durch Daten unterstützte mathematische Modellierung benutzt werden kann um die Komplexität der TCR Aktivierung auf quantitativer Basis detailliert zu analysieren.

# 1. Introduction

The recognition of antigen by the T cell receptor (TCR) is one of the hallmarks of adaptive immunity. Not only is the TCR highly sensitive and can be triggered by only a few ligands it is also very specific and is able to accurately discriminate between ligands with only moderate differences in affinity. For reasons that are still discussed in the field the TCR is able to sense the quality of a ligand rather than its concentration. This discriminative power allows the selection of a T-cell repertoire that mediates effective protection against foreign pathogens but is tolerant towards self peptides.

Despite an ongoing debate on the mechanisms of TCR discrimination, many details of the intricate mechanisms of TCR signaling have been unraveled over the years [62] and the key molecules of this process are thought to be known [31]. The signalosome of the T cell receptor consists of three core modules as defined by Acuto et al. [1]: the Src-family kinase (SFK) regulation module, the signal triggering module and the signal diversification module. The decision whether the TCR is activated by a peptide or not is made during early TCR signaling [61]. Therefore, for a better understanding of antigen discrimination by the TCR, the investigation of the two core modules of SFK activation and TCR signal triggering is crucial.

In this work we combine mechanistic models of early events in TCR signaling and of the regulation of Src-family kinase activation with experimental data to dissect the complexity of TCR signaling on a quantitative basis.

## 1.1. T cell receptor triggering

T cells are constantly presented to antigen by surrounding cells. They are able to distinguish rare foreign antigens from a vast amount of self antigens. Antigens are presented to T cells in form of short peptide sequences.

Antigen presenting cells (APCs) express two classes of the surface molecule major histocompatibility complex (MHC), MHC class I and MHC class II. Both types of MHCs are able to bind the peptides (pMHC) and mediate the interaction of the TCR and its cognate ligand. T cells are subdivided into two groups based on the coreceptor they express. While CD8-T cells interact with pMHC class I molecules that can be found on the surface of more or less all cells, CD4-T cells are triggered

by specialized APCs that carry MHC class II molecules.

The discrimination of antigens takes place during the early stages of TCR-mediated signaling [61] and is based on the affinity of the ligand for the TCR [39]. Nevertheless, the exact cellular response after TCR activation might depend on the strength of the stimuli as well [71].

The T cell receptor itself is an oligomer that is composed of a ligand recognition unit on the surface of T cells and an intracellular signaling module. A dimer of two variable TCR $\alpha$  and TCR $\beta$  chains is responsible for ligand recognition. The core signaling module is a dimer of two  $\zeta$ -chains that is accompanied by a CD3 $\delta/\varepsilon$  and a CD3 $\gamma/\varepsilon$  dimer. All three dimers comprise immunoreceptor tyrosine-based activation motifs (ITAMs) and play an important role in TCR signaling. The ligand recognition subunit of the TCR is distinct from its signaling unit and has only a few intracellular amino acid residues. Hence, it is difficult to envision - based on TCR structure - how the extracellular signal is translated into intracellular signaling. Different theories have been proposed that contribute to the question on how the signal is transmitted through the membrane [68]. We will come back to this question in Section 1.1.3, where we introduce the three main ideas of signal propagation.

ITAMs are TCR intrinsic activation motifs which are located on all six intracellular subunits of the TCR. Each ITAM is comprised of a specific amino acid sequence (Yxx(L/I)x<sub>6–8</sub>Yxx(L/I), where x denotes variable amino acids) which includes two tyrosines (Y) that are around ten amino acids apart [17]. The ITAMs are differently distributed between the subunits of the TCR. While each CD3 chain carries one ITAM, the  $\zeta$ -chains are comprised of three ITAMs each. In total there are ten ITAMs per TCR. Because the TCR is organized in dimers, ITAMs on opposing protein chains are colocated in pairs.

### 1.1.1. Early signaling events

TCR mediated T cell activation coincides with elevated levels of ITAM phosphorylation (although there might be exceptions [54]), which marks the first step of TCR-based signaling. Upon TCR stimulation both tyrosine residues of one ITAM have to be phosphorylated in order to pass on the activation signal. ITAMs are phosphorylated by the Src-family kinase Lck, which will be introduced in more detail later in this chapter.

The predominant effect in TCR signaling is the recruitment of ZAP70 ( $\zeta$ -chain associated protein of 70kDa, introduced in more detail later) to the ITAMs, although the individual ITAMs might have additional functions in TCR activation [49]. The phosphorylation of one ITAM is stabilized by ZAP70 binding. ZAP70 has a high affinity only for double phosphorylated ITAMs [24]. Once it is bound it can get phosphorylated at various tyrosine residues. The two most important phosphoryla-

tion sites for T cell activation are a tyrosine residue in the linker region of ZAP70 that is called interdomain B and one in the kinase domain of ZAP70. The phosphorylation site in interdomain B is, like the ITAMs, phosphorylated by Lck. The activating phosphorylation in the kinase domain of ZAP70 is carried out by trans-autophosphorylation of an opposing ZAP70. The important role of ZAP70 in TCR activation is further discussed in the next section.

Two main substrates of ZAP70 are the adaptor proteins SLP-76 (SH2 domain containing leukocyte protein of 76kDa) and the linker of activation (LAT) [76]. Both orchestrate a number of signaling cascades which ultimately result in a fully activated T cell and an immune response towards the antigen that triggered the TCR [28, 58]. Important signaling pathways that are initiated by these phosphorylation events include the MAP kinase pathway or the PI-3 kinase/Akt pathway [33]. One of the first signs of T cell activation is a massive increase in calcium flux, which is also initiated by the phosphorylation of LAT.

### **1.1.2. ZAP70 is an essential molecule in TCR triggering**

The  $\zeta$ -chain associated protein of 70 kDa (ZAP70) is one of the crucial molecular players in TCR activation. Studies show that T cells deprived of ZAP70 cannot become activated after TCR stimulation. The absence of ZAP70 results in severe combined immunodeficiency (SCID) which is characterized by non functional CD4 T cells and the lack of CD8 T cells in the periphery [6]. The loss of ZAP70 cannot be substituted by other molecules. After the phosphorylation of the T cell receptor, upon stimulation with its specific ligand, ZAP70 is the first protein that interacts with the TCR via the phosphorylated ITAMs.

The structure of ZAP70 contains two N-terminal SH2 domains that are linked to the C-terminal kinase domain by interdomain B. The two SH2 domains of ZAP70 – and their close proximity – make it possible to bind to both phosphorylated tyrosines of an ITAM simultaneously. Unbound ZAP70 is in a closed conformation that shields its activating phosphorylation sites. In order for ZAP70 to change its conformation the two SH2 domains need to be bound in a certain pattern [17]. The incomplete binding pocket of the first SH2 domain is completed by parts of the outside structure of the second SH2 domain [24]. The two tyrosines of an ITAM are spaced in exactly the right distance to allow for high affinity ZAP70 binding. This very specific ITAM-ZAP70 interaction prevents ZAP70 from becoming activated spuriously if it binds to other proteins [70, 7].

Interdomain B of ZAP70 contains three phosphorylation sites (Y292, Y315, Y319) that serve as binding sites for different signaling molecules [74, 48, 7]. While tyrosine 315 is an important phosphorylation site and is often mentioned in the context of TCR activation, the crucial tyrosine residue of interdomain B is Y319 [19]. It is

phosphorylated by Lck and also serves as a binding site for it. But most importantly it is needed for a positive regulation of ZAP70. ZAP70 that is mutated at Y319 cannot be activated, whereas mutations of other tyrosine residues including Y315 also result in decreased TCR activation but with much less severe effects [19]. It is believed that phosphorylation of Y319 further stabilizes the open conformation of ZAP70 and thereby enables the full activation of ZAP70 [7].

The ZAP70 kinase domain holds a pair of tyrosine residues (Y492 and Y493). While phosphorylation of Y492 has an inhibitory effect, the phosphorylation of Y493 fully activates ZAP70 [72]. Experiments with a ZAP70 inhibitor indicate that this tyrosine is phosphorylated mainly by trans-autophosphorylation [39].

To summarize, the activation of ZAP70 is a crucial step in early TCR signaling and is preceded by the decision of TCR activation. Therefore, activated ZAP70 seems to be a good measure of T cell activation and can be used as a readout of successful TCR triggering.

### 1.1.3. Signal propagation

The T cell receptor does not possess intrinsic kinase activity. Nevertheless, the information of extracellular stimulation needs to be transmitted into the cell and translated into stronger phosphorylation of the ITAMs. In this section we will discuss the different underlying mechanisms of signal propagation that have been proposed [68].

**Kinase aggregation model** The most widely accepted mechanism is that of kinase aggregation. Upon stimulation, kinases, in particular the Src-family kinases Lck and to lesser extend Fyn, aggregate in close proximity of the TCR leading to augmented phosphorylation of the ITAMs. Lck can be bound to the coreceptors CD8 and CD4, which have a weak, unspecific affinity for pMHC. If there is a TCR–pMHC interaction, the coreceptors are also recruited to the TCR and with it the bound Lck [66]. The role of the coreceptors CD8 and CD4 is not completely clarified yet. Mature T cells either are CD8 or CD4 positive, so both coreceptors might play different roles in TCR activation. The presence of CD4 enhances the sensitivity of TCR activation [37], whereas CD8 is even able to bind directly to the  $\alpha$ -chain of the TCR [38], which could contribute to the efficiency of TCR antigen discrimination. However, it is also possible to activate T cells that do not have any of the two coreceptors. A finding of Nika et al. [45] supports the aggregation model. In their study the authors report high levels of basal Lck activation (around 40 %) that stay unchanged upon TCR triggering.

**Conformational change model** Another proposed mechanism attributes the signal transduction through the membrane to a conformational change of the TCR. Without stimulation the ITAMs of the TCR are not accessible for Lck, because ITAMs are in close contact to the membrane [73]. Ligand binding releases the intracellular TCR subunits from the membrane, the ITAMs becomes more accessible and can be phosphorylated more easily. The conformational change could either be induced due to a pulling mechanism or by dimerization of TCRs [53, 59]. Although some findings support this theory, the strong activation of the TCR with the phosphatase inhibitor pervanadate is hard to match with this mechanism.

Both the kinase aggregation model and the conformational change model assume that, in one way or the other, the rate of ITAM phosphorylation is enhanced. In contrast, a third possibility assumes a decrease in phosphatase activity following TCR stimulation.

**Phosphatase segregation model** The segregation model assumes that relevant phosphatases are pushed out of the region of TCR–pMHC contact by mechanical forces [16]. The predominant phosphatase at the membrane is CD45. It has very large ectodomains, that exceed the TCR–pMHC complex in size. Upon the formation of the TCR–pMHC complex, CD45 is pushed out of the region of interaction due to its size. A second possibility that would exclude phosphatases could be a rearrangement of the membrane. If the amount of phosphatase is reduced in the proximity of the TCR, phosphorylation is reversed to a much lesser extend and T cells become activated. Recent studies show that, indeed, CD45 is pushed out of the signaling region of the TCR [31].

Both enhanced kinase activity or decreased dephosphorylation results in increased phosphorylation levels of the ITAMs and ZAP70 and can lead to successful TCR triggering. None of the mechanisms is fully validated, nor can be rejected, thus a combination of them is plausible and would explain why none of them is able to satisfactorily explain signal propagation alone.

#### 1.1.4. The high discriminative power of the TCR is explained by different mechanisms

The high discriminative power of the TCR in its accuracy is unmatched by any other known receptor. It is the combination of specificity, sensitivity, concentration independence and its speed that make the TCR so special.

The specificity of the TCR is demonstrated by its ability to sense small changes in ligand affinity. This was impressively shown by Daniels et al. [14] who tested the boundary between positive and negative selection in the thymus for an array of ligands with small differences in affinity. The authors found a sharp threshold

response with a boundary that is mostly independent of ligand concentration; only one of the tested ligand with an affinity close to the threshold could either function as a negative or positive selector depending on its concentration. This implies that weak affinity can not be replaced by a high ligand concentration.

The TCR is sensitive already to a small number of foreign antigens, while on the other hand is able to ignore a high number of self peptides. Around ten ligands are sufficient to reliably trigger sustained T cell activation and the formation of the immunological synapse [75], and even a single ligand could be sufficient to activate the TCR [30]. Additionally the decision whether the TCR is activated or not is made very fast. The up-regulation of signaling events, during which this decision is made [61], only takes seconds [27].

For most receptors there is a trade off between sensitivity and specificity in ligand recognition; the TCR is a rare example that shows a combination of both characteristics. The desire to quantitatively understand this property has guided the formulation of quantitative models, among them kinetic proofreading, feedback regulation and serial triggering models.

The serial triggering model is based on the assumption that high affinity ligands bind to multiple TCRs consecutively [67]. Thereby a small amount of agonists are able to trigger a much higher number of TCRs, which amplifies the signal of the agonist ligand. Serial triggering models were formalized to account for the sensitivity of TCR discrimination. [22].

Various feedback regulations of the TCR have been found experimentally. One important negative regulator of TCR activation is SHP-1. It can be activated by active ZAP70 as well as Lck. But both molecules are also negatively regulated by SHP-1 [50, 12] creating direct negative feedback. On the other hand SHP-1 is inhibited by activated Erk which generates a competitive positive feedback regulation [63]. Other possible feedback mechanism involve the regulation of Ras and SOS [15, 51]. Most of the described feedback regulations have been modeled more or less quantitatively with varying levels of detail, but none of them are directly linked to data [4, 21, 12, 51] and model parameters are mostly either taken from literature or selected by the investigator.

A very detailed model is proposed by Altan–Bonnet et al. [4]. It contains competitive feedback regulations via Erk and SHP-1. Interestingly, they incorporated a kinetic proofreading mechanism into the model. The kinetic proofreading model, which is described in more detail below, accounts especially well for the high specificity of the TCR. But the increased specificity comes at the expense of a reduced sensitivity. In the model of Altan–Bonnet et al. sensitivity is partly restored by combining the kinetic proofreading scheme with the additional feedback regulations.

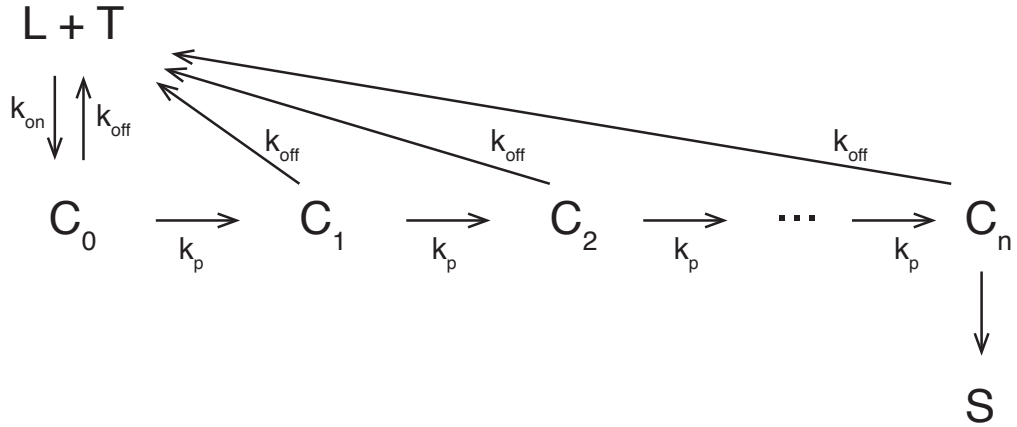


Figure 1.1.: Kinetic proofreading scheme, adapted from McKeithan [40]. Upon contact, the T cell receptor (T) and its cognate ligand (L) form a complex ( $C_i$ ). The complex becomes phosphorylated sequentially with the phosphorylation rate  $k_p$ . The number of phosphorylation steps is indicated by  $n$ . The signal (S) is only passed on if all phosphorylation steps are completed. The TCR and the ligand associate and dissociate with the rates  $k_{on}$  and  $k_{off}$ , respectively.

### Kinetic proofreading in T cells

The principles of kinetic proofreading have first been proposed by Hopfield in 1974 [26]. In his work the author explained the high fidelity of translating the genetic code by means of a mechanism which he termed kinetic proofreading. The proposed model provides a mechanism for the precise molecular discrimination between binding partners with very small differences in binding energies at the expense of metabolic energy. The T cell receptor (TCR) is able to precisely discriminate between ligands with only moderate differences in affinity as well. In 1995 Timothy McKeithan [40] proposed a link between this high discriminative power of the TCR to the principles of kinetic proofreading.

McKeithan's model proposes that downstream signaling is only possible after several, energy consuming, phosphorylation steps. These phosphorylations are triggered by ligands that bind to the TCR. As soon as the ligand dissociates from the TCR, phosphorylation is stopped and – due to very fast dephosphorylation rates in the model – the receptor is immediately cleared of all phosphorylations (see Fig. 1.1).

A signal is only generated if all phosphorylation steps are completed. This implies that the generation of a signal no longer just depends on the ligand concentration ( $[L]$ ) but also on the time that the ligand is bound to the TCR ( $\tau$ ) which is determined by the dissociation rate  $k_{off}$  in the model ( $\tau = 1/k_{off}$ ):

$$\text{Fraction of signaling TCR} = \frac{[L]}{K_d + [L]} \left( \frac{k_p}{k_p + k_{\text{off}}} \right)^n \quad (1.1)$$

where  $K_d$  is the affinity of the ligand given by the ratio of the dissociation and the binding rate ( $K_d = k_{\text{off}}/k_{\text{on}}$ ),  $k_p$  is the phosphorylation rate and  $n$  denotes the number of phosphorylation steps that is required for downstream signaling.

Given constant ligand concentration the discrimination of ligands based on their dwell time  $\tau$  at the TCR that is proposed by the kinetic proofreading model is one of the main features of TCR mediated T cell activation [34, 75].

The precision of ligand discrimination in the kinetic proofreading model is largely dependent on the number of (time consuming) phosphorylation steps that precede signal generation. The decision whether the TCR is activated or not is made within seconds, leading to constraints on the number of proofreading steps in TCR activation.

Despite its elegance, McKeithan's model could not be linked directly to experimental data and biological processes within the T cell so far. Especially the fast dephosphorylation rates, which ensure that the receptor is cleared immediately, are not realistic in a biological context. Slower dephosphorylation rates are problematic, because they lead to an accumulation of phosphorylated complexes and would reduce the specificity of TCR discrimination (cf. Equation 1.1). Additionally, even if activation of the TCR is in principle sequential, it does not exactly follow the scheme that McKeithan proposed. ZAP70 recruitment to the TCR stabilizes its phosphorylation, protecting it from the immediate dephosphorylation that is proposed by McKeithan. It is questionable if the two phosphorylation steps before recruitment are sufficient to generate the high specificity of T cell activation via kinetic proofreading alone.

Different models have been proposed that are based on the idea of McKeithan, but which are more closely related to the biology of actual TCR signaling [13, 23]. One example is a model that combines the kinetic proofreading scheme with a negative feedback that is based on the activation of SHP-1 during signaling [21]. Although this model is less abstract than other models and the used parameters seem to be realistic, it is not directly linked to data and the model features were only qualitatively compared to experimental data.

Taken together this makes the kinetic proofreading scheme proposed by McKeithan difficult to validate experimentally. There is still a need for models that incorporate the idea of kinetic proofreading but are biologically more realistic and are based on experimental data.

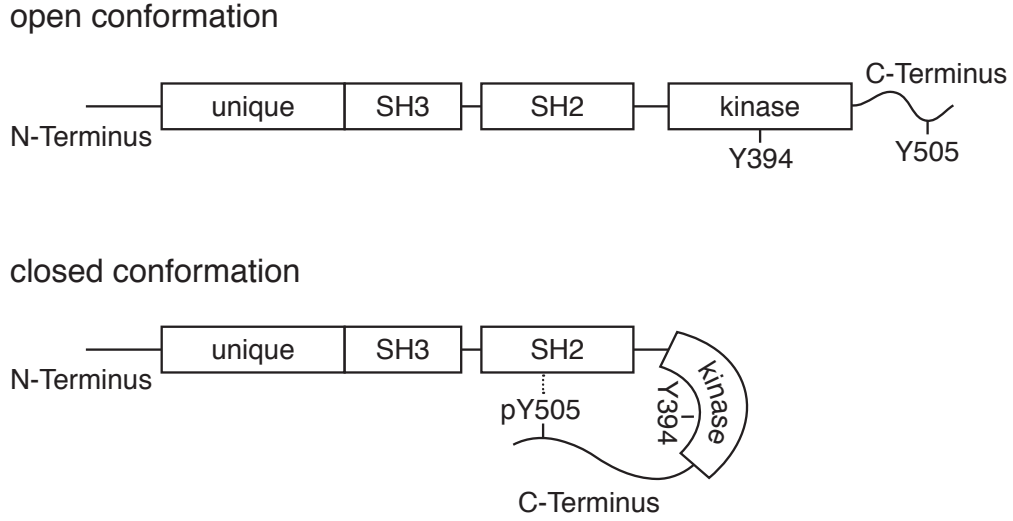


Figure 1.2.: Structure of the Src–family kinase Lck. The structure of Lck is similar to those of other SFKs. It consists of an N–terminal attachment site, a unique region, a Src–homology 3 (SH3) domain, an SH2 domain, a tyrosine kinase domain (also called SH1) and a C–terminal negative regulatory domain. Tyrosine residues 394 and 505 are important for the regulation of Lck activity. Lck is in a closed conformation when phosphorylated at the tyrosine residue 505.

## 1.2. Src-family kinase regulation

Members of the Src–family kinases (SFKs) are expressed in all human cell types. The SFKs found in T cells are Lck and Fyn [55]. Both are able to phosphorylate the ITAMs of the TCR and to some extend ZAP70. Since these are the first phosphorylations in the signaling cascade that are carried out, SFKs are considered to be the key kinases in early TCR signaling. Between the two, Lck is the more important kinase for TCR signaling than Fyn. Although Fyn is able to restore Lck function in T cells to a certain degree, TCR activation is mainly driven by Lck [65]. Hence, we focus on the regulation of Lck in this work.

All SFKs have similar structures and regulation mechanisms. The structure of Lck consists of an N–terminal attachment site, a unique region, a Src–homology 3 (SH3) domain, an SH2 domain, a tyrosine kinase domain (also called SH1) and a C–terminal negative regulatory domain [46, 8] (see Fig. 1.2).

Protein modifications (myristoylation and palmytoylation) at the N–terminus are important for the localization of Lck in the cell and enable the attachment of Lck to specific regions of the membrane [46]. The unique domain mediates interaction with the coreceptors CD8 and CD4 [46]. This interaction is important for the participation of Lck in TCR activation.

Interesting with regards to SFK activation are the phosphorylation sites of the kinase domain and the C-terminus. The kinase domain comprises an activating phosphorylation site at tyrosine residue 394 and facilitates kinase activity of Lck. The C-terminus holds a mostly inhibitory phosphorylation site at tyrosine residue 505. The phosphorylation of this tyrosine residue results in an interaction between the phosphorylated tyrosine and the SH2 domain, thereby promoting an inactive closed conformation of Lck [46] (compare Fig. 1.2). We will refer to this phosphorylation state of Lck as inhibited Lck. The closed conformation shields tyrosine residue 394 in the kinase domain from phosphorylation.

In order to become active, Lck has to be in an unphosphorylated (primed) state. The transition from the closed to the unphosphorylated open conformation of Lck is mediated by CD45 which dephosphorylates tyrosine 505. Lck is active as soon as it is phosphorylated at Y394 by trans-autophosphorylation. After this phosphorylation Lck retains its stable open conformation even if it is additionally phosphorylated at Y505. The single and double phosphorylated active state – as they are called by Nika et al. [45] – yield identical kinase activity. Unless indicated otherwise we will refer to the sum of single and double active Lck as active Lck in the following work.

While the phosphorylation of Y394 is always activating, the C-terminal tyrosine 505 is phosphorylated in the inhibited as well as the double active state of Lck. Nevertheless, Y505 is mostly referred to as the inhibiting phosphorylation site. Mutations of the equivalent phosphorylation site in Src (Y527) result in enhanced activity of Src [55]. This confirms the inhibitory role of that phosphorylation site.

The activity of Lck is dynamically regulated by reversible phosphorylation of the two tyrosine phosphorylation sites. The most important regulators are the phosphatase CD45 and the kinase Csk [46]. While CD45 controls the dephosphorylation of both the inhibitory and the activating phosphorylation site of Lck, the substrate of Csk is only the tyrosine residue 505. If the kinase activity of Csk is inhibited, Lck activation is enhanced and downstream targets are phosphorylated in the absence of TCR stimulation [60]. This shows an inhibiting influence of Csk but also implies a predominant availability of inhibitory Lck over double active Lck.

The substrates of Lck are ITAMs and ZAP70, but the initiation of these phosphorylation events upon TCR triggering are still debated (compare section 1.1). An important question in this regard is how the activation of Lck is regulated when the TCR is stimulated. There are contrary findings that either propose that the activation of Lck is not influenced by TCR triggering or that report massive local upregulation of Lck activity upon ligand binding. An antibody based measurement of global Lck levels in a cell reveals that around 40 % of Lck is constitutively active independent of TCR triggering [45]. This indicates that phosphorylation of the TCR might be influenced by local rearrangement of already active Lck and that the localization of Lck at the membrane is important for TCR activation. Indeed it is shown that clusters of Lck and TCR can be found at the membrane [57] after

TCR triggering. In a different measurement with a Lck biosensor that detects the open conformation of Lck [47] the constitutively active Lck levels were confirmed. This finding is contradicted by a different, more sensitive biosensor experiment that shows a local increase in active Lck after TCR stimulation [64].

### **1.2.1. CD45 is an important regulator of Lck activity**

One of the main regulators of the phosphorylation dynamics of Src-family kinases – including Lck – is the protein tyrosine phosphatase CD45 (cluster of differentiation 45) [46, 31]. CD45 is a membrane protein that is expressed in abundance on T cells and other hematopoietic cells [29, 3].

The function of CD45 is especially interesting because of the dual role it could have on Lck activation. It not only dephosphorylates the inhibitory phosphorylation at Y505, shifting inhibited Lck into the primed state and double active Lck into the single active state, but it also targets the other, activating phosphorylation site. Thereby it is able to regulate the transition from the double active and the single active state of Lck to the inhibitory and primed state, respectively. This dual role of CD45 makes it more difficult to predict the influence of CD45 on the regulation of Lck activation, it could have an activating as well as an inhibitory effect.

Although it is known that for Src the main target of CD45 is Y505 [56], this has not been shown specifically for Lck. This finding could suggest a more inhibitory role of CD45 on Src. But it might well be that dephosphorylation of Y505 results mostly in primed Src, which has neither an inhibitory nor an activating effect. The function of CD45 strongly depends how its negative and positive regulations are balanced [29] and most probably depends on T cell lineage and the developmental stage of a T cell [3].

A study that investigated the effect of different CD45 concentrations on Lck and TCR activation in mice showed that the sensitivity of the TCR depends on CD45 concentration and that the phosphorylation of both tyrosines of Lck were negatively correlated with the concentration of CD45 [41]. With high concentration only high affinity ligands were able to stimulate T cells, whereas T cells were much less sensitive to antigen affinity when CD45 concentration was reduced. This shows that CD45 plays an important regulatory role in Lck and TCR activation.

The trans-autophosphorylation of the activating phosphorylation site adds additional interesting dynamical behavior of Lck regulation and makes it more difficult to predict the behavior of Lck dynamics. This is demonstrated by the model of Src regulation by Kaimachnikov and Kholodenko that predicts bistable switching as well as oscillatory behavior depending on the parameterization of the model [32]. In this work we first adapt their dynamically interesting model by specifying it for the

regulation of Lck. We later use a model that makes less assumptions on underlying enzymatic processes than the model of Kaimachnikov and Kholodenko (which is phrased in terms of Michalis–Menten kinetics). In our model we take into account different localizations of Lck, where it is exposed to different concentrations of CD45 and total Lck. Thereby we are able to study the influence of CD45 regulation and trans-autophosphorylation in more detail.

### 1.3. Structure of this work

Our analysis is motivated by the finding of a sharp threshold response of the TCR that depends on the time an antigen is bound to the TCR. We were interested if this sharp threshold response can be explained by the mechanisms of early TCR activation, which include signal initiation, early signaling events and the regulation of kinase activity after TCR triggering. We investigated these questions in two parts. We first concentrated on the TCR triggering module and then analyzed the influence of Lck regulation on TCR activation.

Chapter 2 explains briefly the methods that we used in this work to estimate model parameters, with a focus on error estimation and the profile likelihood method.

We then introduce a model of early TCR signaling in Chapter 3. Here we develop first a model of basal TCR activation and estimate the model parameters from kinetic data. By extending the model we are able to investigate the relationship between the different signal propagation mechanisms and the kinetic proofreading behavior of the model.

Chapter 4 is dedicated to the analysis of the dynamic regulation of Src–family kinase Lck. The parameterization of the model is based on dose–response data of Lck phosphorylation. We are able to dissect the complex dynamics of Lck activity by means of its localization in the cell and the influence of kinases and phosphatases on Lck regulation.

## 2. Mathematical Methods

### 2.1. Modeling

Modeling biological processes is typically done by two different kind of models: a stochastic or a deterministic approach. Stochastic models are used for simulations of systems with high variability, mostly when only small numbers of molecules are modeled. On the other hand deterministic models may not account for the variability of a system but have the advantage to give an overview on the general dynamics of the model more easily. Additionally it is often less difficult to parameterize such a model by fitting it to experimental data. The models that we introduce in this work are all based on the deterministic modeling approach, hence we will give a short overview on this kind of modeling here. Often deterministic models are phrased in terms of a system of ordinary differential equations:

$$\dot{x}(t) = f(x(t), u(t), \theta)$$

normally  $f$  is given by rate equations and  $u(t)$  denotes the model input such as stimulation or perturbations. The model can be related to data by observables

$$y(t) = g(x(t), \theta)$$

typically these are superposition of states or even more complicated relationships of model states.

The rates of a mechanistic models often describe the kinetics of a biological process. The exact biological process normally is too complex to model explicitly and is always described in a simplified way in the models. Depending on the exact process different descriptions of the kinetics are used, two of the most widely used kinetic assumptions are mass action kinetics and Michaelis–Menten kinetics.

Mass action kinetics assume that the rate of a reaction is proportional to the concentration of the substrate or to the product of substrate concentrations for bimolecular reaction. It is the simplest kind of kinetic and is widely used for models of biological processes.

In contrast, Michaelis–Menten kinetics approximate an enzyme driven catalytic reaction where an enzyme binds a substrates that is then converted into the product and released from the complex. This enzyme kinetics assume that the enzyme–substrate complex is in rapid equilibrium, implying that only a fraction of the total substrate is bound and that there is much more substrate than enzyme. A notion that does not hold true in a lot of cases.

## 2.2. Parameter estimation and identifiability

One of our main goals in this work is to parameterize our models in a biological meaningful way. Mechanistic models often describe complex dynamics that highly depend on the parameterization of the model and can not easily be deduced from the model structure. Especially if an analytic solution can not be calculated. To analyze the model dynamics the parameters of the model have to be known or estimated from data. In most cases the parameters cannot directly be measured, here we will briefly describe how parameters are typically estimated from data.

In order to relate the model to the available experimental data, the model has to have an appropriate structure that is able to explain the data. We are then able to estimate the model parameters such as concentrations or rate constants from the data.

A widely used and well established method for the estimation of the parameters is the maximization of the log–likelihood function [20, 2], which is equivalent to a least-square minimization if the observed noise is normally distributed.

Then the log–likelihood function is defined as

$$\begin{aligned}
\log \mathcal{L}(\theta|D) &= \log \prod_i \frac{1}{\sqrt{2\pi}\sigma_i} e^{-\left(\frac{D_i - \theta_i}{\sqrt{2}\sigma_i}\right)^2} \\
&= \sum_i \log \left( \frac{1}{\sqrt{2\pi}\sigma_i} e^{-\left(\frac{D_i - \theta_i}{\sqrt{2}\sigma_i}\right)^2} \right) \\
&= \sum_i \log \left( \frac{1}{\sqrt{2\pi}\sigma_i} \right) - \sum_i \left( \frac{D_i - \theta_i}{\sqrt{2}\sigma_i} \right)^2 \\
&= \sum_i \left( \log \left( \frac{1}{\sqrt{2\pi}\sigma_i} \right) - \left( \frac{D_i - \theta_i}{\sqrt{2}\sigma_i} \right)^2 \right) \\
&= -\sum_i \log \sqrt{2\pi} - \sum_i \log \sigma_i - \frac{1}{2} \chi^2
\end{aligned}$$

with

$$\chi^2 = \sum_i \left( \frac{D_i - \theta_i}{\sigma_i} \right)^2$$

where  $\theta$  denotes a vector of model parameters,  $D_i$  denotes the observed data and  $\sigma_i$  is the measurement error.

In order to find the best-fit parameters of the model  $\log \mathcal{L}(\theta|D)$  has to be maximized. This is equivalent to minimizing  $\chi^2$ , given that  $\sigma_1$  is constant. In this work we always need to estimate the error of the data  $\sigma_i$  as well. Therefore we had to minimize

$$g(\theta) = \sum_i \log \sigma_i + \frac{1}{2} \chi^2(\Theta) = 2 \sum_i \log \sigma_i + \chi^2(\Theta) \quad (2.1)$$

where  $\theta$  is a vector that is comprised of the vectors  $\Theta$  and  $\sigma$ .

### 2.2.1. The profile likelihood approach

In this work we use the profile likelihood method [43, 69] to assess the uncertainty of our estimated model parameters as described in [52, 35].

Mechanistic models such as the models investigated in this work are typically nonlinear and confidence regions can have complex shapes. Therefore the nonlinear likelihood function is appropriate to use in such settings. [35]

Using the profile likelihood method we can analyze which possible values of a single model parameter are in statistical agreement with the available experimental data. Additionally the profile likelihood method can be used to calculate confidence intervals of the estimated parameters.

In principle we keep the parameter that we investigate fixed and re-fit the model for a series of parameter values.

In our case the profile likelihood PL as a function of these values  $p$  is then defined as

$$\text{PL}_j(p) = \min_{\theta \in \{\theta | \theta_j = p\}} g(\theta|D)$$

$g(\theta)$  is given in equation 2.1,  $D$  denotes the given experimental data and  $\theta_i, i \neq j$  is reoptimized.

On the basis of this we are able to estimate confidence intervals for the investigated parameter. The confidence interval CI is thereby defined by

$$\text{CI}_\alpha(\theta_j) = \{p \mid PL_j(p) \leq \min_\theta g(\theta|D) + \chi_{\alpha,1}^2\} \quad (2.2)$$

with  $\chi_{\alpha,1}^2$  denoting the  $\alpha$  quantile of the  $\chi^2$  distribution with one degree of freedom.

### 2.2.2. Prediction confidence intervals can be estimated by using the profile likelihood method

The estimation of confidence intervals for model predictions is a generalization of the profile likelihood method [11, 36]. Instead of investigating which parameters values are in statistical agreement with the data, we can also test which values of a model prediction are in statistical agreement with the measurements. Here we will introduce the prediction profile likelihood method as described in [36, 35].

For the classical calculation of prediction profile likelihoods the analytical solution is needed [25], which is not feasible for our models. Therefore we utilize the profile likelihood method to evaluate the uncertainties of the model prediction. In principle we re-fit the model while introducing a constraint for the prediction value instead of fixing a parameter like described above.

A prediction  $F$  could be any characteristic of the model. The corresponding prediction profile likelihood then is a function of different values  $z$  of the prediction:

$$\text{PPL}_F(z) = \min_{\theta \in \{\theta | F(\theta) = z\}} g(\theta|D)$$

the minimization is performed for the subset of parameters with model response  $F(\theta) = z$ . The corresponding confidence interval is obtained similar to Equation 2.2 and is defined as

$$\text{PCI}_\alpha(F) = \{z \mid \text{PPL}_F(z) \leq \min_\theta g(\theta|D) + \chi_{\alpha,1}^2\}$$

with  $\chi_{\alpha,1}^2$  denoting the  $\alpha$  quantile of the  $\chi^2$  distribution with one degree of freedom. The estimated confidence interval of the prediction is the set of values  $z$  for which PPL is below a threshold that is given by the  $\chi^2$  distribution.

In this work we analyzed the uncertainties of all parameters that we estimated and used the prediction profile likelihood method extensively in Chapter 3 to assess the uncertainties of our model predictions.



### **3. A mechanistic model of early T cell receptor signaling**

One of the core modules of T cell receptor (TCR) activation is the TCR signal triggering module as described by Acuto et al. [1]. It includes the phosphorylation of the immunoreceptor tyrosine-based activation motifs (ITAMs) and the recruitment of ZAP70 ( $\zeta$ -chain associated protein of 70 kDa) to the TCR complex followed by the activation of ZAP70 by sequential phosphorylation. The phosphorylation of the adapter molecule LAT (linker of activation) by ZAP70 marks the transition to another module of TCR activation which is described in [1] as the signal diversification and regulation module.

It is known that the decision whether the T cell is activated or not is made during the early events of TCR signaling [61]. However, the exact mechanism that is able to distinguish between different ligands is still debated. The kinetic proofreading theory – first presented by McKeithan in 1995 in the context of T cell activation [40] – is a promising mechanism to explain the observed threshold response. But up to date no experimental prove of this theory has been found. Here we focus on quantitative modeling of the early signaling events of TCR activation; especially we will demonstrate the kinetic proofreading capability of the model and will provide a mechanistic explanation for the sharp threshold response of the TCR to stimuli with only little difference in affinity.

We will first introduce a model describing the basal phosphorylation of the TCR in the absence of external TCR triggering. In the second part of the chapter we will include the effects of stimulation into the model and scrutinize the kinetic proofreading capabilities of the model. We will conclude the chapter by dissecting the impact of the different possibilities of signal transduction into the cell on the kinetic proofreading behavior.

#### **3.1. Modeling basal activation of the T cell receptor**

Without external stimulation T cells exhibit low phosphorylation levels of ITAMs and ZAP70. A fine balance of dephosphorylation and phosphorylation rates prevents the T cell from becoming activated, but maintains basal activation of the TCR that

builds the foundation of T cell activation upon ligand stimulation.

In this first part of the chapter we build a model of early signaling events that considers only basal activation. We use time-resolved data of basal T cell activation to parameterize our mechanistic model. The obtained parameter estimates will then be used in the second part of the chapter where we incorporate external TCR stimulation into the model.

### **3.1.1. Basal TCR activation is measured by stimulating T cells with the phosphatase inhibitor pervanadate**

#### **Triggering T cell activation**

T cell activation is triggered by external stimulation of the TCR. This shifts the phosphorylation of the TCR from its basal state to higher phosphorylation levels. In a living organism TCR activation is triggered by an encounter between the TCR and its specific ligand. Experimentally this can be achieved by either stimulation of the TCR with its specific antibody or unspecific TCR triggering. This kind of TCR triggering can be attained by using antibodies that bind to the CD3 unit of the TCR, usually together with antibodies for the coreceptors CD4, CD8 and/or CD28. Both – specific and unspecific TCR triggering – is supposed to initiate the usual activation mechanism of the TCR and first signs of activation (like calcium flux) can be measured within seconds after stimulation.

But T cells can also be activated by stimulating them with pervanadate, a strong and unspecific phosphatase inhibitor which inhibits 80-90 % of the phosphatase activity in the cell [42]. It thereby shifts the basal phosphorylation level to a higher state, by only decreasing dephosphorylation rates and without changing the kinase activity in the cell. Although with this method the TCR is not triggered directly, common characteristics of T cell activation like higher phosphorylation levels of several signaling molecules and calcium flux are observed. However, the time scale of activation is shifted from seconds to minutes compared to the more physiological stimulations.

Pervanadate stimulation allows us to decouple TCR activation from mutual binding events of ligands, by directly addressing phosphorylation kinetics in a controlled and consistent way. But it is of course not fully comparable to a more physiological stimulation and does not give insight into the mechanism of signal initiation. While the TCR is activated within seconds if stimulated with ligands, the activation by pervanadate takes minutes. It is nevertheless a very strong activation.

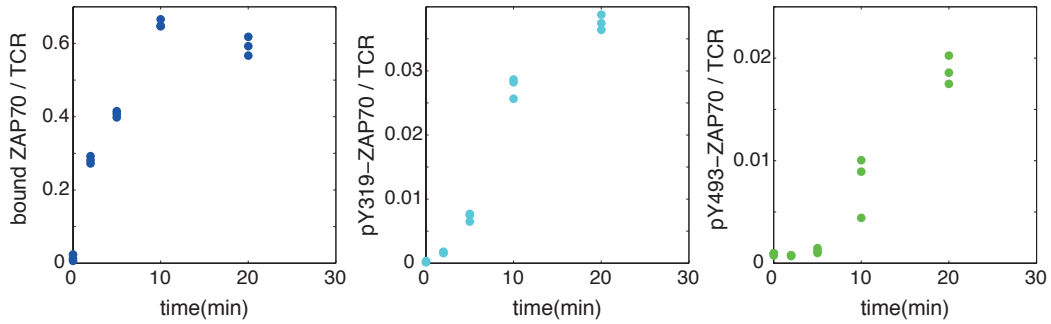


Figure 3.1.: Measurements of TCR activation kinetics. T cells have been stimulated with pervanadate and recruitment and phosphorylation of ZAP70 at different time points after stimulation have been measured. Bound ZAP70 (left panel) and phosphorylation of Y319-ZAP70 (middle panel) were measured in a multicolor IP-FCM experiment. The data of Y493-ZAP70 phosphorylation (right panel) was conducted by Western blot experiments. For each of the time points we have three replicates. (Experiments by S. Deswal and W. Schamel)

### IP-FCM and Western blot measurements reveal a hierarchy of activation

The data used in this part of the work are based on experiments conducted by Sumit Deswal from the laboratory of Wolfgang Schamel at the University of Freiburg and have been published in [18].

Our collaborators measured the kinetics of different early signaling events at the TCR, with a focus on the activation dynamics of ZAP70, following treatment with pervanadate using two experimental techniques.

Employing a multicolor IP-FCM approach, the experimentalists were able to quantify the amount of ZAP70 that is bound to the ITAMs, as well as the phosphorylation at interdomain B (at Y319) of bound ZAP70. We will refer to those measurements as bound ZAP70 per TCR and pY319-ZAP70 per TCR, respectively. The kinetics of the activating phosphorylation site at Y493 were measured using Western blot techniques. For all measurements data at time points 0, 2, 5, 10 and 20 minutes are available.

Multicolor IP-FCM, introduced by Deswal et al. [18], is a powerful and very quantitative measurement approach. Antibody (anti-TCR $\beta$ ) coupled beads are used for immunoprecipitation of the TCR complex at different time points after stimulation with pervanadate. Next, the probes are stained with differently fluorescent-labeled antibodies for ZAP70 and for pY319-ZAP70. The fluorescence intensity is then determined by flow cytometry. Additionally, the usage of quantibeads makes it possible to determine the absolute number of measured molecules per TCR. With this method quantitative measurements were obtained simultaneously of the amount of

ZAP70 bound to the TCR and the number of ZAP70 that is phosphorylated at Y319 per TCR at different time points. Thus, both data sets can be easily compared to each other.

Unfortunately, it was difficult to also measure the amount of ZAP70 phosphorylated at Y493 with IP-FCM. The phosphorylation at Y493 is necessary for ZAP70 to be fully activated and can be used as an indicator for active ZAP70. To obtain more information about the activation state of ZAP70 the amount of pY493-ZAP70 per TCR was measured in a Western blot experiment, again at time points 0, 2, 5, 10 and 20 minutes. Although this measurement is not as quantitative as IP-FCM it gives good additional indication on the activation kinetics of pY493-ZAP70. This data set was made comparable to the IP-FCM data sets by using additional data from the literature; a normalization procedure that is necessary for the estimation of the parameters and is explained in more detail in Section 3.1.3.

The measurements demonstrate a hierarchy of ZAP70 recruitment and activation (Fig 3.1). First ZAP70 is bound, then Y319–ZAP70 and later Y493–ZAP70 is phosphorylated. This hints at a sequential phosphorylation of ZAP70; an important finding that impacts the model set up discussed below.

In the next section we will describe a mechanistic model that was motivated by the measured data and incorporates the canonical knowledge of early signaling events. In Section 3.1.3 we use these measurements to parameterize the model.

### 3.1.2. A model of early events in TCR signaling

We develop a mechanistic model of basal activation of the TCR that is based on the early signaling events after T cell triggering at the level of the TCR. It consists of the following three main parts:

- Random phosphorylation of ITAMs
- Binding of ZAP70 to the double phosphorylated ITAMs
- Activation of ZAP70 by subsequent phosphorylation

The TCR contains ten ITAMs that are distributed among the different intracellular subunits of the TCR and are colocated in distinct pairs. Even though they might be phosphorylated at different rates in our modeling framework we assume that they are independent, and set up a model for one pair of ITAMs.

The complete scheme of the basal model is depicted in Figure 3.2 with all possible model states and transitions between those states. Each ITAM has two tyrosine residues that are phosphorylated by the Src-family kinase Lck with same rate but in no particular order upon TCR triggering. In the model this random phosphorylation

is described by the rate  $a_1$ , while  $b_1$  is the dephosphorylation rate of the ITAMs. The dephosphorylation is carried out by phosphatases like CD45, which is implicitly modeled by summarizing its concentration in the rate constants. An ITAM that is phosphorylated then serves as a docking site for the kinase ZAP70.

The structure of ZAP70 contains two SH2 domains that simultaneously bind to the two phosphorylated tyrosines of an ITAM. This binding event induces a conformational change in ZAP70 making it more accessible for kinases such as Lck. The recruitment of ZAP70 is described in the model by the binding rate  $k_{\text{on}}$  and the dissociation rate  $k_{\text{off}_1}$ . The kinase domain of ZAP70 is linked to the two SH2 domains by interdomain B which contains several phosphorylation sites (including tyrosine 319). The kinase domain of ZAP70 itself is activated by phosphorylation of Y493.

Although ZAP70 has several phosphorylation sites, only two of them are considered in the model. Tyrosine 319 in the interdomain B of ZAP70 is a critical regulator of T cell activity [19] and is phosphorylated by Lck. In the model phosphorylation and dephosphorylation of Y319 are characterized by the rates  $a_2$  and  $b_2$ , respectively. This phosphorylation stabilizes the open conformation of ZAP70, which is necessary for the subsequent phosphorylation of tyrosine 493. Y493 is localized in the kinase domain of ZAP70 and needs to be phosphorylated in order for ZAP70 to become active. Because ZAP70 has to be in an open confirmation it cannot be phosphorylated at Y493 before Y319 is phosphorylated. But once the second phosphorylation is established, the open conformation of ZAP70 is further stabilized and ZAP70 stays active even without Y319 being phosphorylated. This forms the possible signaling state (Y319–pY493–ZAP70) in the model.

We assume that the TCR-ZAP70 complex is much more stable when ZAP70 is phosphorylated, but could still dissociate. Therefore we introduce a second dissociation constant  $k_{\text{off}_2}$  in the model.

It was shown that phosphorylation of Y493 is mostly due to trans-autophosphorylation [39] of opposing ZAP70. Hence we develop a model of a pair of ITAMs as the minimum model. The phosphorylation of Y493-ZAP70 can only occur if ZAP70 is bound to both of the ITAMs and is at least phosphorylated at Y319. This trans-autophosphorylation is described in the model by the rate  $a_3$  and its reverse rate of dephosphorylation by the parameter  $b_3$ .

We assume that the pairs of ITAMs are independent from each other, for two reasons. First, studies on the individual contributions of different ITAMs in TCR activation are not conclusive yet and cannot quantify ITAMs that have a pronounced role in TCR activation [49]. Second, we are not able to distinguish between individual ITAMs based on the pervanadate data that we used. Therefore the smallest possible model that still might be able to explain the observed behavior of the TCR and that can be related to data is the one described.

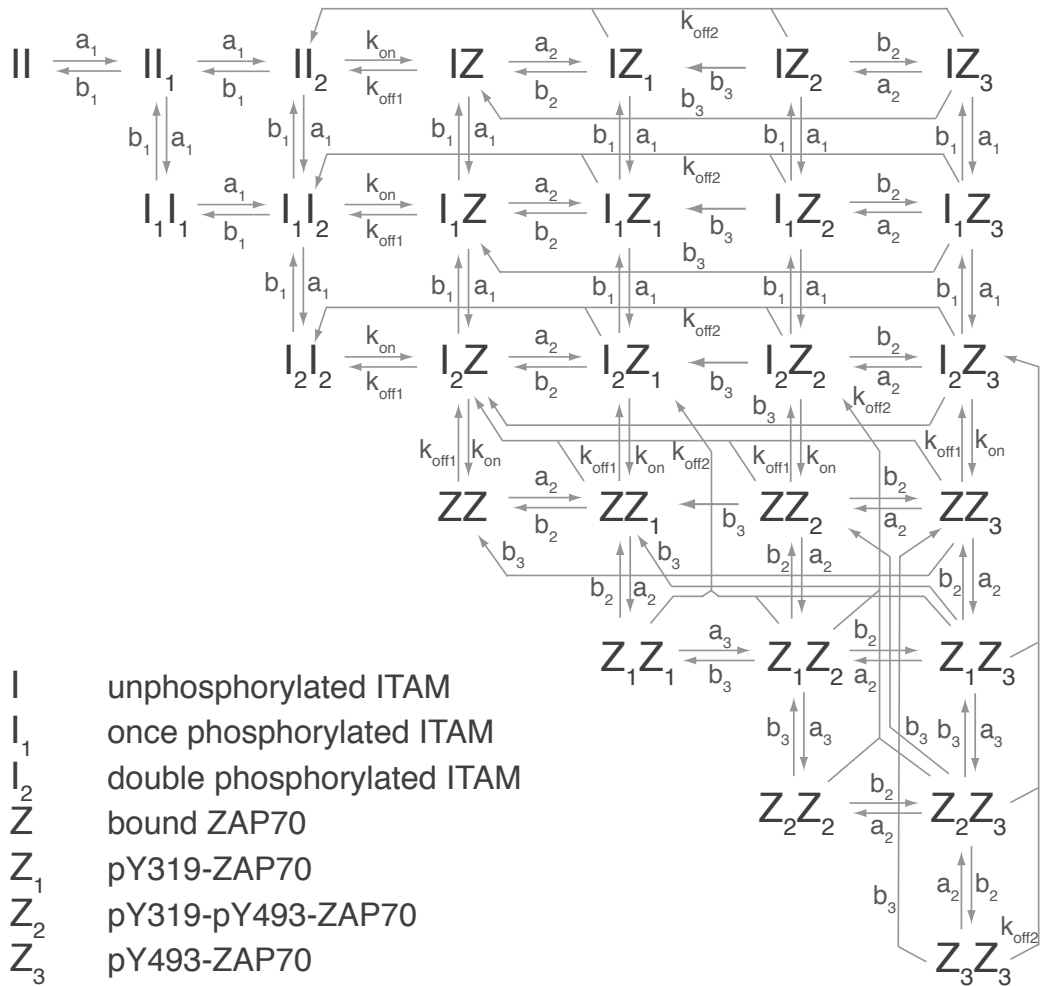


Figure 3.2.: Reaction scheme of the canonical model of basal T cell receptor signaling for a pair of ITAMs. The three modules of the model are ITAM phosphorylation, ZAP70 recruitment and the subsequent phosphorylation of ZAP70. Each ITAM can be in different states: unphosphorylated (I), phosphorylated once ( $I_1$ ) or twice ( $I_2$ ). ZAP70 only binds to double phosphorylated ITAMs (Z) and is then phosphorylated sequentially. First ZAP70 is phosphorylated at Y319 ( $Z_1$ ), then it is activated by trans-autophosphorylation at Y493 ( $Z_2$  and  $Z_3$ ) by an opposing phosphorylated ZAP70. The transitions between the states are indicated by arrows.

By combining all of the relevant signaling events we obtain 28 distinguishable states for a pair of ITAMs that are composed of all possible combinations of the seven signaling states for a single ITAM (Fig. 3.2). The corresponding system of ordinary differential equations that was developed using mass action kinetics can be found in Chapter A.1.1 of the appendix.

Typically, T cells have a much higher number of ZAP70 than of TCRs (compare Fig. 2C in [4]). For this reason we assumed an abundance of ZAP70 for the model. This entails that all of the rate constants are independent of the concentration of ZAP70 and have the dimension of one over time.

ZAP70 that is phosphorylated at either one or both of the tyrosines considered in the model (pY319-ZAP70, pY493-ZAP70 or pY319-pY493-ZAP70) is able to mediate trans-autophosphorylation. Even though ZAP70 is only fully active if phosphorylated in its kinase domain (at Y493) and thereby might be better capable to phosphorylate the opposing ZAP70, we cannot distinguish between those two possible rates based on the pervanadate data. Hence, we include a single rate for any trans-autophosphorylation into the model ( $a_3$ ).

Since we only have measurements for a certain subset of combined model states, we will see in the next section that the data give only limited information about the nine rate constants ( $a_1, b_1, k_{on}, k_{off_1}, a_2, b_2, a_3, b_3, k_{off_2}$ ) that connect the individual states.

### 3.1.3. Estimation of the basal rates from kinetic measurements

The nine rate parameters ( $a_1, b_1, k_{on}, k_{off_1}, a_2, b_2, a_3, b_3, k_{off_2}$ ) of our model have not been measured before, except for a measurement in 1995 by Bu et al. of the affinity of ZAP70 [10]. Therefore we aim to estimate these parameters from the kinetic data of bound ZAP70 and both phosphorylations of ZAP70 that is summarized in Figure 3.1. Since the measurements are obtained from stimulations with pervanadate, we can only estimate basal rates. The affinity measurements of Bu et al. [10] are later used for comparison with the estimated binding rate constant of ZAP70.

In order to fit the model to the data, we have to make assumptions on the efficiency pervanadate stimulation. Pervanadate reduces the activity of the phosphatases in the cell to 10 - 20 % [42]. In the model the pervanadate stimulation is described by the parameter  $p = 0.2$ , which is multiplied to all dephosphorylation rates ( $b_1, b_2$  and  $b_3$ ) of the model. This enables us to still estimate the individual dephosphorylation rates.

While the absolute number of bound ZAP70 per TCR and pY319-ZAP70 per TCR are available from the IP-FCM measurements, the data derived from the Western blot experiment are not as quantitative and are not directly comparable to the

IP-FCM data. Therefore, we can either estimate an additional scaling factor for these data or try to assess this factor from the literature. Attempting the first possibility by introducing an extra fitting parameter results in huge uncertainties in the fitted parameters, especially for the parameter that describes the rate of trans-autophosphorylation  $a_3$ . We find this rate to be nonlinearly dependent on the fitted scaling factor – a fact that cannot easily be seen directly in the model equations. Most of these fitting attempts result in a huge scaling factor and very small amounts of active ZAP70 in the model, which is biologically not plausible. Therefore we resort to the second option of fixing the scaling factor with data from Mallaun et al. [39] (Fig 1 and 2) and roughly estimate a 2-fold difference in pY319-ZAP70 and pY493-ZAP70. Accordingly we keep the scaling factor fixed for the remaining fitting procedure.

Western blot experiments are less accurate than measurements with IP-FCM. Therefore the margins of the errors vary widely between the data sets. For the fitting this means that data from the IP-FCM are weighted more. This is reasonable, because we would trust the more accurate experiment more. However in the present case the difference was so striking that the data for pY493-ZAP70 (Western blot experiment) almost got neglected in our fitting attempt. We decided to rather estimate the absolute error of each data by including the error into the objective function that we aim to minimize (as described in Chapter 2.2)

Time point zero in the data represents the equilibrium state of the TCR before pervanadate stimulation. The steady state of the model without pervanadate stimulation ( $p = 1$ ) is fitted to the measurements of time point zero of all three data sets.

The data of bound ZAP70 per TCR, pY319-ZAP70 per TCR and pY493-ZAP70 per TCR is described by the model in terms of the following observables:

$$\begin{aligned}\Theta_{1i} &= 5 \sum_{j=1}^{28} \varphi_j = \text{ amount of ZAP70/TCR at time point } i \\ \Theta_{2i} &= 5 \sum_{j=1}^{28} \eta_j = \text{ amount of pY319-ZAP70/TCR at time point } i \\ \Theta_{3i} &= 5 \sum_{j=1}^{28} \nu_j = \text{ amount of pY493-ZAP70/TCR at time point } i\end{aligned}$$

with  $\varphi_j, \eta_j, \nu_j \in (0, 1, 2)$  being the number of bound ZAP70, pY319-ZAP70 and pY493-ZAP70 in state  $x_j$  of the model, respectively.

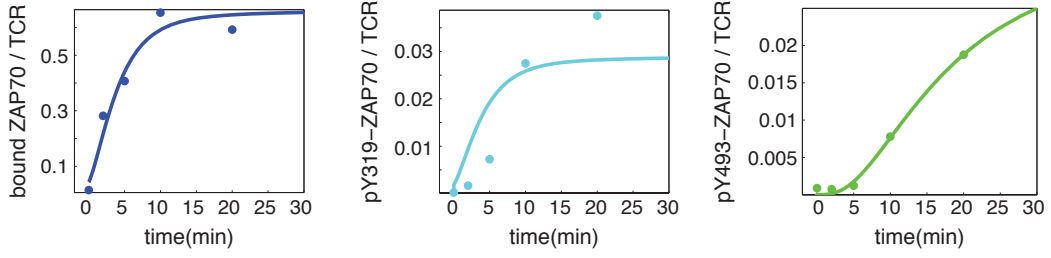


Figure 3.3.: The model (solid line) of basal TCR activation was fitted to the time course data of pervanadate stimulation experiments measured with IP-FCM and Western blot (right panel). (Experiments by S. Deswal and W. Schamel)

Thus we had to minimize the objective function

$$f(\vec{p}) = 2 \cdot 5 \sum_{j=1}^3 \log \sigma_i + \chi^2,$$

where the first term of the right hand side is due to the estimation of the errors (compare Chapter 2.2) and

$$\chi^2 = \sum_{i=1}^5 \left( \frac{D_{1i} - \Theta_{1i}}{e_1} \right)^2 + \sum_{i=1}^5 \left( \frac{D_{2i} - \Theta_{2i}}{e_2} \right)^2 + \sum_{i=1}^5 \left( \frac{D_{3i} - \Theta_{3i}}{e_3} \right)^2.$$

Here  $D_{1i}$  denotes the measured ZAP70,  $D_{2i}$  pY319-ZAP70 and  $D_{3i}$  pY493-ZAP70 per TCR at time points  $i = 0, 2, 5, 10, 20$ , and  $e_i$  are the estimated errors.

For the parameter estimation we used the simplex based algorithm *fminsearch* from the software MathWorks MATLAB. The resulting best fit is shown in Figure 3.3. We capture the overall behavior of the data well, especially the data of bound ZAP70 per TCR and pY493-ZAP70 per TCR are nicely reproduced by the model.

The estimated parameters of basal TCR activation are summarized in Table 3.1. The basal dephosphorylation rates  $b_1$  and  $b_2$ , that describe dephosphorylation of the ITAMs and pY319-ZAP70, respectively, are fast. Whereas the corresponding phosphorylation rates are estimated to be slow. A behavior that is expected for the basal rates of TCR activation since the TCR needs to be kept in a more or less unphosphorylated state before it gets activated. Slow phosphorylation and fast dephosphorylation rates ensure that this is the case, and that the TCR is not activated by accident. In contrast, the dephosphorylation of pY493-ZAP70 ( $b_3 = 4 \times 10^{-5}$ ) as well as the dissociation rate of phosphorylated ZAP70 ( $k_{\text{off}_2} = 0.002$ ) are estimated to be very slow. This might ensure that ZAP70 stays in its active state once it is fully activated.

parameter	estimated value	confidence interval
ITAM phosphorylation ( $a_1$ )	$0.002 \text{ s}^{-1}$	$[0.0007, \infty]$
ITAM dephosphorylation ( $b_1$ )	$0.025 \text{ s}^{-1}$	$[0.005, \infty]$
binding of ZAP70 ( $k_{\text{on}}$ )	$2.96 \text{ s}^{-1}$	$[0.0004, \infty]$
dissociation of ZAP70 and ITAM ( $k_{\text{off}_1}$ )	$3.73 \text{ s}^{-1}$	$[0.001, \infty]$
phosphorylation of Y319-ZAP70 by Lck ( $a_2$ )	$0.29 \text{ s}^{-1}$	$[0.004, \infty]$
dephosphorylation of Y319-ZAP70 ( $b_2$ )	$31.4 \text{ s}^{-1}$	$[0.47, \infty]$
trans-autophosphorylation of Y493-ZAP70 ( $a_3$ )	$0.36 \text{ s}^{-1}$	$[0.15, \infty]$
dephosphorylation of Y493-ZAP70 ( $b_3$ )	$4 \times 10^{-5} \text{ s}^{-1}$	$[0, \infty]$
dissociation on phospho-ZAP70 and ITAM ( $k_{\text{off}_2}$ )	$0.002 \text{ s}^{-1}$	$[0, \infty]$
estimated error for first data set ( $e_1$ )	0.051	$[0.03, 0.21]$
estimated error for second data set ( $e_2$ )	0.008	$[0.003, 0.02]$
estimated error for third data set ( $e_3$ )	0.0005	$[0.003, 0.001]$

Table 3.1.: Best fit parameters as estimated from fitting the model to the pervanadate stimulation data. For each parameter the best fit value is given as well as the estimated 95%-confidence interval.

### Profile likelihoods show one-sided parameter bounds

The uncertainties of the estimated parameters are analyzed by calculating the respective profile likelihoods as described in Chapter 2.2.1. The profile likelihoods are shown in Figure 3.4 together with the threshold for  $\chi^2_{95\%}$  (solid red line) and  $\chi^2_{90\%}$  (dashed red line). The quantified confidence intervals from the shown profile likelihoods are given in Table 3.1.

Since our model is quite detailed and part of the model states are not covered by the data, none of the estimated rate constants is fully identifiable. But we find lower bounds for all phosphorylation rates ( $a_1$ ,  $a_2$  and  $a_3$ ), for the dephosphorylation rates of the ITAMs and pY319-ZAP70 ( $b_1$  and  $b_2$ ), for the binding rate of ZAP70 ( $k_{\text{on}}$ ) and for the dissociation rate of unphosphorylated ZAP70 ( $k_{\text{off}_1}$ ). Our analysis shows that all of these reactions have to happen with a certain minimal rate, but could also be much faster.

The other two rate constants of the model ( $b_3$  and  $k_{\text{off}_2}$ ) are estimated to be very small. The dephosphorylation rate of pY493-ZAP70  $b_3$  is even practically zero. Because both of these rates are small, ZAP70 is kept in its active form once it is fully activated. In the case of the dissociation rate this could be explained by the open conformation of phosphorylated ZAP70, which could stabilize the ITAM-ZAP70 interaction. However, the data do not support an upper bound of the 95%-confidence interval for both rates. Even though the fit becomes worse for higher rates, the change in  $\chi^2$  is not significant.

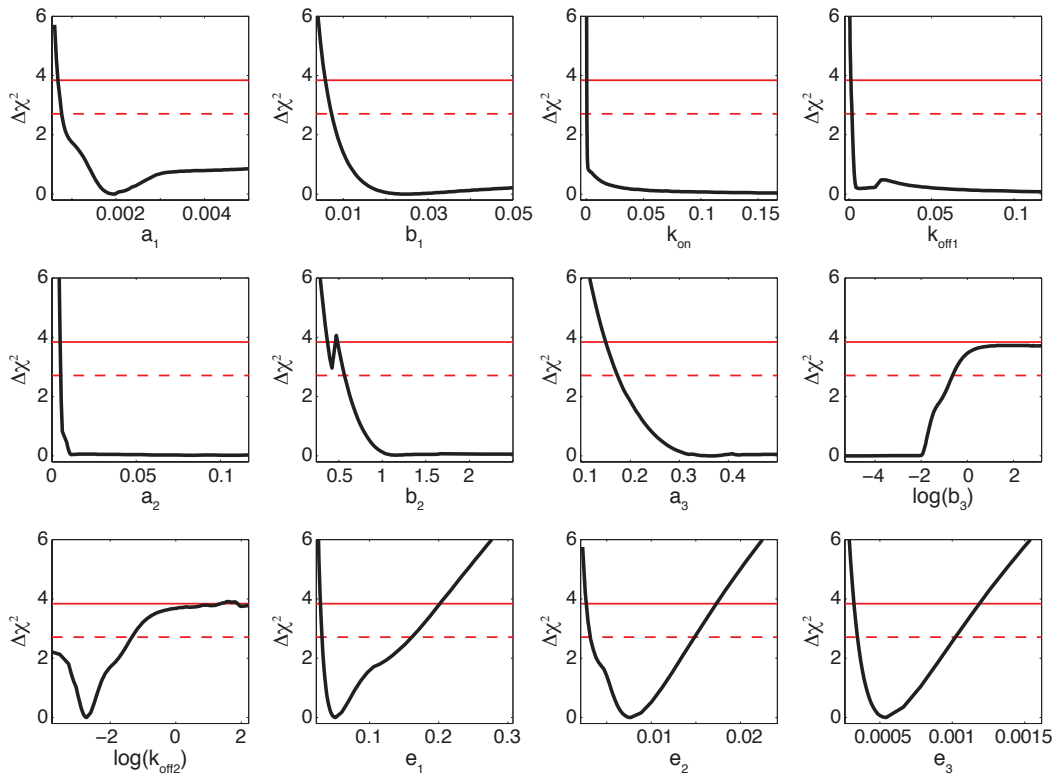


Figure 3.4.: Profile likelihoods of the best fit parameters. For each estimated parameter the corresponding profile likelihoods have been calculated. The rate constants all have either a lower or upper bound. The errors for the three data sets have been estimated with narrow confidence bounds. The threshold for  $\chi^2_{95\%}$  and  $\chi^2_{90\%}$  are marked for each profile in red by the solid and the dashed line, respectively.

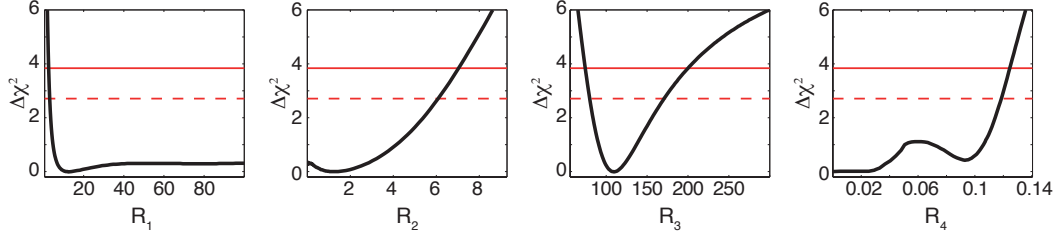


Figure 3.5.: Profile likelihoods for the ratios  $R_1 = b_1/a_1$ ,  $R_2 = k_{\text{off}_1}/k_{\text{on}}$ ,  $R_3 = b_2/a_2$  and  $R_4 = b_3/a_3$  of model parameters. Only the ratio  $R_3$  is fully identifiable. The other ratios have one-sided bounds.

The estimation of the errors for each of the three data set is justified by the profile likelihoods. All three errors are well defined, have narrow bounds and correspond well to the scale of each data set.

We can compare the binding rates of ZAP70 to measured data from Bu et al. [10]. The authors measured the affinity  $K_d$  of ZAP70 by surface plasmon resonance and found a  $K_d$  of 21.4 nM and an association rate of  $k_a = 6.0 \times 10^6 \text{ M}^{-1}\text{s}^{-1}$ . This results in

$$k_{\text{off}} = K_d k_a = 0.128 \text{ s}^{-1}$$

which is smaller than our best fit value for  $k_{\text{off}_1}$  but is well inside the confidence interval of the estimated parameter. Additionally it is difficult to compare the measured value directly because in our model we have a second off-rate for the phosphorylated ZAP70.

### Analysis of parameter ratios

Dependencies between parameters can be the reason why individual parameters are not fully identifiable. In our model, strong dependencies are expected between the phosphorylation and dephosphorylation rates of reversible phosphorylation events as well as between the rates of ZAP70 binding and dissociation. Taking the best fit parameters, we can calculate the following ratios which we hypothesized to have a lower relative uncertainty than the individual rates:

$$\begin{aligned} R_1 &= \frac{b_1}{a_1} = 12.5 & R_2 &= \frac{k_{\text{off}_1}}{k_{\text{on}}} = 1.26 \\ R_3 &= \frac{b_2}{a_2} = 108.3 & R_4 &= \frac{b_3}{a_3} = 0.0001 \end{aligned}$$

To test this hypothesis we re-parameterize the model in terms of these ratios and

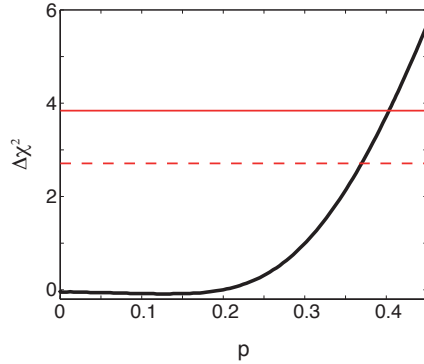


Figure 3.6.: The influence of the assumed pervanadate efficiency on the fitting results analyzed by means of the profile likelihood method. Parameter  $p$  describes the reduction of dephosphorylation upon pervanadate stimulation.

compute the corresponding profile likelihoods (Figure 3.5). For the ratios  $R_1, R_2$  and  $R_4$  we again find one sided bounds, whereas the ratio  $R_3 = b_2/a_2$  is now fully identifiable.

Furthermore, we can draw the following conclusions from the results. We find that  $R_1 > 1$  and also  $R_3 \gg 1$ , indicating that  $b_1 > a_1$  and  $b_2 \gg a_2$ . Like we expected for basal rates, the dephosphorylation has to be faster than the phosphorylation. Although we already found this result for the best fit, it was not clear before that this is always the case for all parameter values that are in accordance with the data. The calculation of  $R_2$  did not help to infer more information about ZAP70 recruitment. The 95% -confidence interval is quite wide and  $R_2$  could be greater as well as smaller than 1.

In contrast to the other ratios the upper limit for the ratio  $R_4$  is  $< 1$ . This implies that phosphorylation of Y493 is faster than its dephosphorylation. This finding indicates that after ZAP70 is phosphorylated at Y319, the activation of the TCR is stabilized by fast and stable activation of ZAP70.

### The influence of simulating pervanadate stimulation on the parameter estimation

We want to evaluate the influence that the efficiency of pervanadate inhibition (which we fixed to be 80 % according to [42]) has on the parameter estimation. This efficiency of pervanadate is expressed in the model by the parameter  $p = 0.2$  that was multiplied to all dephosphorylation rates to simulate pervanadate stimulation. We can analyze the influence of  $p$  on the fit by using the profile likelihood method. The observed change in our  $\chi^2$ -function in dependence on  $p$  is shown in Figure 3.6.

The efficiency of pervanadate has been measured to be 80% - 90% by Mikalsen et al. [42]. The calculated profile likelihood reveals that we can find a good fit that is in accordance with the data for values of  $p$  between 0 and 0.4 which translates into a range of full to 60% efficiency of pervanadate. The best fit was obtained for a value of  $p = 0.13$  with only marginal better  $\chi^2$  than for  $p = 0.2$ , the value we used in all of the calculations.

## 3.2. Ligand binding can induce kinetic proofreading

The sharp threshold response of the TCR after ligand binding is highly discussed in recent literature [39, 14, 15], but the exact mechanisms remain unresolved. It has been hypothesized that one of the mechanisms responsible for this unique feature of the TCR might be the kinetic proofreading mechanism, that was introduced by McKeithan [40], and is described in Section 1.1.4 of the introduction. The rather abstract concept of kinetic proofreading has not yet been phrased in terms of a physiological meaningful way and, thus, could not be proven experimentally. Instead of writing down yet another model with build-in kinetic proofreading, we introduce a biologically more meaningful mechanistic model and test it for its kinetic proofreading capabilities. For this purpose the model of basal TCR activation was extended by the ability to bind ligand. We then simulated the activation of the TCR and analyzed the ability of the model to distinguish between ligands with different TCR affinities in terms of its kinetic proofreading capabilities.

### 3.2.1. Adding ligand binding to the basal model

The model described in the previous section together with the estimated basal parameters was used to further analyze early TCR signaling events. To investigate the kinetic proofreading capabilities of the model we need to incorporate activation by ligand binding into the existing model of basal TCR activation.

We expand the existing model by assuming that a ligand is able to bind to the TCR independent of its basal state. Specifically, this means that a ligand can bind to any of the 28 states of the basal model. This is different from the McKeithan model, where it is assumed that ligands only bind to TCRs that are unphosphorylated. The model expansion results in twice as many states, because every already existing state of the basal model can now be in a ligand bound or unbound state (see also Fig. 3.7).

The addition of model states with bound ligands also introduces new model parameters. We now have to take into account the binding rate of the ligand and the dissociation rate of ligand and TCR. Both cannot be estimated from the per-

vanadate stimulation experiments described in Chapter 3.1.1. But we know typical ligand affinities and their dwell times from the literature.

To model the effect of ligand binding on TCR activation, we have to know how the ligand–TCR interaction influences the phosphorylation levels of the TCR. There are different theories on how signaling is initiated [68] (compare Chapter 1.1.3), which postulate either enhanced phosphorylation or decreased dephosphorylation of the TCR. First, Lck could be recruited to the TCR because of its association with the coreceptors CD4 and CD8 (aggregation model). A different mechanism that would also enhance the phosphorylation rate is a conformational change of the TCR upon ligand binding which makes the ITAMs more accessible for Lck. Both mechanisms would enhance the rate in which the ITAMs and potentially ZAP70 are phosphorylated. The other possibility is a decrease in phosphatase activity. Upon ligand binding the phosphatase CD45 might be pushed out of the region of TCR activation due to its large extracellular tail (segregation model). As a result local phosphatase activity would be reduced. Independent of the exact mechanism of these different possibilities, they would all yield higher overall phosphorylation levels after ligand binding.

Since there is evidence for all of these theories we did not want to base the model on a single theory, but rather systematically test various theories with respect to the kinetic proofreading capability of the model. Therefore we introduced two additional parameters that scale either the rates of basal phosphorylation (parameter  $\alpha$ ) or dephosphorylation (parameter  $\beta$ ) when parameter is bound. Both parameters are chosen to simulate a change in the enzymatic activity of up to 100-fold.

The binding and the dissociation rates of ZAP70 are assumed to be unaffected by ligand binding. This means that the estimated rates can be used for the ligand bound and unbound situations.

The full model that now includes ligand binding is shown in Figure 3.7. The upper right part of the figure illustrates again the basal model and the lower left part depicts the ligand bound states of the model. As before the model is based on mass action kinetics; the corresponding system of ordinary differential equation is given in Chapter A.1.2 of the appendix. Although the full model has twice as many states (56) as the basal model, there are only four additional parameters (ligand binding  $l_{\text{on}}$  and dissociation  $l_{\text{off}}$ , and the factors  $\alpha$  and  $\beta$ ). However none of these parameters are known or could be estimated from the existing data.

Kinetic proofreading has the characteristic feature that the activation of the TCR depends on the time that a ligand is bound to the TCR. We want to analyze if our model possess the same characteristic. The dwell time of the ligand is directly related to the dissociation rate  $l_{\text{off}}$  and is defined as

$$d = \frac{1}{l_{\text{off}}}.$$

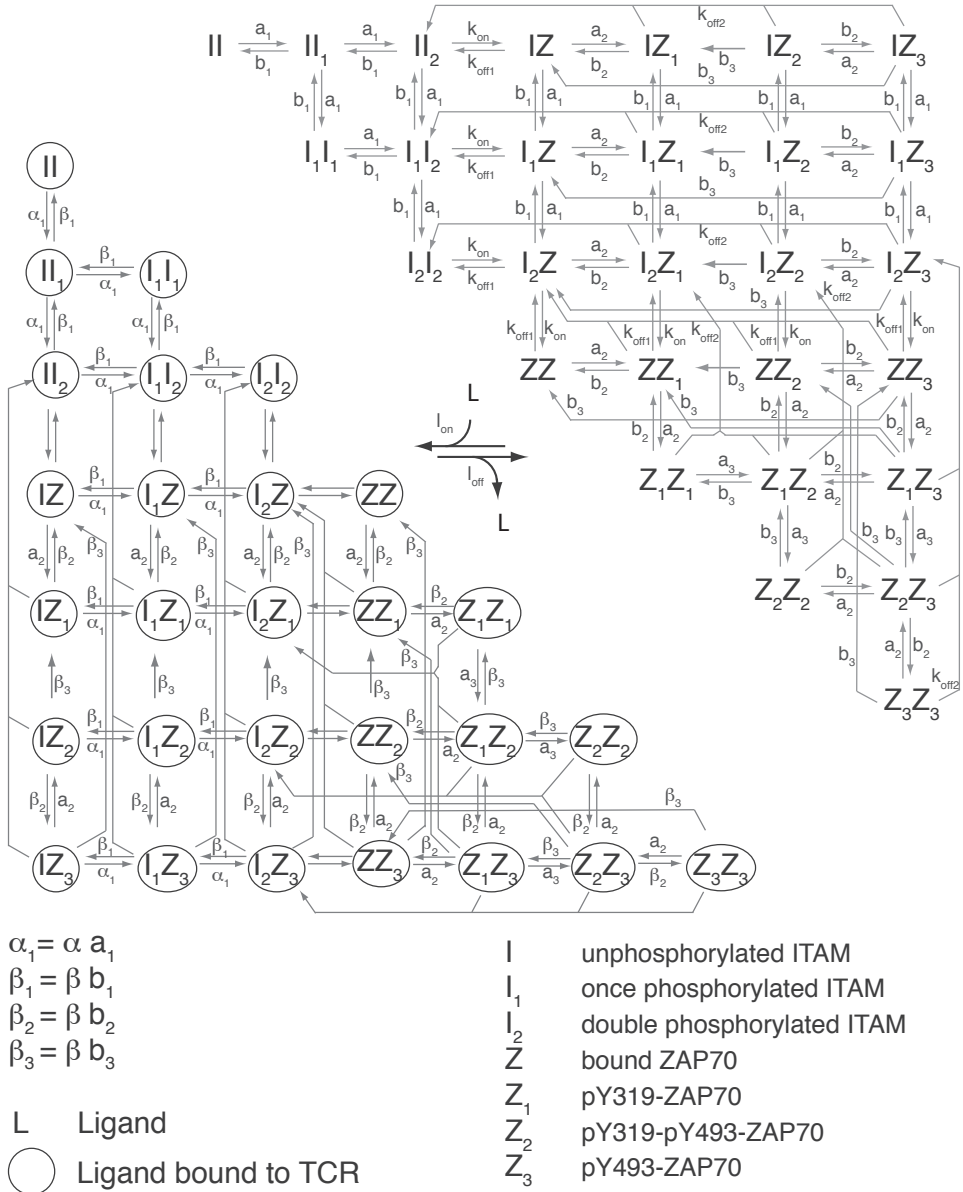


Figure 3.7.: The canonical model of T cell receptor activation. Only the signaling at the TCR level is included in the model. The three important parts of the model are ITAM phosphorylation, ZAP70 recruitment and the subsequent phosphorylation of ZAP70. Ligand can bind to the TCR in any of its signaling states. Upon Ligand binding phosphorylation is enhanced by the factor  $\alpha$  and phosphatase activity is decreased by factor  $\beta$  as indicated in the scheme.

The longer the dwell time of the ligand, the stronger is the signal at the end of the signaling cascade that is initiated by the ligand. A typical dwell time of a high affinity ligand is assumed to be around 2 seconds [44, 75].

In our model, signaling ends with the activation of ZAP70 (pY493-ZAP70 and pY319-pY493-ZAP70). This is defined in the model as follows

$$\text{active ZAP70/TCR} = 5 \sum_{j=1}^{56} \nu_j$$

with  $\nu_j \in (0, 1, 2)$  being the number of phosphorylations at Y493 in state  $x_j$  of the full model.

In the following simulations we always use active ZAP70 as the indicator of TCR activation. If not stated otherwise, we assume a ligand occupancy of around 10% for all our model simulations. This corresponds to a ligand affinity

$$K_d = \frac{l_{\text{off}}}{l_{\text{on}}} = 10$$

By defining the dwell time and the  $K_d$  of the ligand, we can fix two of the unknown parameters of the extended model. For the simulations we will systematically vary the dwell time of the ligand and thereby define  $l_{\text{off}}$ . Together with a constant  $K_d = 10$  this also fixes the rate of ligand binding  $l_{\text{on}}$ .

### 3.2.2. Regulated kinase access or phosphatase exclusion can trigger TCR signaling

The TCR is not able to transmit the information of a bound signal to its intracellular units by itself. Therefore the binding of a ligand to the TCR has to affect the phosphorylation of the ITAMs by other means. The different mechanisms of signal propagation [68] that we introduced in Chapter 1.1.3 result in two apparent possibilities, the regulation of kinase access to the ITAMs or phosphatase exclusion from the TCR. Here, we use the full model of TCR signaling to independently test how the two mechanisms of TCR triggering influence its activation. We will first explain how kinase access can be regulated and how this mechanism influences the model simulations. We then have a closer look at the mechanism of phosphatase exclusion.

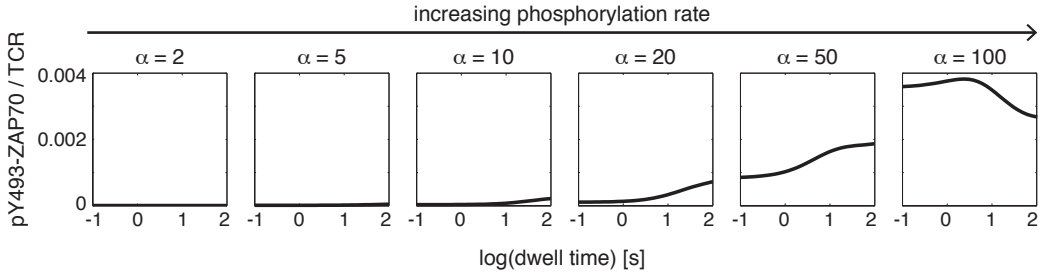


Figure 3.8.: The influence of kinase accessibility on TCR triggering. The amount of active ZAP70 is shown as a function of ligand dwell time for different values of the phosphorylation enhancement factor  $\alpha = 2, 5, 10, 20, 50, 100$ . Fast phosphorylation rates only result in a slight increase in the amount of active ZAP70 and is independent of the dwell time. An enhancement of phosphorylation rates on its own is not sufficient for a kinetic proofreading behavior of the TCR.

### Regulated kinase access

The ITAMs of the TCR are phosphorylated by the Src-family kinase Lck. The access of Lck to the TCR can be regulated by different means.

First, Lck normally is attached to the membrane, but can also be bound to the coreceptors CD4 or CD8, depending on the type of T cell. These coreceptors have a binding site for MHC. If peptide loaded MHCs are recognized by the TCR and a pMHC–TCR complex is formed, the coreceptor will also bind to the pMHC and thereby move into close proximity of the TCR complex. Lck that is bound to the coreceptor intracellularly will automatically be recruited to the ITAMs and is able to better phosphorylate them. This is generally called the kinase aggregation model.

Second, there is evidence that the TCR undergoes a conformational change when ligands bind to it. This could either happen because of dimerization of TCRs or pulling forces on the TCR. In both cases a conformational change would give rise to more accessible ITAMs. Since Lck is always active in T cells [45] it has better access to the ITAMs as soon as the conformation of the TCR changes, and higher phosphorylation levels of the TCR and the following signaling steps can be achieved.

Our model is not able to differentiate between both mechanisms. However, we are able to simulate the higher phosphorylation rates that are implied by any of the two possibilities with our model (parameter  $\alpha$ ). The enhanced kinase activity was simulated for eight different values of  $\alpha$ . Independently, we varied the dwell time of the ligand, while keeping the ligand affinity and the ligand occupancy constant. For each simulation we calculated the steady state of the model at different dwell times and analyzed the amount of active ZAP70.

Each graph in Figure 3.8 shows one simulation and is marked with the value of  $\alpha$  that

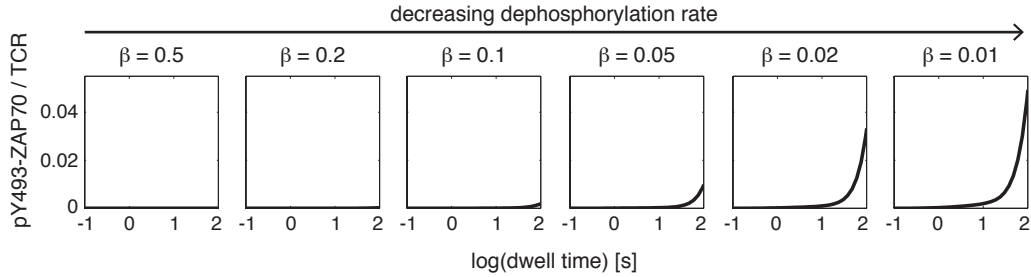


Figure 3.9.: The influence of phosphatase exclusion on TCR triggering. The amount of active ZAP70 is shown as a function of ligand dwell time for different values of decreasing phosphatase set by the factor  $\beta = 0.5, 0.2, 0.1, 0.05, 0.02, 0.01$ . Decreased dephosphorylation rates together with long dwell times result in higher amounts of active ZAP70. The activation of ZAP70 is dependent on the dwell time which could indicate kinetic proofreading behavior.

was used. The figure shows how the activation of ZAP70 could depend on the dwell time and the increasing phosphorylation rate. The more the phosphorylation rate is increased, the more active ZAP70 can be found. But the amount of pY493-ZAP70 hardly depends on the dwell time since the rise in active ZAP70, if there is any, exists already for small dwell times. Although we find a change of ZAP70 activation depending on  $\alpha$ , the highest amount of active ZAP70 is still very small ( $\sim 0.004$  pY493-ZAP70 per TCR) compared to the possible number of ten pY493-ZAP70 per TCR.

### Phosphatase exclusion

The TCR could also be activated by excluding phosphatases from the area of triggering. This would also shift the phosphorylation of ITAMs and ZAP70 to higher levels.

The main phosphatase that regulates dephosphorylation of the TCR is the trans-membrane protein CD45. It has a large extracellular tail compared to the size of the TCR. This ectodomain of CD45 is even larger than the TCR–pMHC complex that forms when the TCR recognizes its specific ligand. In the phosphatase exclusion model it is assumed that CD45 has not enough room in the proximity of the TCR–pMHC complex and is pushed out of that region by physical forces. This in turn prevents CD45 from dephosphorylating the TCR. In our model the resulting decreased dephosphorylation rates after ligand binding are modeled by the parameter  $\beta$ .

We again analyze how the amount of active ZAP70 per TCR depends on the dwell time of the ligand for eight different values of  $\beta$ . The result of these calculations is

shown in Figure 3.9. Decreased dephosphorylation rates result in increased amounts of active ZAP70. But in contrast to the previous calculations for varying phosphorylation rates, the signal also depends strongly on the dwell time of the ligand. For bigger values of  $\beta$  the simulation shows very low amounts of pY493-ZAP70 for short dwell times but higher amounts of active ZAP70 for longer dwell times. Also here, we find that the level of active ZAP70 ( $\sim 0.05$  pY493-ZAP70 per TCR) is still very low when compared to the maximum number of ten pY493-ZAP70 per TCR. It is questionable if any of these simulated low levels of ZAP70 would be able to activate the cell.

The dependence of a signal on the ligand dwell time, while the occupancy of the receptor is constant is the hallmark of kinetic proofreading [40]. Using this criteria we find noteworthy proofreading capabilities only in the case of phosphatase exclusion. However, the overall amount of active ZAP70 remains quite low in all our calculations. We will see in the next chapter that this discrepancy might be resolved by allowing phosphatase exclusion and regulated kinase activity to act together.

### **3.2.3. Kinetic proofreading requires a synergistic effect of enhanced phosphorylation and reduced dephosphorylation**

Since regulated kinase activity and phosphatase exclusion can act independently of one another, both mechanisms could in principle occur simultaneously in the cell. Here we test the influence of a combination of both mechanisms on the activation of the TCR and its kinetic proofreading abilities.

To this end we systematically vary the phosphorylation enhancement factor  $\alpha$  and the dephosphorylation reduction factor  $\beta$ . The simulation is carried out for all possible combinations of  $\alpha = 1, \dots, 100$  and  $\beta = 1, \dots, 0.01$ , resulting in 10000 tested combinations. Like before we are interested in the amount of active ZAP70 per TCR (in steady state) as a function of the dwell time.

Especially we want to investigate in which cases the activation of the TCR is dependent on the dwell time of the ligand, thereby giving rise to kinetic proofreading behavior. For this purpose we introduce a measure of kinetic proofreading by calculating the difference of active ZAP70 at dwell times 0.1 s and 100 s

$$\Delta pY493-ZAP70/TCR = pY493-ZAP70/TCR(100s) - pY493-ZAP70/TCR(0.1s)$$

An example on how  $\Delta pY493-ZAP70/TCR$  is calculated is shown in Figure 3.10 A for one of the simulated parameter combination ( $\alpha = 65$  and  $\beta = 0.015$ ). Like in the previous section, the steady state of active ZAP70 is plotted against different ligand dwell times. For this particular parameter set a strong dependency of the signal on the dwell time is found, indicating kinetic proofreading behavior.

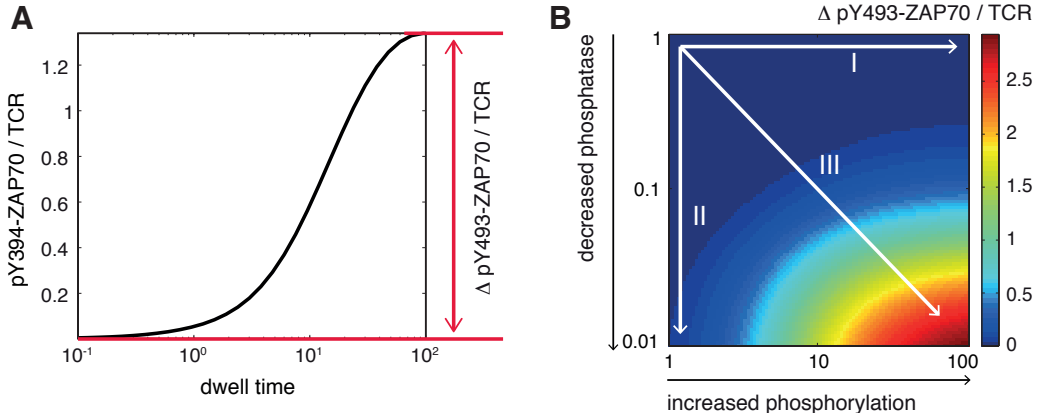


Figure 3.10.: Kinetic proofreading requires a synergistic effect of increased kinase and decreased phosphatase activity. (A) Kinetic Proofreading is measured as the difference in the amount of active ZAP70 ( $pY394\text{-ZAP70}$ ) per TCR at ligand dwell times of 0.1 s and 100 s. The example for  $\alpha = 65$  and  $\beta = 0.015$  shows that kinetic proofreading is possible. (B) The different kinetic proofreading abilities of the model are demonstrated by systematically varying the influence of  $\alpha$  (enhanced phosphorylation upon ligand binding) and  $\beta$  (decreased dephosphorylation upon ligand binding). We do not find kinetic proofreading behavior when only phosphorylation is increased (I;  $\alpha > 1$  and  $\beta = 1$ ) or when the dephosphorylation alone is decreased (II;  $\beta < 1$  and  $\alpha = 1$ ) (compare also Section 3.2.2). Kinetic proofreading is found when ligand binding induces increased phosphorylation as well as decreased dephosphorylation (III).

The measure  $\Delta pY493\text{-ZAP70}/TCR$  compares the low level of active ZAP70 at a short dwell time to the higher level of  $pY493\text{-ZAP70}$  at a long dwell time. We choose these dwell times because typical ligand dwell times should lie within this interval, and therefore we focus on kinetic proofreading behavior within this range of dwell times.

Figure 3.10 B summarizes all differences in active ZAP70 for the tested combinations of  $\alpha$  and  $\beta$ . The change in ZAP70 activation ranges from zero difference in activation (blue) to more than 2.5  $\Delta pY493\text{-ZAP70}/TCR$  (dark red) in the lower right corner of the diagram. The top row of the graph (indicated by arrow I) demonstrates again the effect of enhanced phosphorylation rates ( $\alpha > 1, \beta = 1$ ). As discussed previously the amount of active ZAP70 is independent of the dwell time, thus the difference in  $pY493\text{-ZAP70}$  per TCR is around 0. When we analyzed the single effect of only a reduction of phosphatase activity ( $\alpha = 1, \beta < 1$ ) we found a dependency of active ZAP70 on the dwell time, but very little overall ZAP70 activation. This is depicted in the most left column of the figure (indicated by arrow II). Compared to other regions of the diagram, the kinetic proofreading effect can hardly be seen.

The most pronounced kinetic proofreading behavior is found when both mechanisms are combined. A high phosphorylation rate together with a decreased dephosphory-

$\alpha$	$\beta$	
10	1	
100	1	
1	0.1	single effect
1	0.01	
2	0.5	minimal change
10	0.1	
100	0.1	
65	0.015	mixed effect
10	0.01	
100	0.01	

Table 3.2.: Combinations of  $\alpha$  and  $\beta$  that were chosen to calculate corresponding prediction profile likelihoods.

lation rate, depicted in the lower right corner of Figure 3.10, results in a synergistic increase in the kinetic proofreading capabilities of the model.

Thus, the model simulations predict that the high discriminative power that enables the TCR to distinguish between ligands with different affinities, could be facilitated by a synergistic effect of two activation mechanisms that only together give rise to kinetic proofreading.

### Analysis of the uncertainties of the model predictions

The model predictions that we discussed above were calculated using the best-fit estimates of basal parameters. We will now take into account the uncertainties of the predictions as well, by calculating the corresponding prediction profile likelihoods (see also 2.2.2).

Before, we made 10000 predictions on the effect of different combinations of  $\alpha$  and  $\beta$  on the kinetic proofreading behavior of the model. To reduce computational effort, we now strategically choose predictions that cover a wide variety of the tested parameter combinations and calculate the confidence intervals for those predictions. The chosen predictions are marked by white dots in Figure 3.11 A and are summarized in Table 3.2. The prediction profile likelihood for each of them are calculated and shown in Figure A.1. We quantified the 95%- confidence interval for each of the analyzed predictions (Figure 3.11 B).

First we evaluate the predictions where kinetic proofreading was not apparent. The corresponding 95% confidence intervals (Fig. 3.11 B, left side and Fig. A.1, upper row) for those cases are very narrow, confirming that kinetic proofreading can neither

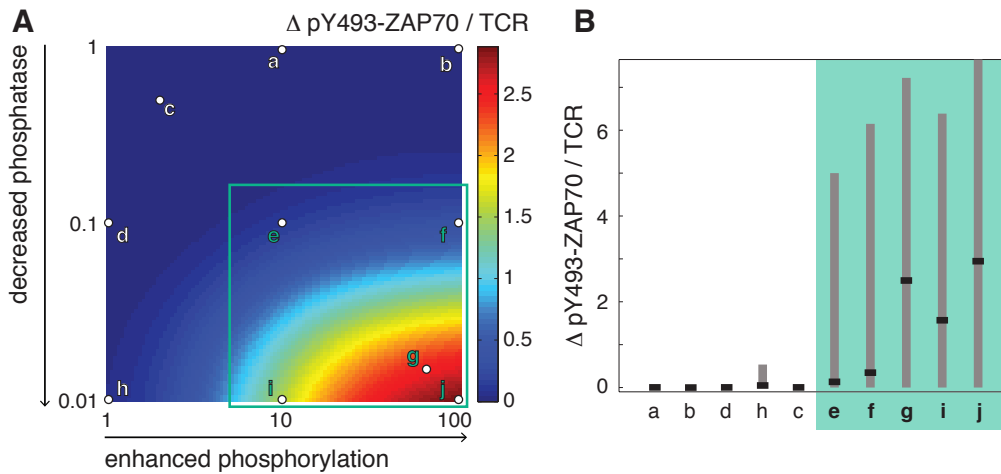


Figure 3.11.: The uncertainty of 10 selected predictions were calculated. (A) The selected predictions are marked by white dots. The turquoise square marks the area of high kinetic proofreading ability. (B) 95%-confidence intervals were calculated for the selected predictions. For the non-mixed effects, bands are very narrow, excluding the possibility of kinetic proofreading. Only for the mixed effect kinetic proofreading is possible.

be introduced by only one of the triggering mechanisms nor by only small impacts on the rates of the signaling machinery after stimulation.

Second, we evaluate the uncertainties of those predictions that indicate kinetic proofreading behavior. Those are only found for cases where both triggering mechanisms are combined (the predictions inside the turquoise square of Figure 3.11 A). The 95%-confidence interval for these cases are much wider, some of them span almost the whole possible range from zero to ten (compare also Fig. A.1, lower row). This means that although we find kinetic proofreading behavior when we simulate with the best fit basal parameters, using other parameter sets that statistically still yield a good fit could give rise to situations where no kinetic proofreading behavior can be found or where the kinetic proofreading behavior is even more pronounced.



## 4. Modeling the dynamics of Lck regulation

The primary kinase that drives TCR phosphorylation is the Src–family kinase Lck. In order to phosphorylate the TCR, Lck has to be in its active form. The regulation of its activation is highly dynamic and depends on different factors like its accessibility for phosphatases and kinases, but also on the concentration of Lck. Here we use a generic model of Lck regulation mechanism to dissect the influence of these different factors on Lck activity.

We will first discuss two different approaches that can be taken to model Lck regulation. Later in this chapter we focus on a mass action kinetic model of Lck regulation. We use dose–response data of Lck phosphorylation in dependence on the amount of total Lck to parameterize the model. Based on these parameters we investigate the influence of Lck localization on its activity. We are also able to further analyze the regulatory influence of the two enzymes (CD45 and Csk) that drive the phosphorylation dynamics of Lck.

All data that we introduce in this chapter has been generated and provided to us by Oreste Acuto and Konstantina Nika from the University of Oxford.

### 4.1. Modeling Lck regulation: two different approaches

In this section we will first introduce a model of Src–family kinase (SFK) regulation that is phrased in terms of Michaelis–Menten kinetics. We will then discuss how this model can be specified to analyze Lck regulation and show that it allows for bistable behavior in Lck activation. Next, we will introduce a second modeling attempt that is based on mass action kinetics and elucidate why this model can be linked to data much better than the other model.

#### 4.1.1. Bistability in the model with enzymatic kinetics

Kaimachnikov and Kholodenko [32] created a generic model of SFK regulation based on reversible phosphorylations. Although SFKs differ in function and exact struc-

ture, in general they all share the same regulatory mechanisms.

Their model consists of four SFK states (inhibited, primed and two active SFK forms) that are defined by the phosphorylation status of an inhibitory and an activating tyrosine residue. The authors study the dynamic regulation of these four states. The model is phrased in terms of Michaelis–Menten kinetics and parameterized with parameters from the literature. They find that the intrinsic features of SFK regulation, like autophosphorylation and reversible phosphorylations together with a non-reversible dephosphorylation, are sufficient for complex dynamic behavior, such as oscillations, bistability and excitability. External feedback loops that might exist are not needed to explain any of the observed dynamics.

In particular the authors investigate how the steady state behavior of the model depends on the amount of phosphatase RPTP (receptor-type tyrosine phosphatase) and on the kinase Csk (C-Src kinase). In this generalized model two phosphatases are introduced; RPTP dephosphorylates only the inhibitory phosphorylation site while PTP1B targets the activating phosphorylation site. The influence of PTP1B concentration on the dynamic behavior of SFK activity is not further characterized by the authors. In contrast, for Lck it is supposed that only one phosphatase (CD45) is mostly responsible for all possible dephosphorylations. It is pointed out by the authors that autophosphorylation most likely plays an important role in the complex dynamic behavior of the system. In this case the phosphorylation dynamics are dependent on the amount of total SFK. However, they did not discuss the influence of varying levels of total SFK on its activation dynamics.

We will now particularize the model of Kaimachnikov and Kholodenko to analyze the dynamical regulation of Lck activation. Specifically we analyze the dependence of Lck activity on the amount of total Lck and total CD45. Since the main phosphatase of both phosphorylation sites of Lck is CD45, we simplify the model by assuming all dephosphorylations to be carried out by the same phosphatase.

Using the same parameterization as proposed by Kaimachnikov and Kholodenko [32] for the generic model reveals a bistable behavior that is dependent on the total Lck concentration (Figure 4.1). The phosphorylation of both, the activating phosphorylation site (Y394) and the Lck inhibitory phosphorylation site Y505 correlates positively with the amount of total Lck and shows bistable behavior. In contrast, a generic parameterization of the model, where we assume most of the parameters to be the same, does not exhibit bistable behavior. Nevertheless, here as well the phosphorylation of both phosphorylation sites increases monotonically with the concentration of Lck.

Bistable behavior can also be found when analyzing the influence of the phosphatase CD45 on Lck regulation (Fig 4.2). Increasing the amount of CD45 leads to decreased phosphorylation both for the inhibitory and the activating phosphorylation site. This inhibitory effect of CD45 on Lck phosphorylation is also found using the generic

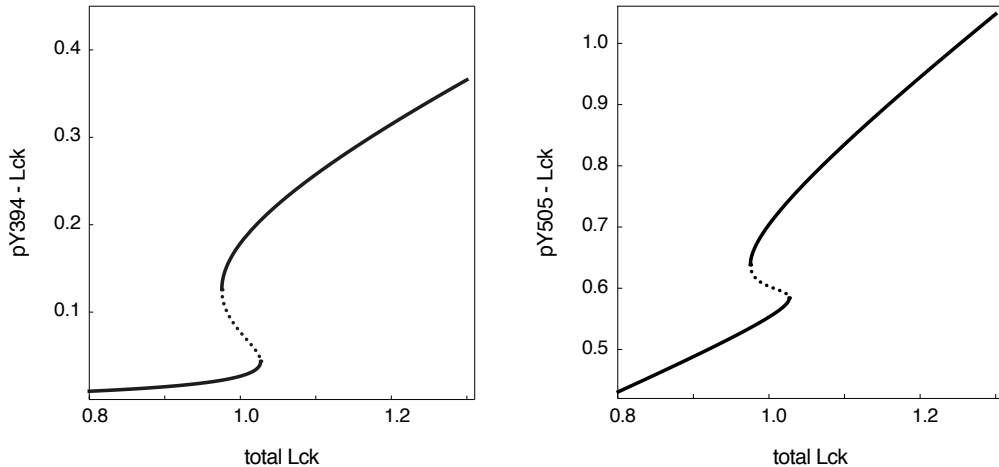


Figure 4.1.: Bistability in the model that is based on enzymatic kinetics. Both phosphorylation sites of Lck Y394 (A) and Y505 (B) exhibit bistable behavior depending on the concentration of total Lck.

parameterization, but again no bistability is observed.

Here we demonstrate that a model of Lck regulation, which is phrased in terms of Michaelis–Menten kinetics can show bistability. However, this behavior does depend on the parameterization of the model. A disadvantage of the model is that Kaimachnikov and Khodenko used parameters from literature that are not necessarily specific for the model setting. Also the authors choose the used parameter values from a wide range of possible values. None of the ten model parameters have been validated by additional experiments nor has the model outcome been compared to measurements.

One of our aims in this work is to parameterize a model of Lck regulation using dose–response data of Lck phosphorylation in dependence on the amount of total Lck. In the next section we introduce an even further simplified model that is based on mass action kinetics. It needs less parameters to describe Lck regulation and is better suited to compare it to the available dose–response data.

#### 4.1.2. A mass–action kinetics model without bistability

An alternative to enzymatic kinetics is the use of mass action kinetics to describe the same regulatory processes. Here, we develop a model of the regulation of reversible phosphorylation of Lck based on mass action kinetics. Each state transition (indicated by the arrows in Figure 4.3) is now characterized by only one parameter, a simplification that is based on assuming fast enzyme-substrate complex turnover.

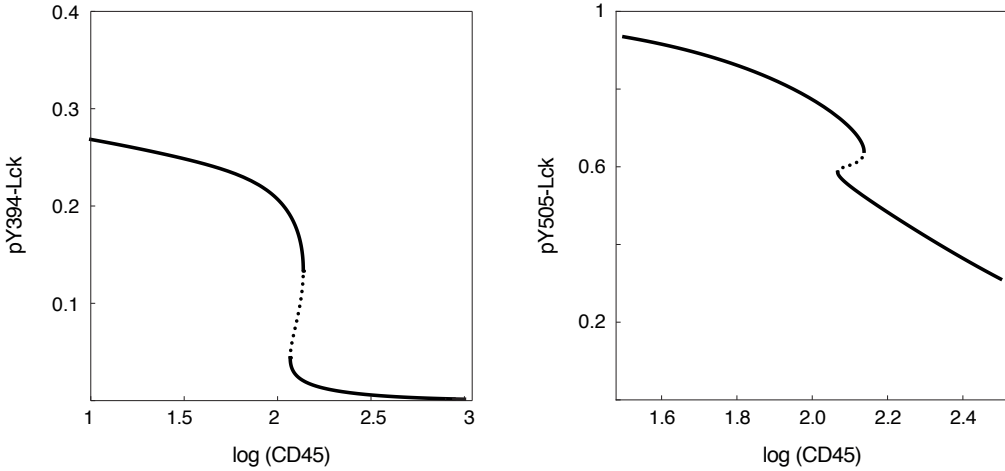


Figure 4.2.: The influence of the amount of CD45 on Lck phosphorylation in the model with enzymatic kinetics. The phosphorylation of both Lck phosphorylation sites (Y394(A) and Y505(B)) correlates negatively with CD45 concentration and shows bistable behavior.

We thereby reduce the number of parameters needed to describe the regulation of Lck activation.

Our model is composed of the four important regulatory states of Lck (inhibited, primed, single and double active Lck) that play a role in the regulation of Lck activity [45]. In the following the four different states of Lck marked by the combination of the phosphorylation state of the two tyrosine residues Y394 and Y505 of Lck. A binary code is used to distinguish whether either site is phosphorylated or not. As a reminder, Lck(0,1) (inhibited) is in a closed conformation due to intramolecular interactions. All other Lck forms are in an open conformation and possess either weak kinase activity (Lck(0,0)) or – when phosphorylated at Y394 – full kinase activity (Lck(1,0) and Lck(1,1)).

Lck regulation is driven by C-Src kinase (Csk) and the phosphatase CD45 as shown in the scheme of Lck regulation in Figure 4.3. Two distinctive features drive the dynamics of Lck regulation. First, the autophosphorylation of tyrosine residue 394, which is phosphorylated by active Lck (Lck(1,0) and Lck(1,1)) and unphosphorylated primed Lck (albeit less strong). Second, the direct transition from Lck(0,1) to Lck(1,1) is not allowed in the model. This transition is excluded because the closed conformation of Lck completely blocks the activating phosphorylation site from kinases and Lck has to be primed first before becoming activated [46]. All other phosphorylation steps are reversible.

The phosphatase CD45 is a membrane protein and hardly expressed in the cytoplasm, while the kinase Csk is a cytoplasmic molecule that is only recruited to the

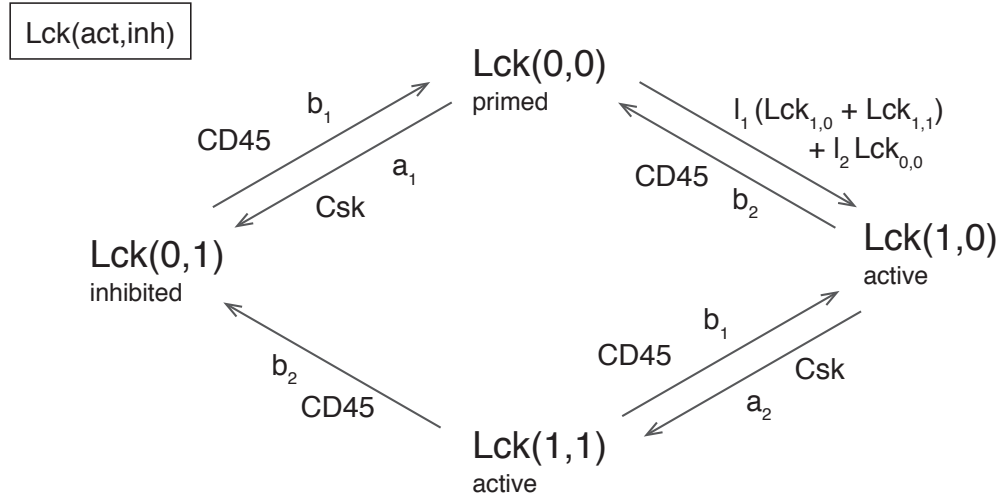


Figure 4.3.: Model scheme of the phosphorylation dynamics of Src-kinase Lck. The phosphorylation is given in a binary code for the activating (Y394) and the inhibitory (Y505) phosphorylation site, respectively. All dephosphorylations are mediated by CD45, while Csk phosphorylates Y505. The conversion from primed to single active Lck is via trans-autophosphorylation by primed and active Lck.

membrane by an adapter protein called Csk binding protein (CBP). In the model we assume constant concentrations of CD45 and Csk at the membrane where Lck is located under normal conditions [46].

The model framework is based on six rate parameters for phosphorylation and dephosphorylation. We describe the phosphorylation of Y505 with parameter  $a_1$  if primed Lck is targeted by Csk and with parameter  $a_2$  if Y505 of single active Lck is phosphorylated by Csk. There are two reasons for the two distinct rates of Csk phosphorylation. First, studies show that Csk interacts with Lck more readily if Lck is phosphorylated at Y394 [5, 9]. Second, the analytic model solution shows that the phosphorylation of Y505 would linearly depend on the total amount of Lck if both rates were the same (compare Section A.2.3 in the appendix), which is in disagreement with the available dose-response data that we later use for parameterization. Since we assume a constant amount of Csk both rates already include its concentration.

Dephosphorylation is characterized by the parameters  $b_1$  and  $b_2$ . While  $b_1$  describes the dephosphorylation of tyrosine residue 505, the rate of dephosphorylation of Y394 is expressed by parameter  $b_2$ . Both dephosphorylation events are carried out by CD45 and again already contain the concentration of CD45.

The rate of trans-autophosphorylation of Y394 depends on the enzymatic activity of the Lck form that executes the phosphorylation. Lck(0,0) has weaker kinase activity

than both active forms of Lck. Hence, we include two parameters  $l_1$  and  $l_2$  in the model to describe trans-autophosphorylation of Y394 by active and primed Lck, respectively.

The model is phrased in terms of mass-action kinetics in the following system of differential equations according to the model scheme in Figure 4.3

$$\begin{aligned} \frac{d}{dt}\text{Lck}_{01}(t) &= -b_1\text{Lck}_{01}(t) + a_1\text{Lck}_{00}(t) + b_2\text{Lck}_{11} \\ \frac{d}{dt}\text{Lck}_{10}(t) &= -(b_2 + a_2)\text{Lck}_{10}(t) + b_1\text{Lck}_{11}(t) \\ &\quad + (l_1(\text{Lck}_{10}(t) + \text{Lck}_{11}(t)) + l_2\text{Lck}_{00}(t))\text{Lck}_{00}(t) \\ \frac{d}{dt}\text{Lck}_{11}(t) &= -(b_1 + b_2)\text{Lck}_{11}(t) + a_2\text{Lck}_{10} \end{aligned} \tag{4.1}$$

where the different Lck forms are indicated by a binary index; with zero being the unphosphorylated and one the phosphorylated state of the activating (Y394) and the inhibitory (Y505) phosphorylation site, respectively.

The total amount of Lck is assumed to be constant:

$$\text{Lck}_{\text{tot}} = \text{Lck}_{01}(t) + \text{Lck}_{00}(t) + \text{Lck}_{10}(t) + \text{Lck}_{11}(t) = \text{const}$$

The steady state of this ODE system can be found analytically. The solutions are given in Chapter A.2.2 of the appendix. In contrast to the model that is based on Michaelis–Menten kinetics the solution does not admit bistable behavior.

In Section 4.2 we will study the introduced model further and will show that parameters can be identified within narrow bounds using steady state data of Lck phosphorylation.

### 4.1.3. Flow cytometry data does not show bistability

Our experimental collaborators performed dose–response experiments and measured phosphorylation of either Y394 or Y505 as a function of total Lck using flow cytometry (for pY394 see Figure 4.4; for pY505 see Figure A.2 in the appendix).

We binned the data into groups of similar Lck expression and calculated histograms of phosphorylation levels for each group (Fig. 4.4, left). Bistable Lck phosphorylation would result in a bimodal distribution of phosphorylation levels. Otherwise, the phosphorylation level distribution of Lck is expected to be unimodal. The histograms reveal distributions that have one clear peak and for some bins a slight

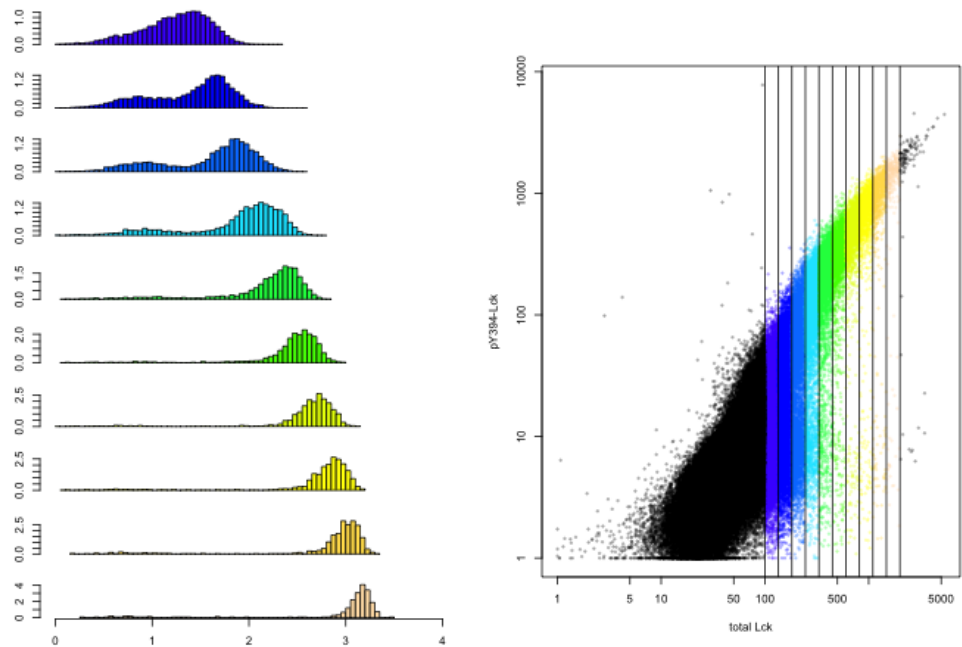


Figure 4.4.: Dose–response data do not indicate bistability in the regulation of Lck. Flow cytometry data (right) is binned into groups of different total Lck expression in the cell. For each bin the corresponding histograms of phosphorylated Y394 are shown left. We do not find clear bimodal distributions as we would expect for bistable behavior. (Experiments by K. Nika and O. Acuto)

elevation in the histogram for low levels of phosphorylation. This holds true for both phosphorylation sites of Lck. The slight elevation in some of the histograms is not pronounced enough to indicate a bistability in Lck regulation.

The approach of modeling the dynamic processes of Lck regulation described in the last section has the advantage over the previous – Michaelis–Menten kinetics based – model to have less parameters. Also the simplified description of enzymatic kinetics using Michaelis–Menten terms is valid if the enzyme concentration is much less than the substrate concentration. In T cells, however, CD45 is one of the most abundant proteins [29, 3]. Additionally, in our data we have varying amounts of total Lck due to the dose–response measurements.

The lack of bistability in the data is an important prerequisite to use the simpler mass action kinetics model instead of the Michaelis–Menten kinetics model. Thus in the next section we use the mass action kinetics model to identify the relevant parameters and later dissect the different features that drive Lck regulation.

## 4.2. A more detailed view on the mass action kinetics model

In this section we carefully parameterize the above described mass action model of Lck regulation using extensive dose–response data about the dependence of Lck concentration and the phosphorylation status of Lck. Here we will first introduce the data and then show that all parameters are fully identifiable within narrow bounds.

### 4.2.1. Phosphorylation of Lck was measured for different Lck chimeras

In the experiments Jurkat cells (an immortalized human T cell line) that lack functional Lck, were transfected with different Lck chimeras and the regulation of Lck activity was measured by means of flow cytometry.

To generate the chimeras the N– terminus of wild type Lck was altered to generate different Lck constructs that then were expressed in Jurkat cells. The N–terminus of Lck mediates the localization of Lck in the cell and hence the different chimeras of Lck are localized differently. An overview of the chimeras that were transfected is given in Figure 4.5. The Lck chimeras are separated into two groups: most of them are still targeted to the membrane, despite the altered N–terminus, but Lck C3,5S and Lck–Δ10 are no longer able to associate with the membrane and can only be found in the cytoplasm.

The membrane–targeted chimeras are constructed to associate to different regions of the membrane. Wild type Lck (Lck–wt), Src–Lck, LAT–Lck and both CD4– Lck variants are targeted to membrane region in close proximity of the TCR. Addition-

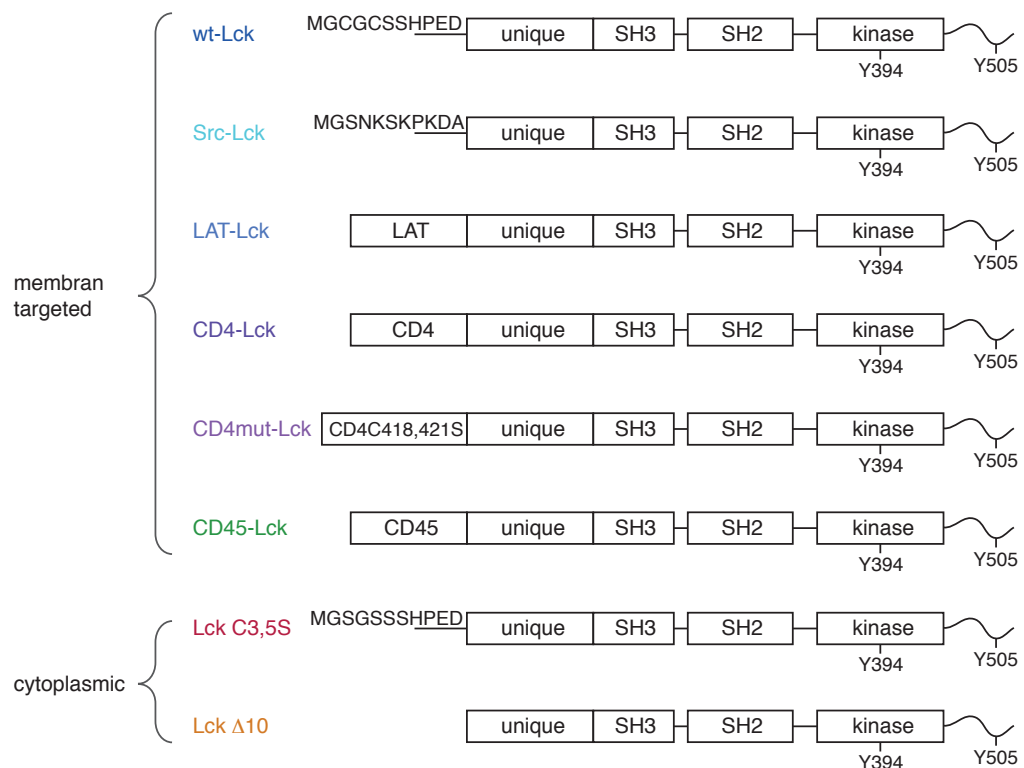


Figure 4.5.: Overview of the different Lck constructs that were transfected into Jurkat cells. Each constructs has a different N-terminus, which alters its localization in the cell. wt-Lck, Src-Lck, LAT-Lck, CD4-Lck, CD4mut-Lck and CD45-Lck are still targeted to the membrane while the two cytoplasmic Lck constructs are not longer able to associate with the membrane.

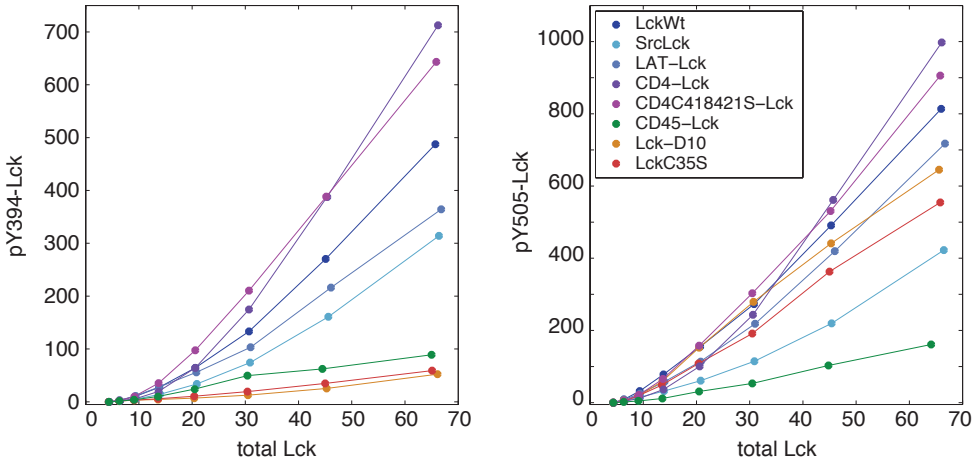


Figure 4.6.: Dose–response data for both phosphorylation sites of Lck and for all eight different Lck constructs. (Experiments by K. Nika and O. Acuto)

ally CD4–Lck and CD4mut–Lck might be able to form dimers at the membrane. Membrane–targeted CD45–Lck is preferably localized in regions with high CD45 content. We will later see that this has direct consequences for the dynamics of Lck regulation.

After transfection the cells expressed different amounts of Lck, which enabled us to analyze how the levels of phosphorylated Lck depend on the amount of total Lck in the cell. Using flow cytometry the amount of Lck, the amount of CD45 and either the phosphorylation level of the activating or the inhibitory phosphorylation site was measured simultaneously. Additionally the effect of Lck localization on its regulation is investigated by conducting these measurements for all eight chimeras.

For the analysis, the data was gated for total Lck levels and the corresponding phosphorylation level of either Y394 phosphorylation or Y505 were quantified from the flow cytometry data (Figure 4.6). We find differences in the regulation of Lck phosphorylation for the different chimeras: For active Lck (pY394–Lck) a clear distinction can be made between the membrane–targeted Lck (except for CD45–Lck) and the cytoplasmic Lck and CD45–Lck. While the phosphorylation of the first group is highly up–regulated with increasing total Lck concentration, the other group is only mildly up–regulated with an increasing amount of total Lck. For high levels of total Lck concentration we find a clear hierarchy of phosphorylation: both CD4–Lck > wt–Lck, Src–Lck and LAT–Lck > CD45–Lck > cytoplasmic Lck.

For the phosphorylation of tyrosine residue 505 the result is not that definite. CD45–Lck is still phosphorylated at low levels, but cytoplasmic Lck is phosphorylated at Y505 similarly to the remaining membrane–bound Lck chimeras.

We want to use these dose–response data to parameterize the mass action model of Lck regulation – for this purpose we have to incorporate different behavior of the individual Lck constructs into the model.

#### 4.2.2. Parameters can be estimated from dose-response data

Here we show that we can fully identify all six parameters ( $a_1$ ,  $a_2$ ,  $b_1$ ,  $b_2$ ,  $l_1$  and  $l_2$ ) of the model of Lck regulation that we introduced in Section 4.1.2 by using the dose–response data, which we introduced in the previous section.

We will first discuss how the effects of the different chimeras are integrated into our model framework. The different Lck constructs have only been altered at the N–terminus, which mediates the localization of Lck [46]. Therefore we assume that the different Lck chimeras are exposed to different densities of CD45 and Lck, which we take into account in the model by introducing additional parameters for some of the phosphorylation and dephosphorylation events for each of the mutants as follows.

The parameter  $b_1$  is estimated individually for each Lck construct to account for different densities of CD45 within the membrane as well as in the cytoplasm. Since the enzymatic activity of CD45 is the same for all chimeras, the ratio of both dephosphorylation rates  $c_1 = b_2/b_1$  is kept constant for all chimeras in the parameter estimation.

It can be assumed that the different chimeras equally affect the binding of activated and primed Lck, so we take  $c_2 = l_2/l_1$  to be the same for all of them, while introducing individual rates  $l_1$  for each chimera.

Csk is a cytoplasmic protein that can also be recruited to the membrane. There is no apparent reason to assume that the availability for phosphorylation by Csk is altered within the different Lck mutants. For simplicity we thus take the rates for phosphorylation by Csk ( $a_1$  and  $a_2$ ) to be the same for all Lck chimeras.

We simultaneously fitted the resulting model to the dose–response data of all eight chimeras. Since there is no information about the phosphorylation kinetics of the process in the dose–response data, we scaled all parameters to  $a_1$  and kept  $a_1 = 1$  fixed in the fitting. This eliminates the time dependency of the rates.

Besides the rate parameters we have to estimate two scaling factors to take into account the arbitrary units of the flow cytometric measurement: The parameter  $s_1$  scales the measurement of pY416-Lck (active Lck) and the parameter  $s_2$  the measurement of pY505-Lck. Finally, two additional parameters,  $\varepsilon_1$  and  $\varepsilon_2$ , were included in the fitting procedure to estimate the absolute measurement errors of pY394-Lck and pY505-Lck, respectively as described in Chapter 2.2.

The above described data contains no information on the unphosphorylated state of Lck. In order to distinguish all four states of Lck we used an additional data set from Nika et al. [45], where all four states were measured separately (see Table 1 of [45], first row) for the estimation of the parameters.

The measurements of the phosphorylation of Y394 and Y505 are expressed by the model in terms of the following observables:

$$\begin{aligned} pY394-Lck &= \Theta_1(\vec{p}, L) = Lck_{10}(\vec{p}, L) + Lck_{11}(\vec{p}, L) \\ pY505-Lck &= \Theta_2(\vec{p}, L) = Lck_{01}(\vec{p}, L) + Lck_{11}(\vec{p}, L) \end{aligned}$$

where  $\vec{p}$  denotes the chimera-specific set of parameters and  $L$  is the concentration of total Lck.

This yields the following objective function, which is to be minimized:

$$f(\vec{p}) = 2 \cdot 8 \sum_{j=1}^2 \log \varepsilon_i + \chi_1^2 + \chi_2^2. \quad (4.2)$$

Here the first part of the left hand side is due to the estimation of the errors (compare Chapter 2.2) and

$$\chi_1^2 = \sum_{j=1}^8 \sum_{i=1}^8 \left( \frac{D_{1ij} - \Theta_1(\vec{p}_j, L_i)}{\varepsilon_1} \right)^2 + \sum_{j=1}^8 \sum_{i=1}^8 \left( \frac{D_{2ij} - \Theta_2(\vec{p}_j, L_i)}{\varepsilon_2} \right)^2$$

where the index  $i$  enumerates the different total Lck concentrations, the index  $j$  denotes one of the eight chimeras and  $D_{1ij}$  and  $D_{2ij}$  denote the corresponding measurements of pY394 and pY505, respectively.

The third part of eqn. 4.2 is given by

$$\begin{aligned} \chi_2^2 &= \left( \alpha \left( \frac{Lck_{01}(\vec{p}_1, L=50)}{50} - 0.14 \right) \right)^2 + \left( \alpha \left( \frac{Lck_{00}(\vec{p}_1, L=50)}{50} - 0.48 \right) \right)^2 \\ &\quad + \left( \alpha \left( \frac{Lck_{10}(\vec{p}_1, L=50)}{50} - 0.17 \right) \right)^2 + \left( \alpha \left( \frac{Lck_{11}(\vec{p}_1, L=50)}{50} - 0.21 \right) \right)^2. \end{aligned}$$

Here  $\vec{p}_1$  is the parameter set for wt-Lck and  $\alpha$  is a weight that we introduced to make  $\chi_2^2$  comparable in size to  $\chi_1^2$ .

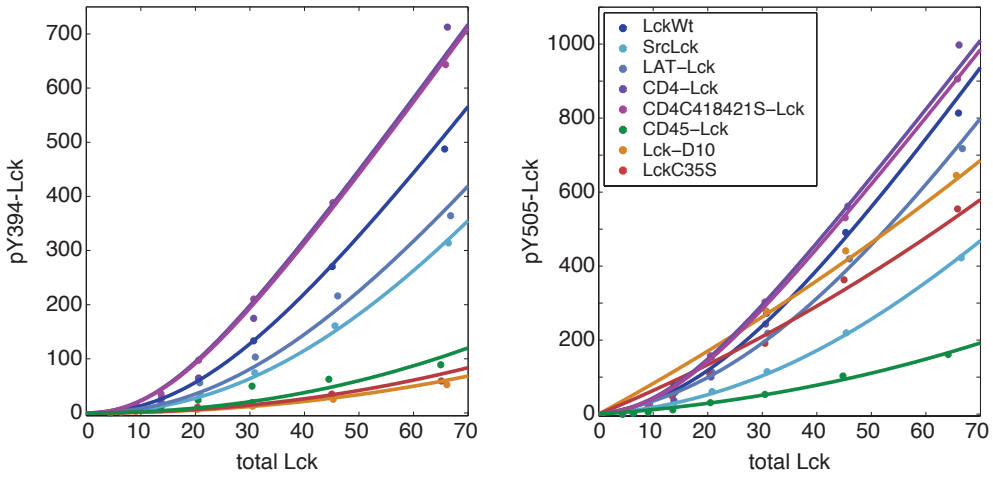


Figure 4.7.: The model (solid lines) was fitted to the dose–response data of the two phosphorylation sites of Lck at Y394 and Y505 and the eight different chimeras of Lck. (Experiments by K. Nika and O.Acuto)

The parameter estimation was carried out with a trust region method (interior point algorithm implemented in matlab). The resulting best fit (with  $\chi^2_{\min} = 866.46$ ) is depicted in Figure 4.3 where the data is shown together with the fitted model curves (solid lines).

The remaining results that we show are based on a fixed value of  $\alpha = 100$ . Repeating the parameter estimation with a ten fold lower value of  $\alpha$  led to unacceptable fits whereas a ten fold higher values of  $\alpha$  yielded a slightly higher  $\chi^2_{\min} = 869.32$  and almost identical parameters compared to the fitting results with  $\alpha = 100$ . We did not further investigate the influence of  $\alpha$  on the other parameters and their confidence intervals.

The estimated parameters that are the same for all Lck constructs are presented in Table 4.1 and Table 4.2 shows the parameters that differ between the chimeras. The uncertainties of the parameters are analyzed using the profile likelihood method as described in Chapter 2.2.1 and are shown in Fig. 4.8. All parameters are identifiable and have narrow confidence bounds. The estimated 95%-confidence intervals are also given in Tables 4.1 and 4.2.

In Table 4.1 we can see that Csk is more than ten-fold more enzymatically active on active Lck than on the primed form. The ratios  $c_1$  and  $c_2$  are both smaller than 1, indicating that  $b_2 < b_1$  and  $l_2 < l_1$ . This means that CD45 dephosphorylates pY394 more easily than pY505, which has been described before [56]. Since primed Lck is not fully enzymatically active  $l_2 < l_1$  is to be expected.

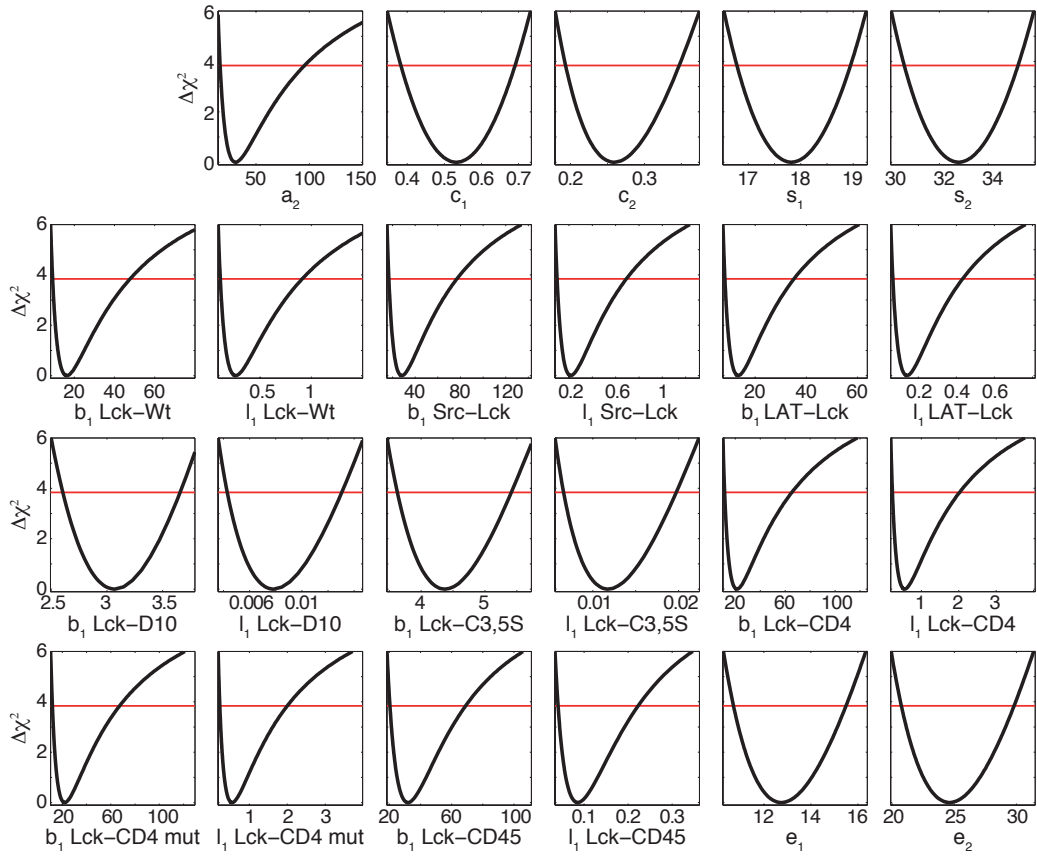


Figure 4.8.: The uncertainties of the estimated parameters is assessed by using the profile likelihood method. The calculation of the profile likelihoods of all parameters show that they are identifiable within narrow bounds. The threshold for  $\chi^2_{95\%}$  is marked for each profile by the red line.

parameter	estimated value	90 % confidence interval
Phosphorylation of Y505 of primed Lck by Csk ( $a_1$ )	1	
Phosphorylation of Y505 of active Lck by Csk ( $a_2$ )	30.77	[16.2, 95.5]
Ratio of dephosphorylation rates of Y505 and Y394 by CD45 ( $c_1$ )	0.53	[0.38, 0.69]
Ratio of autophosphorylation rates ( $c_2$ )	0.26	[0.19, 0.35]
Scaling factor for pY416-Lck measurement ( $s_1$ )	17.82	[16.8, 19]
Scaling factor for pY505-Lck measurement ( $s_2$ )	32.79	[30.6, 35.2]
Error of pY416-Lck measurement ( $\varepsilon_1$ )	12.74	[10.7, 15.5]
Error of pY505-Lck measurement ( $\varepsilon_2$ )	24.61	[20.7, 29.8]

Table 4.1.: Best fit parameters, which are the same for all chimeras, as estimated from fitting the model to the dose response data. The 95%-confidence interval of each parameter is estimated by calculating the corresponding profile likelihoods. The parameters have no units because of the normalization with  $a_1$  (see main text).

	dephosphorylation of pY505 ( $b_1$ )		autophosphorylation by active Lck ( $l_1$ )	
	best fit	90 % conf.	best fit	90% conf.
wt-Lck	16.26	[9.15, 47.9]	0.26	[0.11, 0.91]
Src-Lck	28.11	[16.6, 77.2]	0.216	[0.098, 0.7]
LAT-Lck	13.35	[8.14, 35.4]	0.14	[0.065, 0.4]
Lck-D10	3.1	[2.6, 3.7]	0.008	[0.0043, 0.013]
Lck-C3,5S	4.4	[3.6, 5.4]	0.012	[0.007, 0.02]
Lck-CD4	21.3	[11.4, 65.5]	0.55	[0.22, 2]
Lck-CD4 mut	21.97	[11.7, 67.5]	0.54	[0.22, 2]
Lck-CD45	31.9	[20.4, 69.2]	0.088	[0.04, 0.2]

Table 4.2.: Best fit parameters, which are different for each chimera, as estimated from fitting the model to the dose response data. The 95%-confidence interval of each parameter is estimated by calculating the corresponding profile likelihoods. The parameters have no units because of the normalization with  $a_1$  (see main text).

Also interesting are the estimated chimera-specific parameters that should reflect the different localizations of the Lck chimeras in the cell (Table 4.2). We find similar estimates of the autophosphorylation rate ( $l_1$ ) and the dephosphorylation rate ( $b_2$ ) for the membrane bound chimeras wt-Lck, Src-Lck and LAT-Lck. Both Lck-CD4 mutants have dephosphorylation rates similar to the other membrane-bound Lcks but they differ in the autophosphorylation rates which are bigger in the CD4-Lck mutants. This might reflect their ability to form dimers.

Compared to the other chimeras both mutants that are cytoplasmic have small dephosphorylation rates. This can be explained by the absence of CD45 in the cytoplasm. Like expected, because they diffuse in a much bigger volume, the autophosphorylation rates are very small.

Surprisingly, CD45-Lck also has a small autophosphorylation rate, but a dephosphorylation rate that is comparable to the rates of the other membrane-targeted chimeras.

Based on the estimated dephosphorylation rates there is a clear distinction between the membrane-targeted Lck constructs and the cytoplasmic Lck which shows almost ten-fold smaller dephosphorylation rates. The estimated parameters also imply a hierarchy with respect to autophosphorylation: CD4 targeted Lck > wt-Lck, LAT-Lck and Src-Lck > CD45-Lck > cytoplasmic Lck. The same hierarchy that we found in the measurements of phosphorylated Y394-Lck (compare Chapter 4.2.1).

## 4.3. Model simulations show the regulation of Lck activity

### 4.3.1. Autoactivation of Lck occurs in trans

So far, we assumed in our model framework that Y394 is trans-autophosphorylated. But the question whether this phosphorylation occurs in trans or cis is not fully resolved. Trans-autophosphorylation would be dependent on the concentration of Lck, because the autophosphorylation is executed by another Lck molecule. In contrast, if Y394 is cis-autophosphorylated, the phosphorylation would be mediated by the Lck molecule itself and is not dependent on the concentration of Lck. Additionally it could also only be carried out by primed Lck, since the active Lck is already phosphorylated and does not need to phosphorylate itself. The available experimental data can be used to infer the dependence of the phosphorylation levels on the amount of total Lck and thereby give insights into the question whether Y394 is cis- or trans-autophosphorylated.

We want to explore the possibility of cis-autophosphorylation and rephrase the model that we introduced in the previous section in such a way, that the phosphorylation of the activating phosphorylation site is independent of Lck concentration. Hence

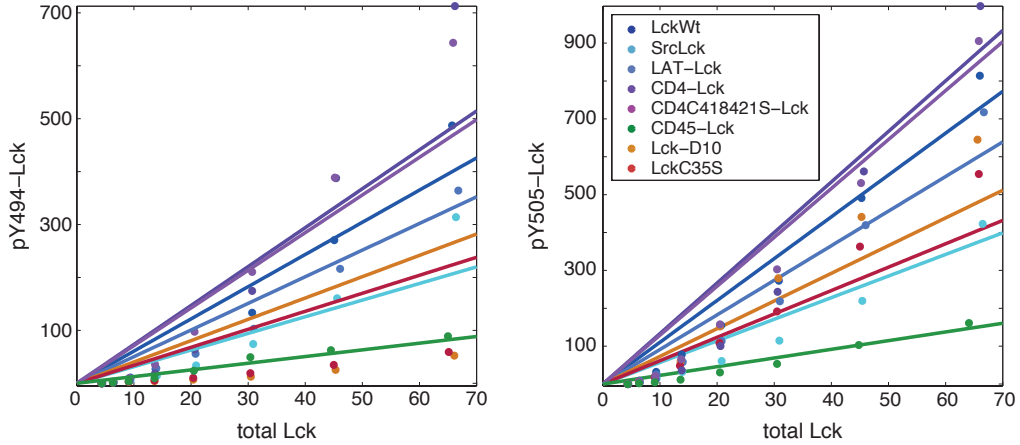


Figure 4.9.: Fit of the modified Lck regulation model that assumes cis-autophosphorylation. Since the steady states of the modified model only depend linearly on total Lck, the model cannot reproduce the observed dependencies in the data. (Experiments by K. Nika and O. Acuto)

eliminating the second order reaction from the model. This notion is phrased in terms of mass action kinetics again in the following system of ODEs

$$\begin{aligned}\frac{d}{dt} \text{Lck}_{01}(t) &= -b_1 \text{Lck}_{01}(t) + a_1 \text{Lck}_{00}(t) + b_2 \text{Lck}_{11} \\ \frac{d}{dt} \text{Lck}_{10}(t) &= -(b_2 + a_2) \text{Lck}_{10}(t) + b_1 \text{Lck}_{11}(t) + l_1 \text{Lck}_{00}(t) \\ \frac{d}{dt} \text{Lck}_{11}(t) &= -(b_1 + b_2) \text{Lck}_{11}(t) + a_2 \text{Lck}_{10}\end{aligned}$$

with

$$\text{Lck}_{\text{tot}} = \text{Lck}_{01}(t) + \text{Lck}_{00}(t) + \text{Lck}_{10}(t) + \text{Lck}_{11}(t) = \text{const.}$$

The steady state of the modified model can be solved analytically:

$$\begin{aligned}\text{Lck}_{00} &= \frac{b_1 b_2 (a_2 + b_1 + b_2) \text{Lck}_{\text{tot}}}{(a_1 + b_1) b_2 (a_2 + b_1 + b_2) + (a_2 + b_1) (b_1 + b_2) l_1} \\ \text{Lck}_{11} &= \frac{a_2 b_1 l_1 \text{Lck}_{\text{tot}}}{(a_1 + b_1) b_2 (a_2 + b_1 + b_2) + (a_2 + b_1) (b_1 + b_2) l_1} \\ \text{Lck}_{01} &= \frac{(a_1 (a_2 + b_1 + b_2) + a_2 l_1) b_2 \text{Lck}_{\text{tot}}}{(a_1 + b_1) b_2 (a_2 + b_1 + b_2) + (a_2 + b_1) (b_1 + b_2) l_1}\end{aligned}$$

$$Lck_{10} = \frac{b_1(b_1 + b_2)l_1 Lck_{tot}}{(a_1 + b_1)b_2(a_2 + b_1 + b_2) + (a_2 + b_1)(b_1 + b_2)l_1}$$

Like expected the solution is only linearly dependent on the total Lck concentration.

We used the same fitting routine as described before using 500 random sets of initial parameters. We find a best fit with  $\chi^2_{\min} = 1222.7$ , which is much higher than the  $\chi^2_{\min}$  of the previous fitting.

The reason for the bad performance of the model is the experimentally observed non-linear dependence of the Lck phosphorylation levels on the total Lck concentration. This is also demonstrated in Figure 4.9, which shows the best-fit result. We clearly see that the model (given by solid lines) cannot reproduce the data.

Thus, we think that cis-autophosphorylation alone is not sufficient to activate Lck in a manner that corresponds to the measurement. For all further analysis of Lck regulation we are using the model that is proposed in Section 4.1.2 and the best fit parameters from Section 4.2.2.

### 4.3.2. Csk phosphorylates the primed and the single active Lck differently

In the model the phosphorylation of the residue of tyrosine 505 of Lck by Csk is described by two rates. The rate  $a_1$  denotes the phosphorylation that is carried out by Csk on primed Lck ( $Lck(0,0)$ ), whereas we assume a different phosphorylation rate ( $a_2$ ) of that site if Lck is already phosphorylated at Y394.

Both phosphorylation rates are kept the same for all chimeras, thus we can directly compare the estimated rate  $a_2 = 30.77$  to  $a_1$ . We find a more than ten-fold higher rate of  $a_2$  which clearly influences how Lck activation is regulated. We did not find any other parameterization compatible with the data that does not show this feature (compare the analysis of parameter uncertainties in Figure 4.8).

The effect is demonstrated in Figure 4.10 by visualizing all four Lck states separately for each chimera. For low total Lck concentrations we would not expect Lck to be active because of the necessary autophosphorylation. But it could be in the inactive or the primed form. Our simulation with the estimated parameters show that it is mostly in the primed form at low Lck concentrations. The relative amount of primed Lck decreases for the membrane bound chimeras of Lck (with the exception of CD45–Lck) with an increase in total Lck. For these isoforms the relative amount of active Lck is high at high amounts of total Lck. Note, that in Figure 4.10 both active forms are depicted individually; the sum of both represents the total amount

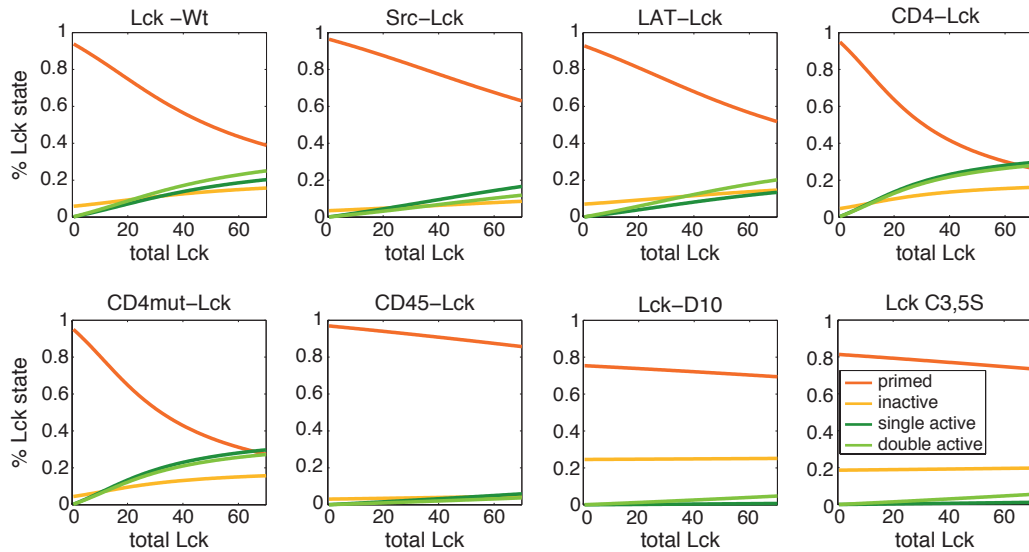


Figure 4.10.: The different chimeras show distinctive phosphorylation dynamics. The regulation of Lck phosphorylation for membrane-bound Lck (with the exception of CD45-Lck) and cytoplasmic Lck varies largely. Membrane-targeted Lck is phosphorylated at Y505 only after its activation. Cytoplasmic Lck and CD45-Lck is hardly influenced by changing Lck and is mostly in its primed form.

of active Lck. Lck is stabilized in its active forms by the higher enzymatic activity of Csk on single active Lck.

For the two cytoplasmic mutants primed Lck is as well the dominant state for low Lck concentrations even though not as dominant as for the membrane bound Lck chimeras. But in contrast to the other chimeras it remains the dominant form almost independent of the Lck concentration. The relative amount of inactive Lck also differs greatly from that of the membrane bound forms of Lck. Around 20–25% of the total Lck is in the inactive state, again independent on the Lck concentration. The two cytoplasmic mutants are not autophosphorylated as easily because of the much bigger reaction volume (the whole cytoplasm) they are in. But because the Csk activity on primed Lck is rather low only a small part of Lck is in the inactive state.

An exception to all the membrane bound Lck isoforms is CD45-Lck, which has very different phosphorylation dynamics, because of its proximity to CD45. Here, Lck is mostly in its primed state, since CD45 clears it from all phosphorylations. Probably the effects of the different enzymatic activities of Csk play hardly a role in this case.

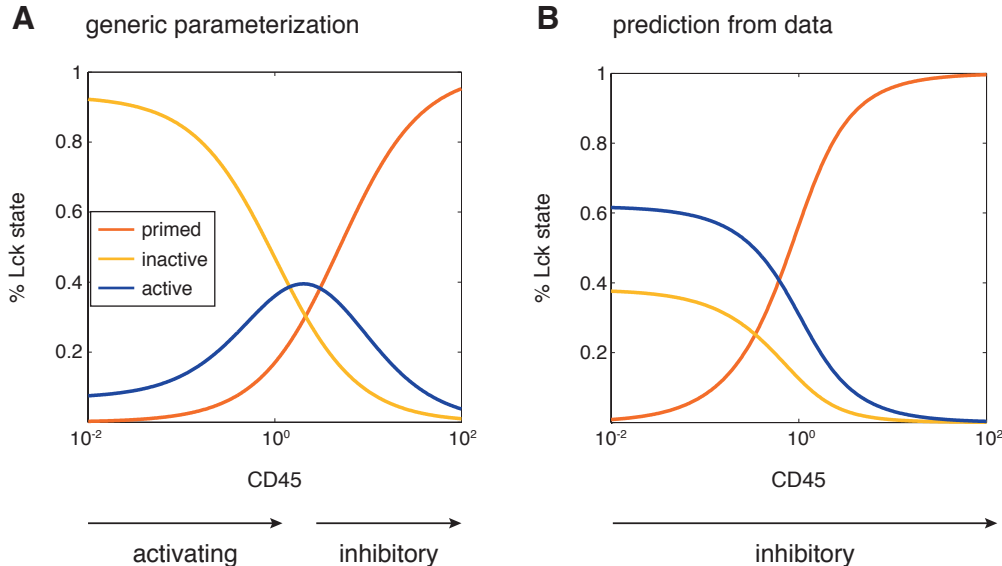


Figure 4.11.: CD45 influence on the activation of Lck. (A) A generic parameterization of the model shows that CD45 could have an activating or an inhibitory effect on Lck. (B) The model simulation with the estimated parameters indicate that CD45 has an inhibitory effect on Lck

### 4.3.3. CD45 has an inhibitory effect on Lck activity

CD45 has a dual role in the activation dynamics of Lck. On the one hand it dephosphorylates the mostly inhibiting Y505 phosphorylation. On the other hand it also mediates the transition from double active Lck to inhibitory Lck by dephosphorylating pY394. Here, we investigate the possible influence of CD45 on Lck in general as well as in terms of our model predictions.

We investigated the influence of CD45 on the phosphorylation levels at a total Lck concentration of 40 (arbitrary units), which corresponds to a medium Lck concentration in the experiments. An increase or decrease of the dephosphorylation rates  $b_1$  and  $b_2$  of up to 100-fold was then employed to simulate different CD45 concentrations.

The dual role of CD45 is shown in Figure 4.11 A. We use a generic parameterization (with most of the parameters set equal) of the model and demonstrate that the activation of Lck depends on the concentration of CD45 in a biphasic manner. In such a way that low amounts of CD45 have an activating effect on Lck activity until an optimum CD45 concentration is reached, then the effect is reversed and more CD45 has an inhibitory influence on Lck activity.

When we use the estimated parameters of wt-Lck for the same simulation we find

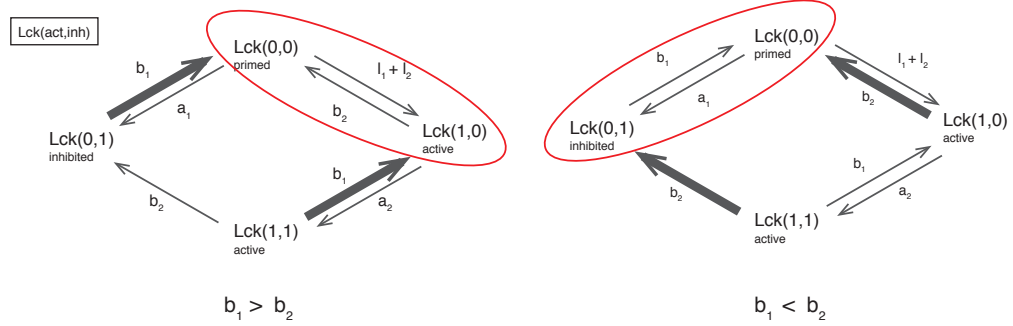


Figure 4.12.: The effect of the two dephosphorylation rates. If  $b_1$  is dominant over  $b_2$  either primed Lck or single active Lck ( $Lck(1,0)$ ) are most likely the predominant forms of Lck. In the case of a stronger  $b_2$  Lck tends to be either primed or inhibited.

a solely inhibitory effect of CD45 on the activation of Lck (see Figure 4.11 B), the amount of active Lck monotonically decreases with the amount of CD45.

These two qualitatively different effects of CD45 can be ascribed to the relation between  $b_1$  and  $b_2$  (see Figure 4.12). If  $b_2$  is bigger this increased would be bigger (demonstrated in Figure 4.12 B by the thick arrows). For our estimated parameters the opposite is the case,  $b_1 > b_2$ . This implies that Lck has a tendency to be either in the primed or in the single active state. We can see in Figure 4.11 B that indeed the fraction of primed Lck positively correlates with CD45 concentration, but given the remaining parameters it has not the same effect on the activation of Lck.



## 5. Discussion

The ability of the T cell receptor to precisely differentiate between antigens with only moderately different affinities is pivotal for the reliable distinction between self and nonself antigens of the adaptive immune system. However, the exact underlying mechanism of antigen discrimination leading to either tolerance or T cell activation has remained elusive.

In this work we utilized mathematical modeling to provide a mechanistic explanation for the emergence of the sharp threshold response of the TCR by scrutinizing the dynamics of the early T cell activation events including signal initiation, early signaling events and the regulation of kinase activity after TCR triggering. We based our modeling on extensive data from experiments that were conducted by our collaborators Sumit Deswal and Wolfgang Schamel at the University of Freiburg and Konstantina Nika and Oreste Acuto at the University of Oxford.

Our model of the early events of TCR signaling revealed that these signaling steps contribute to the kinetic proofreading capability of the TCR, which can explain ligand discrimination based on its dwell time. Interestingly, the kinetic proofreading behavior of the mathematical model depends strongly on the activation mechanisms that initiate TCR signaling. We find a synergistic effect on the ability of the TCR to distinguish between ligands for a combination of enhanced kinase and decreased phosphatase activity.

In a second mathematical model we concentrated on the dynamic regulation of the Src-family kinase Lck that drives TCR signaling. Analysis of the model enabled us to dissect the effect of the phosphatase CD45 on Lck regulation. CD45 has been shown to both dephosphorylate an inhibiting and an activating Lck phosphorylation site. Using our parameterized model we were able to quantify both effects and found that the phosphatase acts as an inhibitor of Lck activation while its activating effects can be neglected. In the light of the result of our mathematical model for the early TCR signaling events, CD45 reduction upon TCR signaling could therefore contribute to the kinetic proofreading capabilities of the T cell receptor.

## The TCR signaling model

The model of early events in TCR signaling, which we introduced in the first part of this work, is solely based on known mechanisms of TCR signaling. In contrast, previous studies [4, 21, 67] made additional assumptions on the underlying processes of antigen discrimination, like implementing an explicit kinetic proofreading scheme into the model.

We first parameterized a model of basal TCR activation by fitting it to kinetic data of ZAP70 recruitment and phosphorylation after pervanadate stimulation. For this we had to quantify the dephosphorylation effect of pervanadate, which we fixed to be 80% based on literature estimates [42]. In a second step we then treated this ratio as a free parameter and used the profile likelihood method to show that the literature value is consistent with the available data, but based on these data can only be estimated with large uncertainties. Another assumption we had to make concerned the estimate of the scaling factor for the Western blot data. This factor could not be estimated directly from our data. We could partly resolve this issue by fixing the factor using former measurements of the ratio between the absolute amount of ZAP70 phosphorylation at the sites Y319 and Y493 [39]. However, future experimental work should be done to address this question again. Especially since we could not extract the uncertainty of the phosphorylation ratio estimate from the paper.

With the data at hand we only found lower bounds for the estimates of most rate constants using the profile likelihood method. Even though we took into account a quite extensive set of data, clearly more data would be needed to improve parameter estimation. However, using the method of prediction profile likelihoods we found that we can still draw many important quantitative conclusions from the modeling. We will discuss these in the following paragraphs.

An analysis of parameter ratios revealed that in order to maintain basal TCR activity, the phosphorylation of ITAMs and the first phosphorylation of ZAP70 have to be slower than the corresponding dephosphorylations. This prevents the TCR from becoming activated accidentally. The opposite is true for the reversible phosphorylation of the activating tyrosine residue (Y493 in the kinase domain); here, the phosphorylation rate is faster than the dephosphorylation rate. This seems to ensure that once the signal comes through it is intensified. At this point downstream signaling cascades will be triggered leading to activation of the T cell.

We extend the model of basal TCR signaling by incorporating ligand binding and then tested the model for its kinetic proofreading capabilities. The main characteristic of kinetic proofreading is that activation explicitly depends on the dwell time of the ligand and not just its affinity to the TCR. In order to systematically test our model for kinetic proofreading behavior we introduced a measure of kinetic proof-

reading that is based on the difference in TCR activation at fixed ligand dwell times. This is computational more effective than to base the calculation of the differences in activation on the minimum and the maximum of the steady state curve. Since we were only interested in the occurrence of kinetic proofreading behavior at biological realistic dwell times [75] our measure is reasonable.

We find that kinetic proofreading in our model depends on the mechanism of signal initiation: a combination of enhanced phosphorylation and reduced dephosphorylation could synergistically lead to significant kinetic proofreading capabilities of the model. Narrow prediction confidence intervals indicate that either mechanism by itself would not result in such behavior. The different mechanisms of signal initiation have only been investigated separately before; it has however already been suggested to consider a combined effect of both [68].

In contrast to our model, previous models were usually limited to the specific mechanism the researches wanted to analyze [4, 40, 21, 67, 12].

The kinetic proofreading model of McKeithan explains the specificity of ligand discrimination [40]. It relies on very fast dephosphorylation rates and requires that ligands can only bind to unphosphorylated TCRs. In our model framework we deviate from these principles. Although we estimated relatively fast dephosphorylation rates they are not comparable to the infinitely fast dephosphorylation in McKeithan's model. Additionally, we assume that ligands can bind to the TCR independently of its phosphorylation state. While both assumptions seem to be biological more realistic, they lead to a softening of the high specificity of ligand discrimination compared to the idealized situation in the original model. Nevertheless, we still find that our model is able to distinguish ligands with very similar affinities but different dwell times in a kinetic proofreading sense.

Altan-Bonnet and Germain proposed a model that combines a kinetic proofreading scheme with competitive feedback regulations [4]. The aim of the authors is to propose a quantitative model that not only accounts for the specificity of the TCR, but also for the sensitivity and speed of TCR discrimination. In their study the authors carefully measured concentrations of relevant model components, but had to modify kinetic parameters to match the model predictions to experimental data.

The same is true for a model by Francois et al. [21], which also relies on a kinetic proofreading scheme that is extended by a negative feedback mechanism. Again, parameters are not estimates from data but chosen by the investigator based on the recent literature. Additionally, model predictions could only qualitatively be compared to biological measurements.

Both models are able to account for the high discriminative power of the TCR based on ligand dwell time and concentration. However, in comparison to our model there are two striking differences in the modeling approach. First, our model framework

is based on the actual signaling at TCR level. Although the feedback regulations used in both models have been described in the literature [63], the underlying kinetic proofreading scheme incorporates many additional processes. Second, we estimate the parameters from data. Hereby we are able to draw quantitative conclusions from the model whereas predictions from the above described models come without estimates of their statistical uncertainty and rely on the correctness of the parameters, which in some cases only represent ad-hoc estimates.

A model that is solely based on biological processes is a feedback model proposed by Das et al. [15]. In their model, feedback regulations downstream of LAT are important for T cell activation implying that the decision of activation is not made during early TCR signaling. In contrast our results indicate that ligand discrimination can be achieved already upstream of LAT during the initial signaling events. In our model the slow dephosphorylation of active ZAP70 stabilizes the signal and indicates that at this point of the signaling cascade the decision of TCR activation has already been made.

The main drawback of models that aim to dissect the discriminative power of the TCR is their parameterization. Due to the complexity of the models it is difficult to find data that would allow to fully identify all parameters. On the other hand a simplification of the model may not any longer allow a biological interpretation of the modeling results. Thus, it is a necessity to create models that incorporate a reasonable level of detail while still allowing good enough estimates of the parameters to ensure predictability. This balance will be largely dependent on the data at hand.

Our model is parameterized by available kinetic data. However, the estimated parameters have only one-sided bounds and were not constrained by the data completely. Nevertheless, compared to the other studies our model predictions and quantitative conclusions are based on a defined set of data allowing us to provide confidence bounds for these quantitative model predictions.

Further analysis of our model of TCR signaling would largely benefit from a decrease in the uncertainties of the parameters. Two apparent possibilities could improve the fitting result. First, additional measurements would contribute to more constraint parameter estimates. Especially experiments on the phosphorylation of the ITAMs could help to account for the complexity of the model and might improve the parameter estimation. Second and more importantly, to account for the given data the model could be further simplified at the potential loss of exactness in describing the underlying signaling processes. Various options come to mind. Since measurement of ITAM phosphorylation are difficult to obtain, we possibly could merge the two phosphorylation steps into one step that describes how ITAMs are primed for ZAP70 recruitment. Another possibility would be to simplify the model by neglecting trans-autophosphorylation by ZAP70 and estimate parameters with the resulting seven state model. This implies to ignore a possibly important regulatory process in the signaling cascade. A possible analysis that could be done with such

a well-parameterized model would be to explore the model response in dependence of ligand dwell time and ligand concentration and thereby studying the relation between TCR sensitivity and specificity (as an example for such an analysis see [19]). This would also allow to quantitatively explore in which way the incorporation of more realistic processes in our model leads to a reduction in TCR specificity compared to the original kinetic proofreading model.

A crucial experimental demonstration of kinetic proofreading has not been achieved and will be difficult to obtain in the future. We based our model on biologically realistic processes and could show that kinetic proofreading capabilities can occur naturally in such a model without making additional assumptions about unobserved mechanisms. This was not possible before and can be interpreted as an additional indication that kinetic proofreading does indeed take place during T cell activation. We believe that the use of such mechanistic models in a combined approach with experimentation is the key to demonstrate kinetic proofreading in T cell activation by validating quantitative model predictions experimentally. However, in our case it is difficult to design experiments where ligands have exactly the same affinity but different dwell times. But the concentration of ligands can easily be adjusted to result in the same ligand occupancy albeit different ligand affinities. Such data could be used to further constrain the model and to test the kinetic proofreading characteristics that are predicted by it.

## The model of Lck regulation

The kinase that drives TCR signaling is the Src–family kinase (SFK) Lck. Its activity is heavily regulated by various factors, such as its localization and auto-phosphorylation, which we investigated in the second part of this work. For a better understanding of the dynamics of Lck activity we first analyzed an already existing model of SFK regulation [32] and specified it for the regulation of Lck. It is based on Michaelis–Menten kinetics and shows bistability in the regulation of Lck.

We then proposed a model that is based on mass action kinetics. By assuming fast enzyme-substrate complex turnover we build a model with fewer parameters than the Michaelis–Menten kinetics model, but which also does not give rise to bistability. An analysis of flow cytometry data of the dependence of Lck phosphorylation on the amount of total Lck did not show bistability, which justified the use of the simpler mass action kinetics based model for further analysis of Lck regulation.

Our collaborators (K. Nika and O. Acuto) measured the phosphorylation of different Lck chimeras, that either bind to distinct areas of the membrane or are cytoplasmic, in dependence of the amount of total Lck. We parameterized the model using these dose–response data. The data did not contain information about the unphosphorylated Lck state (primed Lck). We thus had to rely on an additional data set where

the relative amount of all four Lck states was measured explicitly for a fixed amount of total Lck [45]. This enabled us to identify all parameters within narrow bounds ensuring a high predictive power of the model.

The difference in the estimated parameters between the considered Lck chimeras contain information about the influence of Lck localization on its phosphorylation. We find a clear distinction in terms of dephosphorylation and trans-autophosphorylation rates between membrane-targeted and cytoplasmic Lck. In terms of trans-autophosphorylation we find the following hierarchy: both CD4–Lck > wt–Lck, Src–Lck and LAT–Lck > CD45–Lck > cytoplasmic Lck. This hierarchy reflects the localization of the different Lck chimeras and the effects it has on the local concentration of Lck.

Lck activity depends on the balance between phosphorylation and dephosphorylation of its activating phosphorylation site. This balance is influenced by the localization of Lck. We find that while cytoplasmic Lck is mostly in its primed form, the membrane-targeted Lck chimeras exhibit a much higher fraction of active Lck. Also their regulation of activity correlates much stronger with the amount of total Lck.

Parameter estimation also yields that Csk kinase activity on Lck is more than ten times higher when Lck is already phosphorylated at the activating phosphorylation site (single active Lck) than in the completely unphosphorylated state (primed state). This is in line with studies that investigated Csk–Lck interactions and found that Csk binds with much higher affinity to single active Lck and thus phosphorylates this Lck state more efficiently [5, 9]. These findings confirms the necessity to have two different phosphorylation rates.

Studies indicate that the efficiency of dephosphorylation of both tyrosine residues by CD45 is different; CD45 has a stronger enzyme activity on Y505 [56]. Our estimated rates corroborate this finding. Dephosphorylation of Y394 is two-fold less efficient than dephosphorylation of Y505. Nevertheless, it is also conceivable that – similar to Csk – the kinase activity of CD45 on each of the two phosphorylation sites of Lck depends on the phosphorylation state of the other site. For example one could imagine that the access of CD45 to pY505 is different if Lck is in its closed or open conformation. However, we are not aware of studies showing this and for simplicity modeled the kinase activity to be the same.

Another important finding of our model simulations is that autophosphorylation is likely to occur in trans or a combination of cis and trans. Explicitly incorporating pure cis-autophosphorylation into our model yielded a linear dependency of Lck phosphorylation on the amount of total Lck. The data, however, clearly show a non-linear dependency, indicating that autophosphorylation is not exclusively cis.

Finally, we quantified the influence of CD45 on Lck regulation. Since CD45 dephosphorylates both the inhibiting and the activating Lck phosphorylation site, its

overall effect on the amount of active Lck is very much dependent on the chosen parameters values. Our finding that CD45 enzyme activity is stronger on tyrosine residue 505 could suggest an overall activating effect of CD45. Instead we find that the best-fit parameters imply an inhibitory influence of CD45 on the activity of wild type Lck. Increasing local concentrations of CD45 results mostly in enhanced levels of primed Lck, whereas the inactive form of Lck is affected by CD45 the same way as active Lck. This finding is an important prerequisite for TCR signaling initiation as proposed by the so-called segregation model [16]: according to this model, CD45 is pushed out of the TCR signaling region upon ligand binding due mechanical forces.

To summarize, we found that the localization of Lck influences has a strong influence on its phosphorylation, which is reflected in the differences between the estimated rates belonging to the different chimeras. Our quantitative model further allowed us to predict an overall inhibitory influence of CD45 on Lck. Finally, we showed that a model that assumes pure *cis*-autophosphorylation is not in accordance with the data.

The model that is most similar to our modeling approach is the one proposed by Kaimachnikov and Kholodenko [32]. We used a slightly modified version of it in the beginning of Chapter 4 as a basis to analyze the regulation of Lck activity. Based on a general model of SFK (including Lck) regulation, the authors discuss a number of possible phosphorylation dynamics, like oscillations and bistability. In contrast to our work, their model is not directly linked to experimental data and their analysis is instead based on rather rough estimates of parameters taken from the literature. Hence the investigators are limited to qualitative predictions about the dynamics of SFK regulation.

A broader approach to model Lck regulation was taken by Chan et al. [12]. The authors model Lck activity in the context of interaction with the TCR and a phosphatase that is not further specified. In their model Lck activity is regulated by several feedback mechanisms. Although feedback mechanisms might also contribute to the dynamic regulation of Lck activity (Chan et al. also find bistable Lck activation), Kaimachnikov and Kholodenko showed that feedback loops are not necessary to explain the complex dynamics of Lck activation. For this reason and for simplicity we did not include additional feedback mechanisms in our model. Again parameters are rough estimates made by the investigators and it remains unclear in which way other biologically justified choices of parameter values would influence the model predictions. For example, the model theoretically shows that feedback regulations of Lck activation could contribute to antigen discrimination by the TCR, but the robustness of this prediction with respect to parameter uncertainties is not assessed.

## Conclusions

In this work we investigated two mechanistic models of early TCR activation that follows TCR triggering. The first model focuses on the induction of TCR signaling by phosphorylation of the ITAMs of the receptor and subsequent ZAP70 recruitment and phosphorylation. In the other model we more closely study the regulation of Lck, which is the kinase that drives TCR signaling. The parameterization for both models is strictly data-based and makes use of extensive measurements to estimate the model parameters and to assess the predictive power of the models.

We analyzed the model of TCR signaling induction with regard to its kinetic proofreading capabilities, implying the ability to discriminate between ligands with different dwell times but similar affinities. We found that the kinetic proofreading capabilities of the model depend on how the signaling is triggered. Neither an enhancement of phosphorylation nor a reduction of phosphatase activity alone would lead to the discriminative power of the TCR based on dwell times. Both mechanisms have separately been proposed to initiate TCR signaling. Contrary to this, we find in our quantitative model that only the synergistic interaction of both mechanisms does result in kinetic proofreading behavior.

With our second model we dissect the complex dynamics of Lck activation. We found that Lck activity is regulated by three main factors: the localization of Lck in the cell, its activation by trans-autophosphorylation and an inhibitory effect of CD45 on Lck activity.

Our models represent two of the core modules of TCR activation that are pointed out by Acuto et al. [1]. Biologically, both of the mechanisms that are described by our models are closely related, because Lck is the key kinase of TCR signaling. It is responsible for the phosphorylation of the ITAMs as well as for the stabilization of the open conformation of ZAP70 by phosphorylation of the tyrosine residue in interdomain B (Y319).

The model of TCR signaling predicts that a combined effect of reduced phosphatase and enhanced kinase activity is needed in order to accurately discriminate antigens in a kinetic proofreading sense. This result is especially interesting in the light of our model on Lck regulation which predicts that a reduction in the phosphatase activity of CD45 results in higher levels of active Lck. Together both models indicate that a reliable ligand discrimination based on dwell times might be induced by a reduction of phosphatase activity alone (which then automatically leads to enhanced Lck activity).

This reduced phosphatase activity has been proposed in the kinetic segregation model [16]: upon TCR triggering CD45 is excluded from the signaling region of the TCR by mechanical forces. This in turn alters the balance of phosphorylation and

dephosphorylation activity at the TCR and initiates signaling. Our modeling shows that kinetic proofreading is possible in the segregation model.

There are contradicting studies about the regulation of Lck that either claim Lck to be constitutively active with TCR triggering having no effect on its global activity [45, 47] or that ligand binding increases Lck activity [64]. According to our model CD45 is a negative regulator of Lck, this implies that the first finding of constitutively active Lck would speak against the proposed kinetic segregation model, whereas the latter finding suggest that TCR signaling might be triggered by exclusion of CD45. While we are not able to resolve this contradiction biologically, we can assess the importance of these findings for the ability of the TCR to discriminate between different ligands.

The decision whether the TCR is activated by the presented antigen takes place within seconds. The threshold of activation is shown to be around 2s [75]. In contrast, the regulation of Lck is seems to be happening on the time scale of minutes [45, 64]. Even though our model proposes that the activation of Lck is enhanced upon CD45 exclusion, this might happen on a time scale that is not relevant for the discrimination of antigen by the TCR. Therefore, it would be interesting to extend the model fit with kinetic measurements (similar to those in [45]) to further elucidate this notion.



# Bibliography

- [1] Oreste Acuto, Vincenzo Di Bartolo, and Frédérique Micheli. Tailoring t-cell receptor signals by proximal negative feedback mechanisms. *Nat Rev Immunol*, 8(9):699–712, Sep 2008.
- [2] John Aldrich. R. a. fisher and the making of maximum likelihood 1912-1922. *Statistical Science*, 12(3):162–176, 1997.
- [3] D. R. Alexander. The cd45 tyrosine phosphatase: a positive and negative regulator of immune cell function. *Seminars in immunology*, 12(4):349–359, Aug 2000.
- [4] Grégoire Altan-Bonnet and Ronald N Germain. Modeling t cell antigen discrimination based on feedback control of digital erk responses. *PLoS Biol*, 3(11):e356, Nov 2005.
- [5] K. E. Amrein, J. Molnos, J. D. zur Hausen, N. Flint, B. Takacs, and P. Burn. Csk-mediated phosphorylation of substrates is regulated by substrate tyrosine phosphorylation. *Farmaco (Società chimica italiana : 1989)*, 53(4):266–272, Apr 1998.
- [6] Enrico Arpaia, Michal Shahar, Harkit Dadi, Amos Cohen, and Chaim M. Rolfman. Defective t cell receptor signaling and cd8+ thymic selection in humans lacking zap-70 kinase. *Cell*, 76(5):947–958, Mar 1994.
- [7] Byron B. Au-Yeung, Sebastian Deindl, Lih-Yun Hsu, Emil H. Palacios, Susan E. Levin, John Kuriyan, and Arthur Weiss. The structure, regulation, and function of zap-70. *Immunological Reviews*, 228(1):41–57, 2009.
- [8] Titus J. Boggon and Michael J. Eck. Structure and regulation of src family kinases. *Oncogene*, 23(48):7918–7927, Oct 2004.
- [9] C. Bougeret, T. Delaunay, F. Romero, P. Jullien, H. Sabe, H. Hanafusa, R. Benarous, and S. Fischer. Detection of a physical and functional interaction between csk and lck which involves the sh2 domain of csk and is mediated by autophosphorylation of lck on tyrosine 394. *The Journal of biological chemistry*, 271(13):7465–7472, Mar 1996.
- [10] J. Y. Bu, A. S. Shaw, and A. C. Chan. Analysis of the interaction of zap-

- 70 and syk protein-tyrosine kinases with the t-cell antigen receptor by plasmon resonance. *Proceedings of the National Academy of Sciences of the United States of America*, 92(11):5106–5110, May 1995.
- [11] Gunnar Cedersund. Conclusions via unique predictions obtained despite unidentifiability - new definitions and a general method. *FEBS Journal*, 279(18):3513–3527, 2012.
  - [12] Cliburn Chan, Jaroslav Stark, and Andrew J George. Feedback control of t-cell receptor activation. *Proc Biol Sci*, 271(1542):931–939, May 2004.
  - [13] D. Coombs and B. Goldstein. T cell activation: Kinetic proofreading, serial engagement and cell adhesion. *Journal of Computational and Applied Mathematics*, 184(1):121–139, 2005.
  - [14] Mark A Daniels, Emma Teixeiro, Jason Gill, Barbara Hausmann, Dominique Roubaty, Kaisa Holmberg, Guy Werlen, Georg A Holländer, Nicholas R Gascoigne, and Ed Palmer. Thymic selection threshold defined by compartmentalization of ras/mapk signalling. *Nature*, 444(7120):724–729, Dec 2006.
  - [15] Jayajit Das, Mary Ho, Julie Zikherman, Christopher Govern, Ming Yang, Arthur Weiss, Arup K. Chakraborty, and Jeroen P. Roose. Digital signaling and hysteresis characterize ras activation in lymphoid cells. *Cell*, 136(2):337–351, Jan 2009.
  - [16] Simon J. Davis and P. Anton van der Merwe. The kinetic-segregation model: Tcr triggering and beyond. *Nature immunology*, 7(8):803–809, Aug 2006.
  - [17] Sebastian Deindl, Theresa A Kadlecak, Tomas Brdicka, Xiaoxian Cao, Arthur Weiss, and J Kuriyan. Structural basis for the inhibition of tyrosine kinase activity of zap-70. *Cell*, 129(4):735–746, May 2007.
  - [18] Sumit Deswal, Anna K Schulze, Thomas Höfer, and Wolfgang W Schamel. Quantitative analysis of protein phosphorylations and interactions by multi-colour ip-fcm as an input for kinetic modelling of signalling networks. *PLoS One*, 6(7), 2011.
  - [19] Vincenzo Di Bartolo, Dominique Mége, Valérie Germain, Michele Pelosi, Eve-lyne Dufour, Frédérique Michel, Giovanni Magistrelli, Antonella Isacchi, and Oreste Acuto. Tyrosine 319, a newly identified phosphorylation site of zap-70, plays a critical role in t cell antigen receptor signaling. *J Biol Chem*, 274(10):6285–6294, Mar 1999.
  - [20] R A Fisher. On the mathematical foundations of theoretical statistics. *Phil. Trans. R. Soc. Lond. A*, 222:309–368, 1922.
  - [21] Paul François, Guillaume Voisinne, Eric D Siggia, Grégoire Altan-Bonnet, and

- Massimo Vergassola. Phenotypic model for early t-cell activation displaying sensitivity, specificity, and antagonism. *Proc Natl Acad Sci U S A*, 110(10):888–897, Mar 2013.
- [22] Andrew J George, Jaroslav Stark, and Cliburn Chan. Understanding specificity and sensitivity of t-cell recognition. *Trends Immunol*, 26(12):653–659, Dec 2005.
  - [23] Byron Goldstein, James R Faeder, and William S Hlavacek. Mathematical and computational models of immune-receptor signalling. *Nat Rev Immunol*, 4(6):445–456, Jun 2004.
  - [24] Marcos H. Hatada, Xiaode Lu, Ellen R. Laird, Jeremy Green, Jay P. Morgenstern, Meizhen Lou, Chris S. Marr, Thomas B. Phillips, Mary K. Ram, Kelly Theriault, Mark J. Zoller, and Jennifer L. Karas. Molecular basis for interaction of the protein tyrosine kinase zap-70 with the t-cell receptor. *Nature*, 377(6544):32–38, Sep 1995.
  - [25] David Hinkley. Predictive likelihood. *The Annals of Statistics*, 7(4):718–728, 1979.
  - [26] John J Hopfield. Kinetic proofreading: a new mechanism for reducing errors in biosynthetic processes requiring high specificity. *Proc Natl Acad Sci U S A*, 71(10):4135–4139, Oct 1974.
  - [27] Jon C Houtman, Richard A Houghtling, Mira Barda-Saad, Yoko Toda, and Lawrence E Samelson. Early phosphorylation kinetics of proteins involved in proximal tcr-mediated signaling pathways. *J Immunol*, 175(4):2449–2458, Aug 2005.
  - [28] Václav Hořejší, Weiguo Zhang, and Burkhardt Schraven. Transmembrane adaptor proteins: organizers of immunoreceptor signalling. *Nat Rev Immunol*, 4(8):603–616, Aug 2004.
  - [29] Nicholas D. Huntington and David M. Tarlinton. Cd45: direct and indirect government of immune regulation. *Immunology letters*, 94(3):167–174, Jul 2004.
  - [30] Darrell J. Irvine, Marco A. Purbhoo, Michelle Krogsgaard, and Mark M. Davis. Direct observation of ligand recognition by t cells. *Nature*, 419:845–849, 2002.
  - [31] John R James and Ronald D Vale. Biophysical mechanism of t-cell receptor triggering in a reconstituted system. *Nature*, 487(7405):64–69, Jul 2012.
  - [32] Nikolai P Kaimachnikov and Boris N Kholodenko. Toggle switches, pulses and oscillations are intrinsic properties of the src activation/deactivation cycle. *FEBS J*, 276(15):4102–4118, Aug 2009.
  - [33] Lawrence P Kane and Arthur Weiss. The pi-3 kinase/akt pathway and t cell

- activation: pleiotropic pathways downstream of pip3. *Immunol Rev*, 192:7–20, Apr 2003.
- [34] G. J. Kersh, E. N. Kersh, D. H. Fremont, and P. M. Allen. High- and low-potency ligands with similar affinities for the tcr: the importance of kinetics in tcr signaling. *Immunity*, 9(6):817–826, Dec 1998.
  - [35] Clemens Kreutz, Andreas Raue, Daniel Kaschek, and Jens Timmer. Profile likelihood in systems biology. *FEBS J*, 280(11):2564–2571, Jun 2013.
  - [36] Clemens Kreutz, Andreas Raue, and Jens Timmer. Likelihood based observability analysis and confidence intervals for predictions of dynamic models. *BMC systems biology*, 6(1):120, 2012.
  - [37] Q J Li, A R Dinner, S Qi, D J Irvine, J B Huppa, M M Davis, and A K Chakraborty. Cd4 enhances t cell sensitivity to antigen by coordinating lck accumulation at the immunological synapse. *Nat Immunol*, 5(8):791–799, Aug 2004.
  - [38] Michel Mallalau, Dieter Naehler, Mark A. Daniels, Pia P. Yachi, Barbara Hausmann, Immanuel F. Luescher, Nicholas R. J. Gascoigne, and Ed Palmer. The t cell receptor’s alpha-chain connecting peptide motif promotes close approximation of the cd8 coreceptor allowing efficient signal initiation. *Journal of immunology (Baltimore, Md. : 1950)*, 180(12):8211–8221, Jun 2008.
  - [39] Michel Mallalau, Gerhard Zenke, and Ed Palmer. A discrete affinity-driven elevation of zap-70 kinase activity initiates negative selection. *J Recept Signal Transduct Res*, 30(6):430–443, Dec 2010.
  - [40] Timothy W McKeithan. Kinetic proofreading in t-cell receptor signal transduction. *Proc Natl Acad Sci U S A*, 92(11):5042–5046, May 1995.
  - [41] Louise McNeill, Robert J Salmond, Joanne C Cooper, Céline K Carret, Robin L Cassady-Cain, Marta Roche-Molina, Panna Tandon, Nick Holmes, and Denis R Alexander. The differential regulation of lck kinase phosphorylation sites by cd45 is critical for t cell receptor signaling responses. *Immunity*, 27(3):425–437, Sep 2007.
  - [42] Svein Ole Mikalsen and Olav Kaalhus. Properties of perva-nadate and per-molybdate. connexin43, phosphatase inhibition, and thiol reactivity as model systems. *J Biol Chem*, 273(16):10036–10045, Apr 1998.
  - [43] S. A. Murphy and A. W. Van Der Vaart. On profile likelihood. *Journal of the American Statistical Association*, 95(450):449–465, 2000.
  - [44] Dieter Naehler, Mark A Daniels, Barbara Hausmann, Philippe Guillaume, Immanuel Luescher, and Ed Palmer. A constant affinity threshold for t cell toler-

- ance. *J Exp Med*, 204(11):2553–2559, Oct 2007.
- [45] Konstantina Nika, Christiana Soldani, Mogjiborhaman Salek, Wolfgang Paster, Adrian Gray, Ruth Etzensperger, Lars Fugger, Paolo Polzella, Vincenzo Cerundolo, Omer Dushek, Thomas Höfer, Antonella Viola, and Oreste Acuto. Constitutively active lck kinase in t cells drives antigen receptor signal transduction. *Immunity*, 32(6):766–777, Jun 2010.
  - [46] Emil H. Palacios and Arthur Weiss. Function of the src-family kinases, lck and fyn, in t-cell development and activation. *Oncogene*, 23(48):7990–8000, Oct 2004.
  - [47] Wolfgang Paster, Christian Paar, Paul Eckerstorfer, Andrea Jakober, Karel Drbal, Gerhard J. Schütz, Alois Sonnleitner, and Hannes Stockinger. Genetically encoded förster resonance energy transfer sensors for the conformation of the src family kinase lck. *Journal of immunology (Baltimore, Md. : 1950)*, 182(4):2160–2167, Feb 2009.
  - [48] Michele Pelosi, Vincenzo Di Bartolo, Virginie Mounier, Dominique Mège, Jean-Marc Pascussi, Evelyne Dufour, Arnaud Blondel, and Oreste Acuto. Tyrosine 319 in the interdomain b of zap-70 is a binding site for the src homology 2 domain of lck. *J Biol Chem*, 274(20):14229–14237, May 1999.
  - [49] Lisa A Pitcher and Nicolai S van Oers. T-cell receptor signal transmission: who gives an itam? *Trends Immunol*, 24(10):554–560, Oct 2003.
  - [50] David R. Plas, Robin Johnson, Jeanette T. Pingel, R. James Matthews, Mark Dalton, Gabrine Roy, Andrew C. Chan, and Matthew L. Thomas. Direct regulation of zap-70 by shp-1 in t cell antigen receptor signaling. *Science*, 272(5265):1173–1176, May 1996.
  - [51] Ashok Prasad, Julie Zikherman, Jayajit Das, Jeroen P. Roose, Arthur Weiss, and Arup K. Chakraborty. Origin of the sharp boundary that discriminates positive and negative selection of thymocytes. *Proc Natl Acad Sci U S A*, 106(2):528–533, Jan 2009.
  - [52] A. Raue, C. Kreutz, T. Maiwald, J. Bachmann, M. Schilling, U. Klingmüller, and J. Timmer. Structural and practical identifiability analysis of partially observed dynamical models by exploiting the profile likelihood. *Bioinformatics (Oxford, England)*, 25(15):1923–1929, Aug 2009.
  - [53] Z. Reich, J. J. Boniface, D. S. Lyons, N. Borochov, E. J. Wachtel, and M. M. Davis. Ligand-specific oligomerization of t-cell receptor molecules. *Nature*, 387(6633):617–620, Jun 1997.
  - [54] Caridad Rosette, Guy Werlen, Mark A Daniels, Philmore O Holman, S Munir

- Alam, Paul J Travers, Nicholas R Gascoigne, Ed Palmer, and Stephen C Jameson. The impact of duration versus extent of tcr occupancy on t cell activation: a revision of the kinetic proofreading model. *Immunity*, 15(1):59–70, Jul 2001.
- [55] Robert Roskoski. Src protein-tyrosine kinase structure and regulation. *Biochemical and biophysical research communications*, 324(4):1155–1164, Nov 2004.
- [56] Robert Roskoski. Src kinase regulation by phosphorylation and dephosphorylation. *Biochemical and biophysical research communications*, 331(1):1–14, May 2005.
- [57] Jérémie Rossy, Dylan M Owen, David J Williamson, Zhengmin Yang, and Katharina Gaus. Conformational states of the kinase lck regulate clustering in early t cell signaling. *Nat Immunol*, 14(1):82–89, 2013.
- [58] L E Samelson. Signal transduction mediated by the t cell antigen receptor: the role of adapter proteins. *Annu Rev Immunol*, 20:371–394, 2002.
- [59] Wolfgang W. A. Schamel, Ignacio Arechaga, Ruth M. Risueño, Hisse M. van Santen, Pilar Cabezas, Cristina Risco, José M. Valpuesta, and Balbino Alarcón. Coexistence of multivalent and monovalent tcrs explains high sensitivity and wide range of response. *The Journal of experimental medicine*, 202(4):493–503, Aug 2005.
- [60] Jamie R. Schoenborn, Ying Xim Tan, Chao Zhang, Kevan M. Shokat, and Arthur Weiss. Feedback circuits monitor and adjust basal lck-dependent events in t cell receptor signaling. *Science signaling*, 4(190):ra59, Sep 2011.
- [61] Joanne Sloan-Lancaster, Andrey S. Shaw, Jonathan B. Rothbard, and Paul M. Allen. Partial t cell signaling: altered phospho-zeta and lack of zap70 recruitment in apl-induced t cell anergy. *Cell*, 79(5):913–922, Dec 1994.
- [62] Jennifer E Smith-Garvin, Gary A Koretzky, and Martha S Jordan. T cell activation. *Annu Rev Immunol*, 27:591–619, 2009.
- [63] Irena Stefanová, Bernhard Hemmer, Marco Vergelli, Roland Martin, William E. Biddison, and Ronald N. Germain. Tcr ligand discrimination is enforced by competing erk positive and shp-1 negative feedback pathways. *Nat Immunol*, 4(3):248–254, Mar 2003.
- [64] Anja Stirnweiss, Roland Hartig, Steffi Gieseler, Jonathan A. Lindquist, Peter Reichardt, Lars Philipsen, Luca Simeoni, Mateusz Poltorak, Camilla Merten, Werner Zuschratter, Yury Prokazov, Wolfgang Paster, Hannes Stockinger, Thomas Harder, Matthias Gunzer, and Burkhardt Schraven. T cell activation results in conformational changes in the src family kinase lck to induce its activation. *Science signaling*, 6(263):ra13, Feb 2013.

- [65] David B. Straus and Arthur Weiss. Genetic evidence for the involvement of the lck tyrosine kinase in signal transduction through the t cell antigen receptor. *Cell*, 70(4):585–593, Aug 1992.
- [66] Alain Trautmann and Clotilde Randriamampita. Initiation of tcr signalling revisited. *Trends in immunology*, 24(8):425–428, Aug 2003.
- [67] Salvatore Valitutti, Sabina Müller, Marina Cella, Elisabetta Padovan, and Antonio Lanzavecchia. Serial triggering of many t-cell receptors by a few peptide-mhc complexes. *Nature*, 375(6527):148–151, May 1995.
- [68] P Anton van der Merwe and Omer Dushek. Mechanisms for t cell receptor triggering. *Nat Rev Immunol*, 11(1):47–55, Jan 2011.
- [69] D. J. Venzon and S. H. Moolgavkar. A method for computing profile-likelihood-based confidence intervals. *Journal of the Royal Statistical Society. Series C (Applied Statistics)*, 37(1):pp. 87–94, 1988.
- [70] Haopeng Wang, Theresa A Kadlecak, Byron B Au-Yeung, Hanna E Goodfellow, Lih-Yun Hsu, Tanya S Freedman, and Arthur Weiss. Zap-70: an essential kinase in t-cell signaling. *Cold Spring Harb Perspect Biol*, 2(5), May 2010.
- [71] Xiaoqian Wang, Luca Simeoni, Jonathan A Lindquist, Julio Saez-Rodriguez, Andreas Ambach, Ernst D Gilles, Stefanie Kliche, and Burkhardt Schraven. Dynamics of proximal signaling events after tcr/cd8-mediated induction of proliferation or apoptosis in mature cd8+ t cells. *J Immunol*, 180(10):6703–6712, May 2008.
- [72] Ronald L. Wange, Ramon Gutián, Noah Isakov, Julian D. Watts, Ruedi Aebersold, and Lawrence E. Samelson. Activating and inhibitory mutations in adjacent tyrosines in the kinase domain of zap-70. *The Journal of biological chemistry*, 270(32):18730–18733, Aug 1995.
- [73] Chenqi Xu, Etienne Gagnon, Matthew E. Call, Jason R. Schnell, Charles D. Schwierers, Christopher V. Carman, James J. Chou, and Kai W. Wucherpfennig. Regulation of t cell receptor activation by dynamic membrane binding of the cd3epsilon cytoplasmic tyrosine-based motif. *Cell*, 135(4):702–713, Nov 2008.
- [74] Qingrong Yan, Tiago Barros, Patrick R. Visperas, Sebastian Deindl, Theresa A. Kadlecak, Arthur Weiss, and John Kuriyan. Structural basis for activation of zap-70 by phosphorylation of the sh2-kinase linker. *Molecular and cellular biology*, 33(11):2188–2201, Jun 2013.
- [75] Dietmar Zehn, Carolyn King, Michael J Bevan, and Ed Palmer. Tcr signaling requirements for activating t cells and for generating memory. *Cell Mol Life*

*Sci*, 69(10):1565–1575, May 2012.

- [76] Weiguo Zhang, Joanne Sloan-Lancaster, Jason Kitchen, Ronald P Trible, and Lawrence E Samelson. Lat: the zap-70 tyrosine kinase substrate that links t cell receptor to cellular activation. *Cell*, 92(1):83–92, Jan 1998.

# A. Appendix

## A.1. Additional material for the T cell signaling model

### A.1.1. ODE-System for the basal model

The ODE-system for the basal model as described in Chapter 3.1 is setup like follows

$$\begin{aligned}
x'_1(t) &= -4a_1x_1(t) + pb_1x_2(t) \\
x'_2(t) &= 4a_1x_1(t) - (3a_1 + pb_1)x_2(t) + 2pb_1(x_3(t) + x_8(t)) \\
x'_3(t) &= a_1x_2(t) - (2a_1 + 2pb_1 + k_{on})x_3(t) + k_{off_1}x_4(t) + k_{off_2}(x_5(t) + x_6(t) + x_7(t)) \\
&\quad + pb_1x_9(t) \\
x'_4(t) &= k_{on}x_3(t) - (2a_1 + k_{off_1} + a_2)x_4(t) + pb_2x_5(t) + pb_1x_{10}(t) + pb_3x_7(t) \\
x'_5(t) &= a_2x_4(t) - (2a_1 + pb_2 + k_{off_2})x_5(t) + pb_3x_6(t) + pb_1x_{11}(t) \\
x'_6(t) &= -(2a_1 + pb_2 + pb_3 + k_{off_2})x_6(t) + a_2x_7(t) + pb_1x_{12}(t) \\
x'_7(t) &= pb_2x_6(t) - (2a_1 + a_2 + pb_3 + k_{off_2})x_7(t) + pb_1x_{13}(t) \\
x'_8(t) &= 2a_1x_2(t) - 2(pb_1 + a_1)x_8(t) + 2pb_1x_9(t) \\
x'_9(t) &= 2a_1x_3(t) + 2a_1x_8(t) - (a_1 + 3pb_1 + k_{on})x_9(t) + 4pb_1x_{14}(t) + k_{off_1}x_{10}(t) \\
&\quad + k_{off_2}(x_{11}(t) + x_{12}(t) + x_{13}(t)) \\
x'_{10}(t) &= 2a_1x_4(t) + k_{on}x_9(t) - (pb_1 + a_1 + k_{off_1} + a_2)x_{10}(t) + 2pb_1x_{15}(t) + pb_2x_{11}(t) \\
&\quad + pb_3x_{13}(t) \\
x'_{11}(t) &= 2a_1x_5(t) + a_2x_{10}(t) - (pb_1 + a_1 + pb_2 + k_{off_2})x_{11}(t) + 2pb_1x_{16}(t) \\
&\quad + pb_3x_{12}(t) \\
x'_{12}(t) &= 2pb_1x_{17}(t) - (pb_1 + a_1 + pb_2 + pb_3 + k_{off_2})x_{12}(t) + 2a_1x_6(t) + a_2x_{13}(t) \\
x'_{13}(t) &= 2pb_1x_{18}(t) + pb_2x_{12}(t) - (pb_1 + a_1 + a_2 + pb_3 + k_{off_2})x_{13}(t) + 2a_1x_7(t) \\
x'_{14}(t) &= a_1x_9(t) - (4pb_1 + 2k_{on})x_{14}(t) + k_{off_1}x_{15}(t) + k_{off_2}(x_{16}(t) + x_{17}(t) + x_{18}(t)) \\
x'_{15}(t) &= a_1x_{10}(t) + 2k_{on}x_{14}(t) - (2pb_1 + k_{on} + k_{off_1} + a_2)x_{15}(t) + 2k_{off_1}x_{19}(t) \\
&\quad + pb_2x_{16}(t) + pb_3x_{18}(t) + k_{off_2}(x_{20}(t) + x_{21}(t) + x_{22}(t)) \\
x'_{16}(t) &= a_1x_{11}(t) + a_2x_{15}(t) - (2pb_1 + k_{on} + pb_2 + k_{off_2})x_{16}(t) + k_{off_1}x_{20}(t) \\
&\quad + pb_3x_{17}(t) + k_{off_2}(2x_{23}(t) + x_{24}(t) + x_{25}(t))
\end{aligned}$$

$$\begin{aligned}
x'_{17}(t) &= -(2pb_1 + k_{\text{on}} + pb_2 + pb_3 + k_{\text{off}_2})x_{17}(t) + k_{\text{off}_1}x_{21}(t) + a_1x_{12}(t) + a_2x_{18}(t) \\
&\quad + k_{\text{off}_2}(x_{24}(t) + 2x_{26}(t) + x_{27}(t)) \\
x'_{18}(t) &= a_1x_{13}(t) + pb_2x_{17}(t) - (2pb_1 + k_{\text{on}} + a_2 + pb_3 + k_{\text{off}_2})x_{18}(t) + k_{\text{off}_1}x_{22}(t) \\
&\quad + k_{\text{off}_2}(x_{25}(t) + x_{27}(t) + 2x_{28}(t)) \\
x'_{19}(t) &= k_{\text{on}}x_{15}(t) - (2k_{\text{off}_1} + 2a_2)x_{19}(t) + pb_2x_{20}(t) + pb_3x_{22}(t) \\
x'_{20}(t) &= k_{\text{on}}x_{16}(t) + 2a_2x_{19}(t) - (k_{\text{off}_1} + a_2 + pb_2 + k_{\text{off}_2})x_{20}(t) + 2pb_2x_{23}(t) \\
&\quad + pb_3(x_{21}(t) + x_{25}(t)) \\
x'_{21}(t) &= pb_2x_{24}(t) + k_{\text{on}}x_{17}(t) - (k_{\text{off}_1} + a_2 + pb_2 + pb_3 + k_{\text{off}_2})x_{21}(t) + a_2x_{22}(t) \\
&\quad + pb_3x_{27}(t) \\
x'_{22}(t) &= pb_2x_{25}(t) + pb_2x_{21}(t) + k_{\text{on}}x_{18}(t) - (k_{\text{off}_1} + 2a_2 + k_{\text{off}_2} + pb_3)x_{22}(t) \\
&\quad + 2pb_3x_{28}(t) \\
x'_{23}(t) &= a_2x_{20}(t) - (2pb_2 + 2a_3 + 2k_{\text{off}_2})x_{23}(t) + pb_3x_{24}(t) \\
x'_{24}(t) &= 2a_3x_{23}(t) - (2pb_2 + pb_3 + a_3 + 2k_{\text{off}_2})x_{24}(t) + a_2x_{21}(t) + 2pb_3x_{26}(t) \\
&\quad + a_2x_{25}(t) \\
x'_{25}(t) &= pb_2x_{24}(t) - (pb_2 + a_2 + 2k_{\text{off}_2} + a_3 + pb_3)x_{25}(t) + a_2x_{22}(t) + pb_3x_{27}(t) \\
x'_{26}(t) &= a_3x_{24}(t) - (2pb_2 + 2pb_3 + 2k_{\text{off}_2})x_{26}(t) + a_2x_{27}(t) \\
x'_{27}(t) &= 2pb_2x_{26}(t) - (2pb_3 + pb_2 + a_2 + 2k_{\text{off}_2})x_{27}(t) + 2a_2x_{28}(t) + a_3x_{25}(t) \\
x'_{28}(t) &= pb_2x_{27}(t) - (2a_2 + 2k_{\text{off}_2} + 2pb_3)x_{28}(t)
\end{aligned}$$

here,  $x_i$  denotes the 28 different model states that are shown in Figure 3.2.

### A.1.2. ODE-System of the model with ligand binding

The ODE-system for the model that is extended by the ability to bind ligand as described in Chapter 3.2.1 is setup like follows

$$\begin{aligned}
x'_1(t) &= -(4a_1 + l_{\text{on}})x_1(t) + b_1x_2(t) + l_{\text{off}}x_{29}(t) \\
x'_2(t) &= 4a_1x_1(t) - (3a_1 + b_1 + l_{\text{on}})x_2(t) + 2b_1(x_3(t) + x_8(t)) + l_{\text{off}}x_{30}(t) \\
x'_3(t) &= a_1x_2(t) - (2a_1 + 2b_1 + k_{\text{on}} + l_{\text{on}})x_3(t) + k_{\text{off}_1}x_4(t) + k_{\text{off}_2}(x_5(t) + x_6(t) + x_7(t)) \\
&\quad + b_1x_9(t) + l_{\text{off}}x_{31}(t) \\
x'_4(t) &= k_{\text{on}}x_3(t) - (2a_1 + k_{\text{off}_1} + a_2 + l_{\text{on}})x_4(t) + b_2x_5(t) + b_1x_{10}(t) + b_3x_7(t) + l_{\text{off}}x_{32}(t) \\
x'_5(t) &= a_2x_4(t) - (2a_1 + b_2 + k_{\text{off}_2} + l_{\text{on}})x_5(t) + b_3x_6(t) + b_1x_{11}(t) + l_{\text{off}}x_{33}(t) \\
x'_6(t) &= -(2a_1 + b_2 + b_3 + k_{\text{off}_2} + l_{\text{on}})x_6(t) + a_2x_7(t) + b_1x_{12}(t) + l_{\text{off}}x_{34}(t) \\
x'_7(t) &= b_2x_6(t) - (2a_1 + a_2 + b_3 + k_{\text{off}_2} + l_{\text{on}})x_7(t) + b_1x_{13}(t) + l_{\text{off}}x_{35}(t)
\end{aligned}$$

$$\begin{aligned}
x'_8(t) &= 2a_1x_2(t) - (2b_1 + 2a_1 + l_{\text{on}})x_8(t) + 2b_1x_9(t) + l_{\text{off}}x_{36}(t) \\
x'_9(t) &= 2a_1x_3(t) + 2a_1x_8(t) - (a_1 + 3b_1 + k_{\text{on}} + l_{\text{on}})x_9(t) + 4b_1x_{14}(t) + k_{\text{off}_1}x_{10}(t) \\
&\quad + k_{\text{off}_2}(x_{11}(t) + x_{12}(t) + x_{13}(t)) + l_{\text{off}}x_{37}(t) \\
x'_{10}(t) &= 2a_1x_4(t) + k_{\text{on}}x_9(t) - (b_1 + a_1 + k_{\text{off}_1} + a_2 + l_{\text{on}})x_{10}(t) + 2b_1x_{15}(t) + b_2x_{11}(t) \\
&\quad + b_3x_{13}(t) + l_{\text{off}}x_{38}(t) \\
x'_{11}(t) &= 2a_1x_5(t) + a_2x_{10}(t) - (b_1 + a_1 + b_2 + k_{\text{off}_2} + l_{\text{on}})x_{11}(t) + 2b_1x_{16}(t) + b_3x_{12}(t) \\
&\quad + l_{\text{off}}x_{39}(t) \\
x'_{12}(t) &= 2b_1x_{17}(t) - (b_1 + a_1 + b_2 + b_3 + k_{\text{off}_2} + l_{\text{on}})x_{12}(t) + 2a_1x_6(t) + a_2x_{13}(t) + l_{\text{off}}x_{40}(t) \\
x'_{13}(t) &= 2b_1x_{18}(t) + b_2x_{12}(t) - (b_1 + a_1 + a_2 + b_3 + k_{\text{off}_2} + l_{\text{on}})x_{13}(t) + 2a_1x_7(t) + l_{\text{off}}x_{41}(t) \\
x'_{14}(t) &= a_1x_9(t) - (4b_1 + 2k_{\text{on}} + l_{\text{on}})x_{14}(t) + k_{\text{off}_1}x_{15}(t) + k_{\text{off}_2}(x_{16}(t) + x_{17}(t) + x_{18}(t)) \\
&\quad + l_{\text{off}}x_{42}(t) \\
x'_{15}(t) &= a_1x_{10}(t) + 2k_{\text{on}}x_{14}(t) - (2b_1 + k_{\text{on}} + k_{\text{off}_1} + a_2 + l_{\text{on}})x_{15}(t) + 2k_{\text{off}_1}x_{19}(t) + b_2x_{16}(t) \\
&\quad + b_3x_{18}(t) + k_{\text{off}_2}(x_{20}(t) + x_{21}(t) + x_{22}(t)) + l_{\text{off}}x_{43}(t) \\
x'_{16}(t) &= a_1x_{11}(t) + a_2x_{15}(t) - (2b_1 + k_{\text{on}} + b_2 + k_{\text{off}_2} + l_{\text{on}})x_{16}(t) + k_{\text{off}_1}x_{20}(t) + b_3x_{17}(t) \\
&\quad + k_{\text{off}_2}(2x_{23}(t) + x_{24}(t) + x_{25}(t)) + l_{\text{off}}x_{44}(t) \\
x'_{17}(t) &= -(2b_1 + k_{\text{on}} + b_2 + b_3 + k_{\text{off}_2} + l_{\text{on}})x_{17}(t) + k_{\text{off}_1}x_{21}(t) + a_1x_{12}(t) + a_2x_{18}(t) \\
&\quad + k_{\text{off}_2}(x_{24}(t) + 2x_{26}(t) + x_{27}(t)) + l_{\text{off}}x_{45}(t) \\
x'_{18}(t) &= a_1x_{13}(t) + b_2x_{17}(t) - (2b_1 + k_{\text{on}} + a_2 + b_3 + k_{\text{off}_2} + l_{\text{on}})x_{18}(t) + k_{\text{off}_1}x_{22}(t) \\
&\quad + k_{\text{off}_2}(x_{25}(t) + x_{27}(t) + 2x_{28}(t)) + l_{\text{off}}x_{46}(t) \\
x'_{19}(t) &= k_{\text{on}}x_{15}(t) - (2k_{\text{off}_1} + 2a_2 + l_{\text{on}})x_{19}(t) + b_2x_{20}(t) + b_3x_{22}(t) + l_{\text{off}}x_{47}(t) \\
x'_{20}(t) &= k_{\text{on}}x_{16}(t) + 2a_2x_{19}(t) - (k_{\text{off}_1} + a_2 + b_2 + k_{\text{off}_2} + l_{\text{on}})x_{20}(t) + 2b_2x_{23}(t) \\
&\quad + b_3(x_{21}(t) + x_{25}(t)) + l_{\text{off}}x_{48}(t) \\
x'_{21}(t) &= b_2x_{24}(t) + k_{\text{on}}x_{17}(t) - (k_{\text{off}_1} + a_2 + b_2 + b_3 + k_{\text{off}_2} + l_{\text{on}})x_{21}(t) + a_2x_{22}(t) + b_3x_{27}(t) \\
&\quad + l_{\text{off}}x_{49}(t) \\
x'_{22}(t) &= b_2x_{25}(t) + b_2x_{21}(t) + k_{\text{on}}x_{18}(t) - (k_{\text{off}_1} + 2a_2 + k_{\text{off}_2} + b_3 + l_{\text{on}})x_{22}(t) + 2b_3x_{28}(t) \\
&\quad + l_{\text{off}}x_{50}(t) \\
x'_{23}(t) &= a_2x_{20}(t) - (2b_2 + 2a_3 + 2k_{\text{off}_2} + l_{\text{on}})x_{23}(t) + b_3x_{24}(t) + l_{\text{off}}x_{51}(t) \\
x'_{24}(t) &= 2a_3x_{23}(t) - (2b_2 + b_3 + a_3 + 2k_{\text{off}_2} + l_{\text{on}})x_{24}(t) + a_2x_{21}(t) + 2b_3x_{26}(t) + a_2x_{25}(t) \\
&\quad + l_{\text{off}}x_{52}(t) \\
x'_{25}(t) &= b_2x_{24}(t) - (b_2 + a_2 + 2k_{\text{off}_2} + a_3 + b_3 + l_{\text{on}})x_{25}(t) + a_2x_{22}(t) + b_3x_{27}(t) + l_{\text{off}}x_{53}(t) \\
x'_{26}(t) &= a_3x_{24}(t) - (2b_2 + 2b_3 + 2k_{\text{off}_2} + l_{\text{on}})x_{26}(t) + a_2x_{27}(t) + l_{\text{off}}x_{54}(t) \\
x'_{27}(t) &= 2b_2x_{26}(t) - (2b_3 + b_2 + a_2 + 2k_{\text{off}_2} + l_{\text{on}})x_{27}(t) + 2a_2x_{28}(t) + a_3x_{25}(t) + l_{\text{off}}x_{55}(t) \\
x'_{28}(t) &= b_2x_{27}(t) - (2a_2 + 2k_{\text{off}_2} + 2b_3 + l_{\text{on}})x_{28}(t) + l_{\text{off}}x_{56}(t) \\
x'_{29}(t) &= -(4\alpha_1 + l_{\text{off}})x_{29}(t) + \beta_1x_{30}(t) + l_{\text{on}}x_1(t) \\
x'_{30}(t) &= 4\alpha_1x_{29}(t) - (3\alpha_1 + \beta_1 + l_{\text{off}})x_{30}(t) + 2\beta_1(x_{31}(t) + x_{36}(t)) + l_{\text{on}}x_2(t) \\
x'_{31}(t) &= \alpha_1x_{30}(t) - (2\alpha_1 + 2\beta_1 + k_{\text{on}} + l_{\text{off}})x_{31}(t) + k_{\text{off}_1}x_{32}(t) + \beta_1x_{37}(t)
\end{aligned}$$

$$\begin{aligned}
& + k_{\text{off}_2}(x_{33}(t) + x_{34}(t) + x_{35}(t)) + l_{\text{on}}x_3(t) \\
x'_{32}(t) &= k_{\text{on}}x_{31}(t) - (2\alpha_1 + k_{\text{off}_1} + a_2 + l_{\text{off}})x_{32}(t) + \beta_2x_{33}(t) + \beta_1x_{38}(t) + \beta_3x_{35} + l_{\text{on}}x_4(t) \\
x'_{33}(t) &= a_2x_{32}(t) - (2\alpha_1 + \beta_2 + k_{\text{off}_2} + l_{\text{off}})x_{33}(t) + \beta_3x_{34}(t) + \beta_1x_{39}(t) + l_{\text{on}}x_5(t) \\
x'_{34}(t) &= -(2\alpha_1 + \beta_2 + \beta_3 + k_{\text{off}_2} + l_{\text{off}})x_{34}(t) + a_2x_{35}(t) + \beta_1x_{40}(t) + l_{\text{on}}x_6(t) \\
x'_{35}(t) &= \beta_2x_{34}(t) - (2\alpha_1 + a_2 + \beta_3 + k_{\text{off}_2} + l_{\text{off}})x_{35}(t) + \beta_1x_{41}(t) + l_{\text{on}}x_7(t) \\
x'_{36}(t) &= 2\alpha_1x_{30}(t) - (2\beta_1 + 2\alpha_1 + l_{\text{off}})x_{36}(t) + 2\beta_1x_{37}(t) + l_{\text{on}}x_8(t) \\
x'_{37}(t) &= 2\alpha_1x_{31}(t) + 2\alpha_1x_{36}(t) - (\alpha_1 + 3\beta_1 + k_{\text{on}} + l_{\text{off}})x_{37}(t) + 4\beta_1x_{42}(t) + k_{\text{off}_1}x_{38}(t) \\
& + k_{\text{off}_2}(x_{39}(t) + x_{40}(t) + x_{41}(t)) + l_{\text{on}}x_9(t) \\
x'_{38}(t) &= 2\alpha_1x_{32}(t) + k_{\text{on}}x_{37}(t) - (\beta_1 + \alpha_1 + k_{\text{off}_1} + a_2 + l_{\text{off}})x_{38}(t) + 2\beta_1x_{43}(t) + \beta_2x_{39}(t) \\
& + \beta_3x_{41}(t) + l_{\text{on}}x_{10}(t) \\
x'_{39}(t) &= 2\alpha_1x_{33}(t) + a_2x_{38}(t) - (\beta_1 + \alpha_1 + \beta_2 + k_{\text{off}_2} + l_{\text{off}})x_{39}(t) + 2\beta_1x_{44}(t) + \beta_3x_{40}(t) \\
& + l_{\text{on}}x_{11}(t) \\
x'_{40}(t) &= 2\beta_1x_{45}(t) - (\beta_1 + \alpha_1 + \beta_2 + \beta_3 + k_{\text{off}_2} + l_{\text{off}})x_{40}(t) + 2\alpha_1x_{34}(t) + a_2x_{41}(t) + l_{\text{on}}x_{12}(t) \\
x'_{41}(t) &= 2\beta_1x_{46}(t) + \beta_2x_{40}(t) - (\beta_1 + \alpha_1 + a_2 + \beta_3 + k_{\text{off}_2} + l_{\text{off}})x_{41}(t) + 2\alpha_1x_{35}(t) + l_{\text{on}}x_{13}(t) \\
x'_{42}(t) &= \alpha_1x_{37}(t) - (4\beta_1 + 2k_{\text{on}} + l_{\text{off}})x_{42}(t) + k_{\text{off}_1}x_{43}(t) + k_{\text{off}_2}(x_{44}(t) + x_{45}(t) + x_{46}(t)) \\
& + l_{\text{on}}x_{14}(t) \\
x'_{43}(t) &= \alpha_1x_{38}(t) + 2k_{\text{on}}x_{42}(t) - (2\beta_1 + k_{\text{on}} + k_{\text{off}_1} + a_2 + l_{\text{off}})x_{43}(t) + 2k_{\text{off}_1}x_{47}(t) + \beta_2x_{44}(t) \\
& + \beta_3x_{46}(t) + k_{\text{off}_2}(x_{48}(t) + x_{49}(t) + x_{50}(t)) + l_{\text{on}}x_{15}(t) \\
x'_{44}(t) &= \alpha_1x_{39}(t) + a_2x_{43}(t) - (2\beta_1 + k_{\text{on}} + \beta_2 + k_{\text{off}_2} + l_{\text{off}})x_{44}(t) + k_{\text{off}_1}x_{48}(t) + \beta_3x_{45}(t) \\
& + k_{\text{off}_2}(2x_{51}(t) + x_{52}(t) + x_{53}(t)) + l_{\text{on}}x_{16}(t) \\
x'_{45}(t) &= -(2\beta_1 + k_{\text{on}} + \beta_2 + \beta_3 + k_{\text{off}_2} + l_{\text{off}})x_{45}(t) + k_{\text{off}_1}x_{49}(t) + \alpha_1x_{40}(t) + a_2x_{46}(t) \\
& + k_{\text{off}_2}(x_{52}(t) + 2x_{54}(t) + x_{55}(t)) + l_{\text{on}}x_{17}(t) \\
x'_{46}(t) &= \alpha_1x_{41}(t) + \beta_2x_{45}(t) - (2\beta_1 + k_{\text{on}} + a_2 + \beta_3 + k_{\text{off}_2} + l_{\text{off}})x_{46}(t) + k_{\text{off}_1}x_{50}(t) \\
& + k_{\text{off}_2}(x_{53}(t) + x_{55}(t) + 2x_{56}(t)) + l_{\text{on}}x_{18}(t) \\
x'_{47}(t) &= k_{\text{on}}x_{43}(t) - (2k_{\text{off}_1} + 2a_2 + l_{\text{off}})x_{47}(t) + \beta_2x_{48}(t) + \beta_3x_{50}(t) + l_{\text{on}}x_{19}(t) \\
x'_{48}(t) &= k_{\text{on}}x_{44}(t) + 2a_2x_{47}(t) - (k_{\text{off}_1} + a_2 + \beta_2 + k_{\text{off}_2} + l_{\text{off}})x_{48}(t) + 2\beta_2x_{51}(t) \\
& + \beta_3(x_{49}(t) + x_{53}(t)) + l_{\text{on}}x_{20}(t) \\
x'_{49}(t) &= \beta_2x_{52}(t) + k_{\text{on}}x_{45}(t) - (k_{\text{off}_1} + a_2 + \beta_2 + \beta_3 + k_{\text{off}_2} + l_{\text{off}})x_{49}(t) + a_2x_{50}(t) + \beta_3x_{55}(t) \\
& + l_{\text{on}}x_{21}(t) \\
x'_{50}(t) &= \beta_2x_{53}(t) + \beta_2x_{49}(t) + k_{\text{on}}x_{46}(t) - (k_{\text{off}_1} + 2a_2 + k_{\text{off}_2} + \beta_3 + l_{\text{off}})x_{50}(t) + 2\beta_3x_{56}(t) \\
& + l_{\text{on}}x_{22}(t) \\
x'_{51}(t) &= a_2x_{48}(t) - (2\beta_2 + 2a_3 + 2k_{\text{off}_2} + l_{\text{off}})x_{51}(t) + \beta_3x_{52}(t) + l_{\text{on}}x_{23}(t) \\
x'_{52}(t) &= 2a_3x_{51}(t) - (2\beta_2 + \beta_3 + a_3 + 2k_{\text{off}_2} + l_{\text{off}})x_{52}(t) + a_2x_{49}(t) + 2\beta_3x_{54}(t) + a_2x_{53}(t) \\
& + l_{\text{on}}x_{24}(t) \\
x'_{53}(t) &= \beta_2x_{52}(t) - (\beta_2 + a_2 + 2k_{\text{off}_2} + a_3 + \beta_3 + l_{\text{off}})x_{53}(t) + a_2x_{50}(t) + \beta_3x_{55}(t) + l_{\text{on}}x_{25}(t) \\
x'_{54}(t) &= a_3x_{52}(t) - (2\beta_2 + 2\beta_3 + 2k_{\text{off}_2} + l_{\text{off}})x_{54}(t) + a_2x_{55}(t) + l_{\text{on}}x_{26}(t)
\end{aligned}$$

$$x'_{55}(t) = 2\beta_2 x_{54}(t) - (2\beta_3 + \beta_2 + a_2 + 2k_{\text{off}_2} + l_{\text{off}})x_{55}(t) + 2a_2 x_{56}(t) + a_3 x_{53}(t) + l_{\text{on}} x_{27}(t)$$

$$x'_{56}(t) = \beta_2 x_{55}(t) - (2a_2 + 2k_{\text{off}_2} + 2\beta_3 + l_{\text{off}})x_{56}(t) + l_{\text{on}} x_{28}(t)$$

here,  $x_i$  denotes the 56 different model states that are shown in Figure 3.7.

### A.1.3. Prediction profile likelihoods

As discussed in Chapter 3.2.3 the uncertainties of selected model predictions is assessed by the use of the prediction profile likelihood method (compare Section 2.2.2). The result is shown in Figure A.1. The quantification of the prediction profile likelihood is given in Figure 3.11.

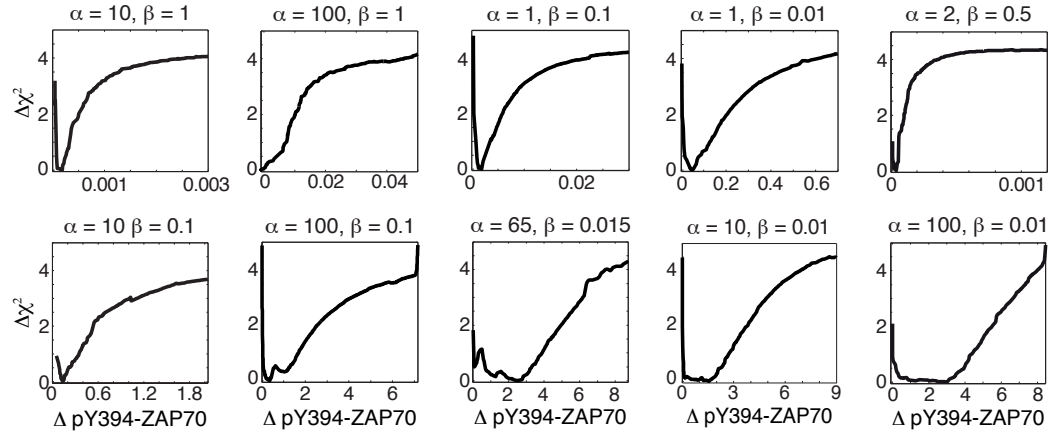


Figure A.1.: The uncertainties of selected model predictions is assessed by the use of the prediction profile likelihood method. The analyzed prediction is defined by the combination of the parameters  $\alpha$  and  $\beta$ .

## A.2. Additional material for the Lck regulation model

### A.2.1. Flow cytometry data of pY505

As discussed in Chapter 4.1.3, flow cytometry data of the phosphorylation of tyrosine residue 505 of Lck do not indicate bisable behavior.

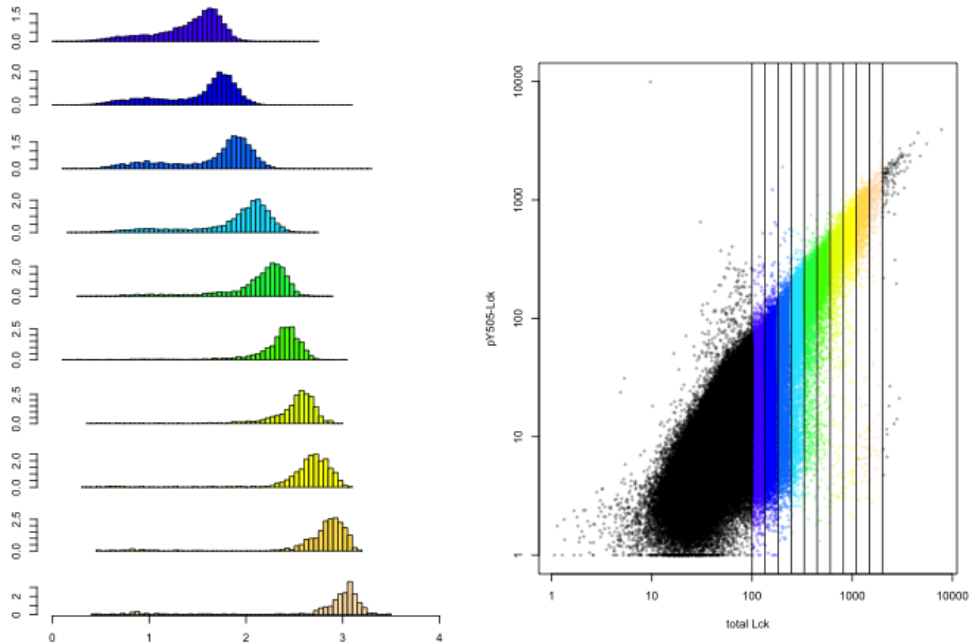


Figure A.2.: Dose–response data do not indicate bistability in the regulation of Lck. Flow cytometry data (right) is binned into groups of different total Lck expression in the cell. For each bin the corresponding histograms of phosphorylated Y505 are shown left. We do not find clear bimodal distributions as we would expect for bistable behavior. (Experiments by K. Nika and O. Acuto)

### A.2.2. Steady state solution of the Lck model

The ODE–system that describes the model of Lck regulation in Chapter 4.1.2 is solved analytically. The four model states are described by the following equations.

$$\begin{aligned}
 sActive = & -(a1^2 * b2 * (a2 + b1 + b2)) + a1 * (-b1 * (a2 + b1 + b2) * (2 * b2 - L * l1)) \\
 & + \sqrt{(a2 + b1 + b2) * ((a2 + b1 + b2) * ((a1 + b1) * b2 - b1 * L * l1)^2} \\
 & + 4 * b1 * (a2 + b1) * b2 * (b1 + b2) * L * l2)) + b1 * (-b1 * (a2 + b1 + b2) * \\
 & (b2 - L * l1)) - 2 * (a2 + b1) * (b1 + b2) * L * l2 + \sqrt{(a2 + b1 + b2) * ((a2 + b1 + b2)
 \end{aligned}$$

```

*((a1+b1)*b2 - b1*L*l1)^2 + 4*b1*(a2+b1)*b2*(b1+b2)*L*l2)))))
/(2*(a2+b1)*((a1+b1)*(a2+b1+b2)*l1 - (a2+b1)*(b1+b2)*l2))

dActive = (a2*(-(a1^2*b2*(a2+b1+b2)) + a1*(-(b1*(a2+b1+b2)*
(2*b2-L*l1)) + sqrt((a2+b1+b2)*((a2+b1+b2)*((a1+b1)*b2-b1*L*l1)^2
+ 4*b1*(a2+b1)*b2*(b1+b2)*L*l2))) + b1*(-(b1*(a2+b1+b2)*
(b2-L*l1)) - 2*(a2+b1)*(b1+b2)*L*l2 + sqrt((a2+b1+b2)*((a2+b1+b2)
*((a1+b1)*b2 - b1*L*l1)^2 + 4*b1*(a2+b1)*b2*(b1+b2)*L*l2))))))
/(2*(a2+b1)*(b1+b2)*((a1+b1)*(a2+b1+b2)*l1 - (a2+b1)*(b1+b2)*l2))

inactive = (a1^2*b2*(a2+b1+b2)^2 + a1*(a2+b1+b2)*(a2*(b1-b2)*b2
+ a2*(b1+2*b2)*L*l1 + b1*(b1+b2)*(b2+L*l1)
- sqrt((a2+b1+b2)*((a2+b1+b2)*((a1+b1)*b2 - b1*L*l1)^2
+ 4*b1*(a2+b1)*b2*(b1+b2)*L*l2))) + a2*b2*(-(b1*(a2+b1+b2)*
(b2-L*l1)) - 2*(a2+b1)*(b1+b2)*L*l2 + sqrt((a2+b1+b2)*((a2+b1+b2)
*((a1+b1)*b2 - b1*L*l1)^2 + 4*b1*(a2+b1)*b2*(b1+b2)*L*l2))))))
/(2*(a2+b1)*(b1+b2)*((a1+b1)*(a2+b1+b2)*l1 - (a2+b1)*(b1+b2)*l2))

primed = ((a2+b1+b2)*((a1+b1)*b2 + b1*L*l1)
- sqrt((a2+b1+b2)*((a2+b1+b2)*((a1+b1)*b2 - b1*L*l1)^2
+ 4*b1*(a2+b1)*b2*(b1+b2)*L*l2)))
/(2*(a1+b1)*(a2+b1+b2)*l1 - 2*(a2+b1)*(b1+b2)*l2)

```

### A.2.3. Csk kinase activity with two different rates

Our model could be further simplified by using the same phosphorylation rate for both phosphorylations that are carried out by Csk, instead of using two rate  $a_1$  and  $a_2$ . We can substitute both rates by the rate  $a$  in our steady state solution of the Lck model. Since we are interested in the phosphorylation of Y394 and Y505 we calculate the steady state solution for pY505 as the sum of inactive and double active Lck for a model system where the rates  $a_1$  and  $a_2$  are lumped into one rate  $a$ .

$$pY505-Lck = \frac{a Lck_{tot}}{a + b_1}$$

The phosphorylation of Y505 depends only linearly on the amount of total Lck, which is in disagreement with the observed data.



# Abbreviations

**APC** antigen presenting cell

**CBP** Csk binding protein

**CD45** cluster of differentiation 45

**Csk** C-Src kinase

**I** interleucine

**ITAM** immunoreceptor tyrosine-based activation motif

**L** leucine

**LAT** linker of activation

**Lck** lymphocyte-specific protein tyrosine kinase

**MAPK** mitogen-activated protein kinase

**MHC** major histocompatibility complex

**ODE** ordinary differential equation

**PI-3** phosphoinositide 3

**pMHC** peptide bound to MHC

**RPTP** receptor-type tyrosine phosphatase

**SFK** Src-family kinase

**SH** Src-homology

**SHP-1** Src homology region 2 domain-containing phosphatase-1

**SLP-76** SH2 domain containing leukocyte protein of 76kDa

**SOS** son of Sevenless

**TCR** T cell receptor

**Y** tyrosine

**ZAP70**  $\zeta$ -chain associated protein of 70 kDa

# Acknowledgments

I would like to express my gratitude to my supervisor Thomas Höfer who gave me the opportunity to work in his group. I could not only learn a lot from him about modeling but also about

Ursula Klingmüller

I would like to thank our collaborators Sumit Deswal and Wolfgang Schamel as well as Konstantina Nika and Oreste Acuto for providing me with the interesting data and for all the helpful insights into the vast field of immunology. My models without their data would have been meaningless. A special thanks to Wolfgang Schamel who was not only part of my Thesis Advisory Committee, but also agreed to come to Heidelberg to be one of my examiners.

Micha was an office mate, but has become a great friend. Thank you for smiling back all the time.

I would like to thank the whole Höfer group for fruitful discussions and the nice working atmosphere. Especially all the people that I share or shared the office with. Florian, thank you, you also have become a good friend.

My friends and room mates supported my throughout the entire time and have been great. I have to point out Elke, who checked on me and provided me with everything I needed whilst finishing the thesis. Paula, Svantje, Rebecca, Eva and Shayda, thank you for the weekly lunch break